UNIVERSITÀ DEGLI STUDI DI SALERNO

Dipartimento di Ingegneria Civile

Dottorato di Ricerca
in
Rischio e sostenibilità nei sistemi dell'ingegneria civile, edile ed ambientale
Curriculum B: Ingegneria delle Strutture e del Recupero Edilizio e Urbano

XXXIV Ciclo N.S. (a.a. 2020-2021)

DESIGN, MECHANICAL MODELLING AND TESTING OF INNOVATIVE SEISMIC ISOLATION DEVICES

Narinder Singh

Il Tutor
Prof. Ada Amendola

Il Coordinatore
Prof. Fernando Fraternali

Co-Tutor
Prof. Fernando Fraternali

Abstract

This work takes a pioneering approach to a bio-inspired design of seismic isolation systems. There is a growing demand for tunable seismic isolation devices to be widely used in developing countries at affordable cost. This thesis work employs architecture materials concepts and a bio-inspired design approach to formulate, manufacture, and experimentally test a novel seismic isolator. The unit cell of the analyzed device is formed by rigid linkages mimicking the bones of the limbs of the human body, which are connected to a central post through stretchable tendons. The central post carries the vertical load transmitted by the superstructure and can slide against the basis of the system.

This seismic 'sliding-stretching' isolator dissipates mechanical energy via friction and the pseudo-elastic recentring force of the tendons. Its displacement capacity can be finely tuned through an optimized design of the geometry of the limb members, while dissipative effects can be adjusted for the application at hand by playing with the geometry, the training cycles, and the material of the tendons.

It can be manufactured in-house using 3D printers and metallic parts provided by local metal framing companies or online suppliers, and hence does not require heavy industry or expensive materials. Its development paves the way to a customizable approach to the protection of artworks, small houses, and essential equipment in industrialized and developing countries.

KEYWORDS: Bio-inspired design, Seismic isolation, 3D printing, Scaling laws

Publications

The work presented in this dissertation and the preparatory research activities originated the following scientific papers published on internationally recognised (ISI) journals.

- F. Fraternali, N. Singh, A. Amendola, G. Benzoni, G.W. Milton, A biomimetic sliding–stretching approach to seismic isolation, Nonlinear Dynamics (2021) 1-13.
- A. Amendola. N. Singh, F. Santos, G. Benzoni, F. Fraternali., Innovative dissipative devices with tensegrity architecture and super elastic behaviour for the seismic protection of structures, EURODYN 2020- XI International Conference on Structural Dynamics, 2020.
- I. Farina, N. Singh, F. Colangelo, R. Luciano, G. Bonazzi, F. Fraternali, High-performance nylon-6 sustainable filaments for additive manufacturing, Materials 12(23) (2019) 3955.
- N. Singh, F. Santos, A. Amendola, F. Fraternali and A. Micheletti., Seismic metamaterials with tensegrity architecture, in: M.F. M. Papadrakakis (Ed.) 8th ECCOMAS Thematic Conference on Computational Methods in Structural Dynamics and Earthquake Engineering, Athens, Greece, 2021.
- N. Singh, A. Amendola, G. Benzoni, and F. Fraternali, 2021, January. Computational modeling of the seismic response of tensegrity dissipative devices incorporating shape memory alloys. In 14th WCCMECCOMAS Congress 2020 (Vol. 100).

To my parents

Acknowledgements

Without the financial support of the DICIV at the University of Salerno, this work would not have been possible. I am especially grateful to Dr. Ada Amendola, Thesis Supervisor, and Dr. Fernando Fraternali, co-supervisor, and Department of Civil Engineering Coordinator, who have been supportive of my career goals and have worked hard to provide me with protected academic time to pursue them.

I am indebted to everyone with whom I have had the pleasure of working on this and other similar initiatives.

I would like to express my gratitude to Dr Filipe Santos, (Civil Engineering Department, Faculty of Science and Technology, Universidade NOVA de Lisboa), the team of F.I.P. MEC srl and Carpenterie Morinelli srl for their invaluable guidance, collaboration, support, and solidarity during this endeavor.

Nobody has been more important to me in the pursuit of this project than the members of my family. I would like to express my gratitude to my parents, whose love and wisdom accompany me in every endeavor I undertake.

They are the exemplars of role models.

Thank you all!

Contents

LIST OF FIGURES

LIST OF TABLES

CHAPTER 1

INTRODUCTION AND MOTIVATION

In the event of earthquakes, seismic isolation offers an effective strategy to ensure the safety of people and the prevention of damage to structures, machinery, and equipment [1][2][3][4][5][6]. The most widespread seismic isolators currently on the market use elastomeric or friction-pendulum bearings [7][8]. These devices partially or completely disconnect the portion of the 'superstructure' above them from the ground motion. As a result, the fundamental vibration period of the structure is significantly increased, avoiding resonance with high-frequency seismic excitations [9].

Seismic isolators offer different levels of damping [10], which is useful for dissipating energy and reducing the amplitude of lateral displacements during earthquakes. The inherent limitations of currently available isolators include their confined operational frequencies, manufacturing complexity, need for advanced technical expertise, and substantial costs. While elastomeric bearings are still widely used and appreciated for their simplicity and consistent performance, even after several decades in service [11][12][13], friction-based devices quickly become the technology of choice when the

displacement demand increases significantly. Sliding bearings generally imply a more complex behavior of the isolated structure, due to the intrinsic complexity of the frictional phenomena and the still limited data about the durability of their critical components [14].

The choice of the appropriate technology for seismic isolation interventions on existing or new structures requires a careful analysis [1][15]. However, even the simplest implementation of the seismic isolation technology offers a major improvement in terms of the level of seismic protection of buildings and infrastructures in both industrialized and developing countries. Residential and rural buildings [16], equipment in hospitals and essential buildings [4][5], artworks in museums [6], and critical industrial facilities are nowadays often protected through many variations and combinations of seismic isolators. The considerable high cost and the perceived complexity of such devices, together with local availability constraints, often discourage a larger use of this reliable technology, particularly in less developed countries. The scientific community senses the need to create the conditions for a broader field of applications, and in this sense, several low-cost solutions for seismic isolators have been proposed in the literature and are currently under investigation [4][16][17][18][19].

The use of architecture material concepts to design next-generation seismic isolators deserves special attention, in consideration of the exceptional properties these systems

exhibit in different fields of mechanics, robotics, and acoustics [21][22][23][24][25][26][27]. This is due to an optimized geometric design of the internal structure [20][21] that can be conveniently manufactured using 3D printing at different scales [28][29][30]. Seismic metamaterials have been successfully proposed to protect buildings from seismic waves by creating shields around the structure through Bragg-scattering structured soils, buried mass or above-surface resonators, auxetic and hierarchical materials [31][32][33][34][35][36]. The periodicity of these media is often at the meter scale, which makes them not suited for use as seismic isolators. The employment of confined pentamode lattices as small amplitude vibration attenuation devices has been the subject of recent discussion in the literature [37].

Ever since Leonardo da Vinci's pioneering anatomic studies [38], the mechanics of human and animal locomotion have attracted researchers' attention. Animals adjust their muscle contraction frequencies to reach a state of resonance with pendulum- and elastic-type oscillation mechanisms during locomotion [39]. This frequency tuning process produces motion at low energy consumption. The bones of the legs and arms behave as pendulum systems that the muscles bend periodically to match their natural frequencies [40][41]. Animals such as jellyfish tune vibration frequencies through the elasticity of their tissues, which is a nonlinear function of the deflection of the mesoglea bell [39].

This thesis work takes a novel approach to a bio-inspired design of seismic isolation systems. It is focused on the design of a hybrid sliding–stretching isolator (SSI)

combining finite kinematics linkages that replicate the bones of human arms and legs, stretchable membranes that mimic the action of the muscle-tendon complex and confinement plates. The proposed device dissipates mechanical energy via friction and the hysteretic recentring force of the tendons. Its displacement capacity can be finely tuned through an optimized design of the geometry of the limb members, while dissipative effects can be adjusted for the application at hand by playing with the geometry, the training cycles, and the material of the tendons.

The SSI can be manufactured on-site or in a fabrication laboratory using 3D printers and metallic parts provided by local metal framing companies or online suppliers, and hence does not require heavy industry or expensive materials. Its development paves the way to novel, tunable seismic isolators that can be fully or partially manufactured through 3D printing techniques.

CHAPTER 2

BIO-INSPIRED DESIGN OF A STRETCHING SLIDING ISOLATOR

This section involves the design and development of the nature-inspired seismic isolation system which is a sliding stretching-based base isolation system. This system employs various parts which were designed with the help of the 3D CAD package and then additive manufacturing (AM) was used to manufacture the components which are described in the upcoming section. AM was used because of the rapid technique as the rapid manufacturing of the parts were needed for various testing purposes and design modifications. Most of the parts were manufactured or printed in filament wire made of polylactic acid (PLA) polymer and restitution elements (tendons) were printed in Thermoplastic Polyurethane (TPU) as they are flexible yet strong. The characterization of such TPU membranes was also carried out in later sections to optimize the response of the tendons. The tendons are the restitution elements that play a major role in the

functioning of the isolator. In the next sections, experimental and numerical modeling of the isolator has been discussed along with the results and discussion section.

2.1 Materials and methods

2.1.1 Unit cell design

An exploded view of the unit cell of the SSI is shown in Figure 1. It is composed of four articulated 'limb' members (arms and legs) branching out from a central post connected to the top plate of the device. This plate carries the vertical load transmitted by the superstructure, consisting, e.g., of a column, a bridge beam, machinery, or an artifact that needs to be isolated from the foundation. A cap screwed to the top plate covers the central post, which cap can exhibit relative rotations with respect to the post, due to a deformable cap cushion positioned between these parts. Such a movement allows the top plate to achieve the correct level (Figure 1). If rocking motions need to be prevented [5], the cushion can be removed, with the cap and the post-forming a single element. The central post ends with a slider made of a low-friction material built into a recess in its base.

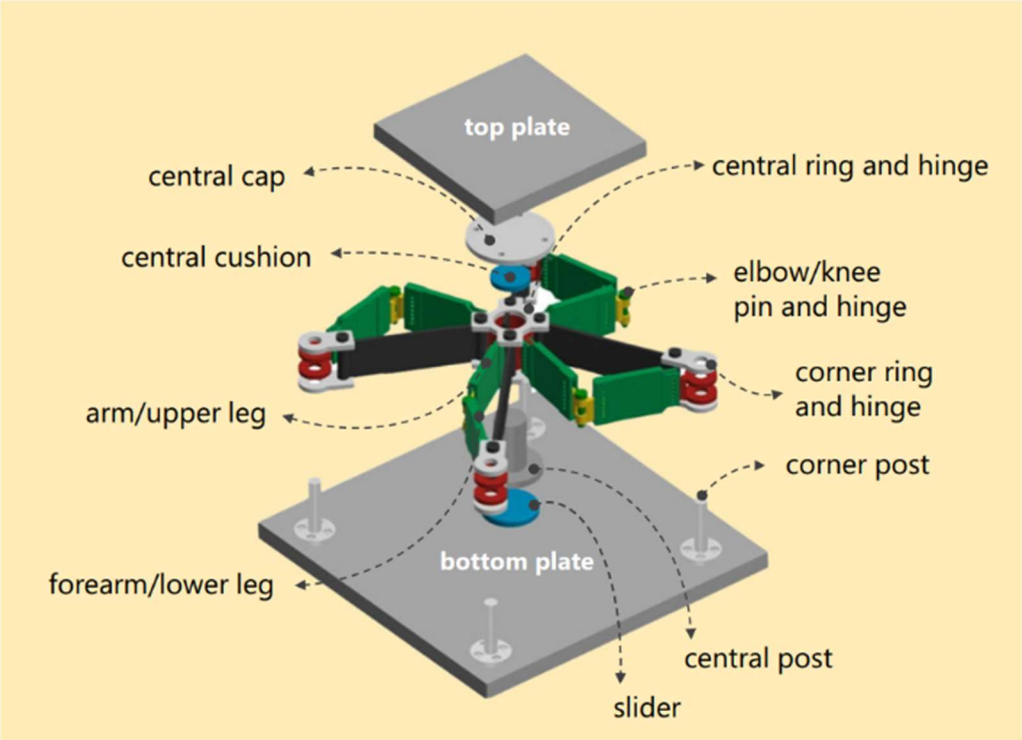

Figure 1 Exploded view of the SSI unit cell

As Figure 1 illustrates, four corner posts are screwed to the bottom plate and connected to the limb members at the ends opposite the central post. Vertical hinges connect the limbs and to the posts, while four membranes–tendons connect the corner posts to the central post (see Figure 1). The tendons are made of a material that can carry large stretching strains and that dissipates energy through hysteretic response [43][44]. The undeformed configuration of the limbs, depicted with red dashed lines in Figure 4 A, shows lower arms and legs with axial length a_1, upper arms and legs with axial length

a_2, and the relative angle between these members equal to $\pi/2+\beta$. Interestingly, the design variable β ('initial foot angle' or 'rest angle' of the limbs) can be easily varied by changing the screw points of the corner posts on the bottom plate.

The kinematics of the unit cell is described by the two parameters illustrated in Figure 4, for a given direction of the displacement of the central node (relative to the foundation): the angle α formed by such a direction with the horizontal axis, and the scalar projection u of the displacement vector of the central node in this direction. The displaced positions of the elbow and knee joints are easily found at the intersection points of the circle with radius a_2, which is centered at the current position of the central post, and the circles with radius a_1 centered at the corner posts. Due to symmetry, the kinematics of the cell is comprehensively studied by assuming $u > 0$ and letting α vary in the interval $[0^0, 90^0]$ deg. It is safe to assume that the design value of the lateral displacement allowed by the biomimetic isolator, hereafter referred to as 'displacement capacity' d, must be sufficiently lower than the minimum value of u producing a 'locking' configuration of the unit cell ($u = u^{lock}$). The locking condition is achieved when one or more tendons overlap the adjacent limb members (see Figure 2). The remarkable increase in '*d'* in systems with negative rest angles is achieved without changing the limbs' length and slightly reducing the footprint of the device (see insets in b). Overall, the displacement capacity depends only on the geometric design variables a_1, a_2 and β.

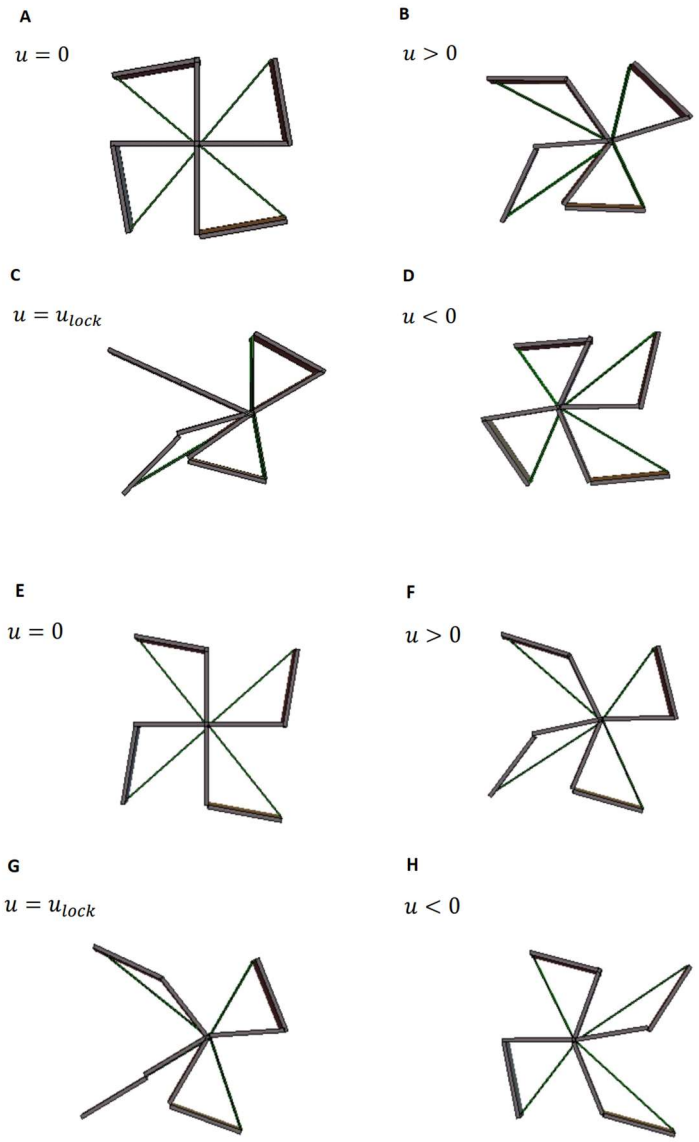

Figure 2 Snapshots extracted from the animations of the unit cell's motion. (A-D) Deformed configurations for different values of the applied displacement u,α= 0, and β=−10 deg. (E-H) Deformed configurations for α= 0 and β= 10 deg.

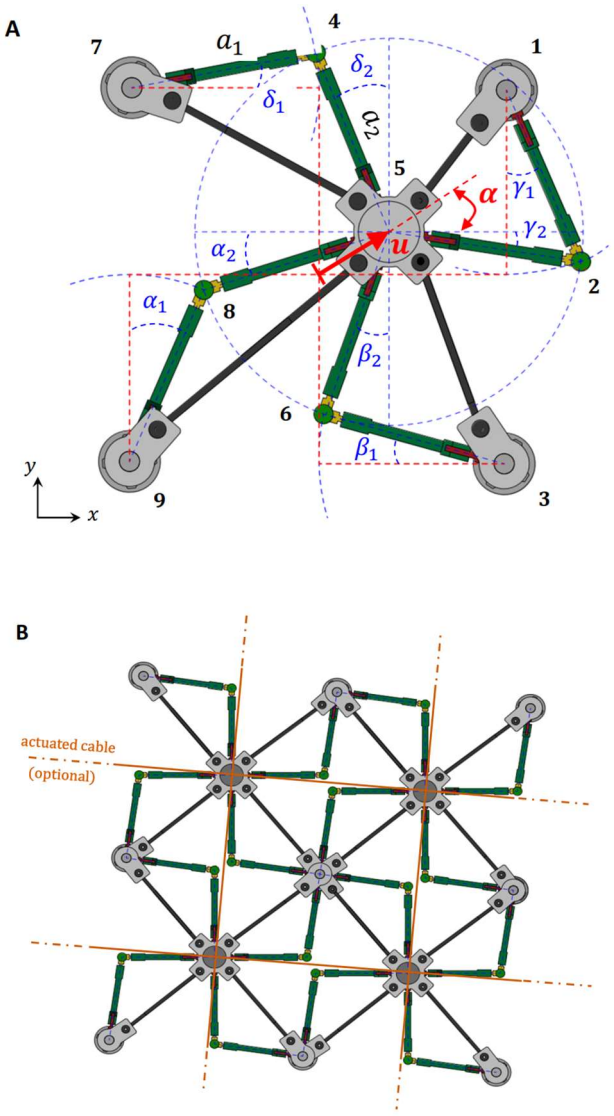

Figure 3 Undeformed and deformed configurations of different models of the SSI. (A) Top view of a deformed configuration of a single unit cell. (B) Top view of a 2x2 array of unit cells (undeformed configuration, β= 8deg).

C

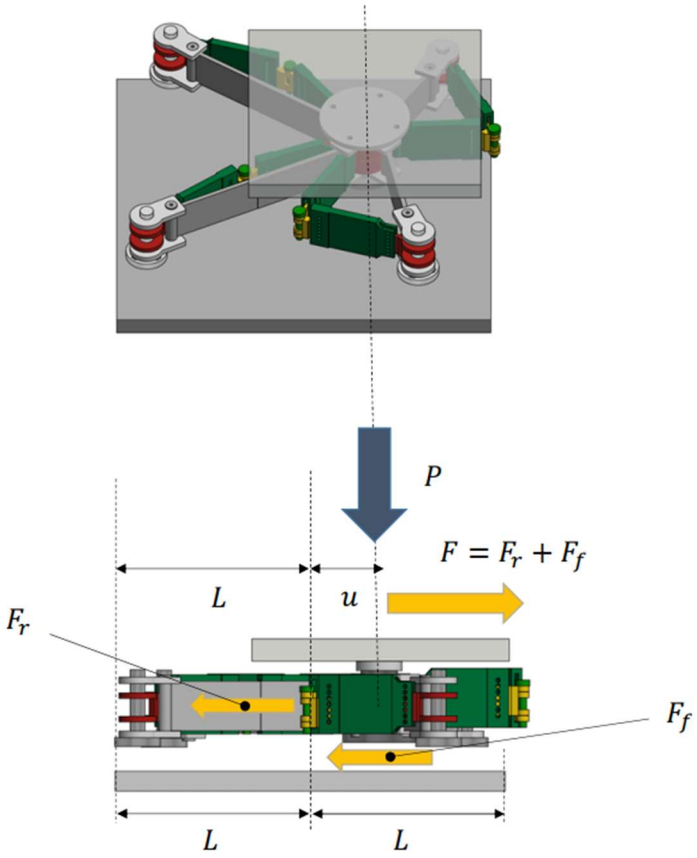

Figure 3 (continued) (C) Different views of the deformed configuration of an assembled model featuring 1 layer.

D

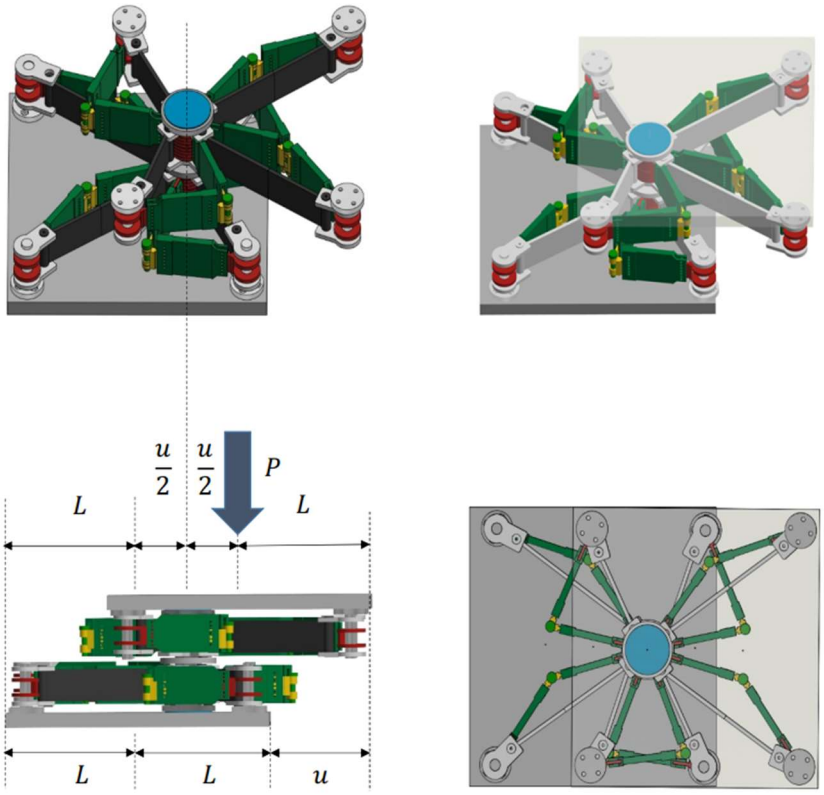

Figure 3 (continued) (D) Different views of the deformed configuration of an assembled model featuring 2 layers.

The plot in Figure 4 shows the variation of the dimensionless locking displacement $\bar{u}_{lock} = u_{lock}/a$ with α, for $a_1 = a_2 = a$. One observes that the minimum value of $\bar{u}_{lock}$ is attained at $\alpha = \pi/4 - \beta/2$, and that such a value grows appreciably when the rest angle changes from positive to negative. Indeed, it increases from 0.468 to 0.714 (≈ 53%) when switching β from 10 deg to -10 deg. It is also possible to double the displacement capacity of the device by stacking 2 unit cells one over the other in the vertical direction, as shown in Figure 4 (see also Figure 3, D).

The remarkable increase in '*d'* in systems with negative rest angles is achieved without changing the limbs' length and slightly reducing the footprint of the device. Overall, the displacement capacity depends only on the geometric design variables a_1, a_2 and β. Positive values of the rest angle are needed to build periodic systems formed by arrays of unit cells since the knee/elbow joints of adjacent cells do not touch one another if β is sufficiently greater than zero (Figure 3, B).

This design approach distributes the vertical load '*P'* transmitted by the superstructure among multiple central posts, creating a periodic metamaterial. The bio-inspired character of the proposed seismic isolator is multi-fold. First, the shape of the unit cell replicates that of a human body with bent arms and legs (Figure 1). Second, the tendon–membranes' capacity to stretch acts as a recentring mechanism of the central post, which regulates the fundamental vibration period of the isolated structure.

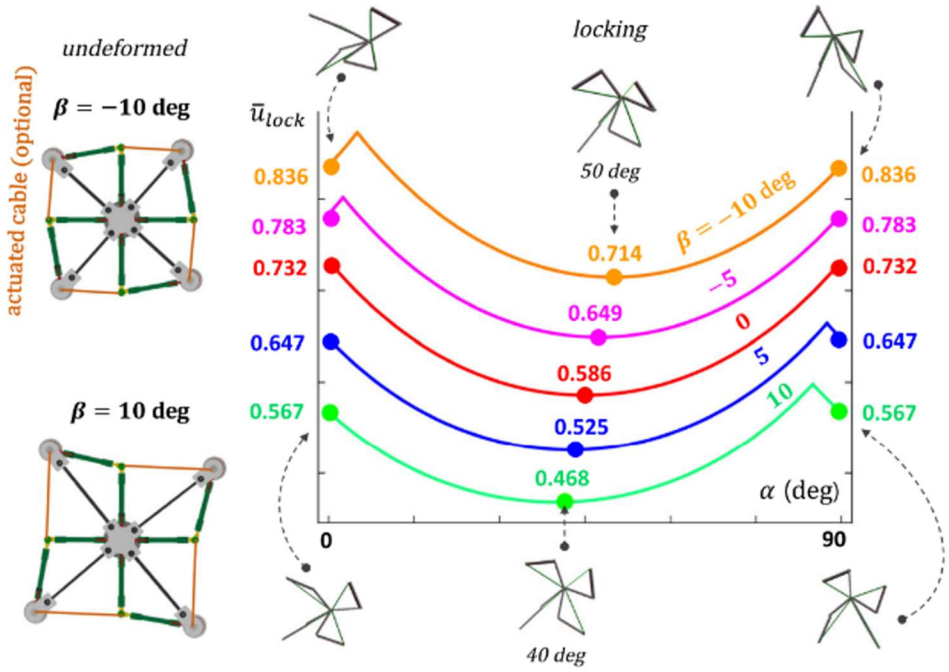

Figure 4 Locking displacements versus loading angle α and rest angle β. Deformed configuration of a two-layer system.

The extension-and-release working principle of the membranes produces time fluctuations of kinetic and stored energies like those induced by the stretching and recoil of animals' tendons during running and hopping [40]. Such a response also converts the frequency tuning mechanism associated with the locomotion of animals [39] into a passive mode. While animals move at resonance through the active control of

locomotion by muscles, tendons, and tissues, the SSI analyzed in this study works oppositely: it tunes the nonlinear stiffness of the tendons to avoid resonance with seismic excitation frequencies [9]. It is also possible to actively control the isolator by equipping the device with actuated cables that run on top of the posts or along the tendons controlled, e.g., by actuators embedded in the joints [42] (Figure 4 and Figure 3, B). This optional feature can be useful because it allows adjustment in real-time of the fundamental vibration period and the dissipation capacity of the isolated structure to the earthquake frequency and energy content during extreme events [3]. The active control provides an additional recentring mechanism of the system.

CHAPTER 3

PREPARATION OF PROTOTYPES

Physical models of the SSI were manufactured at the Rapid Prototyping Laboratory of the University of Salerno. This was achieved using fused deposition modeling (FDM) 3D printers, a lathe from a partner metal framing company, and Aluminum 7075-T651 (Ergal) confinement plates. The analyzed prototypes feature a single unit cell with the properties a_1 = 97.0 mm, a_2 = 100.5 mm, β = 0, and an overall height of 95 mm (including the confinement plates). The non-structural components were 3D printed using eco-friendly polylactic acid (PLA) filaments. The load-carrying members of the tested prototypes were fabricated in S235 steel through a parallel lathe (Figure 6 B). The slider underneath the central post (Figure 1) is a circular disk made of polytetrafluoroethylene (PTFE).

One of the tested prototypes (prototype #1) does not have tendons and was analyzed to study the pure friction sliding response of the central post (Figure 5A). Prototype #2 features tendons 3D-printed using thermoplastic polyurethane (TPU) filament for FDM

(Figure 5 D). Prototypes equipped with fully 3D-printed unit cell parts were also manufactured for demonstrative purposes (Figure 5 A, B). Table 1 illustrates the key manufacturing parameters of the biomimetic isolator prototypes.

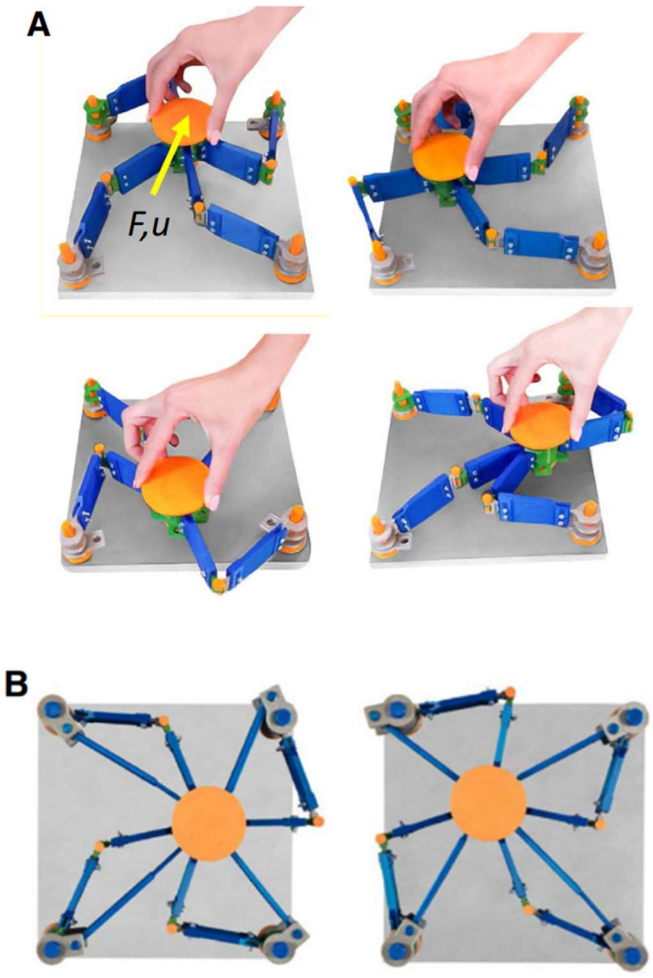

Figure 5 Physical models and experimental validation. (A) Motion animation of a demonstrative version of prototype #1 equipped with fully 3D-printed unit cell parts, which can be moved by hand. (B) Demonstrative version of prototype #2 equipped with telescopic tendons

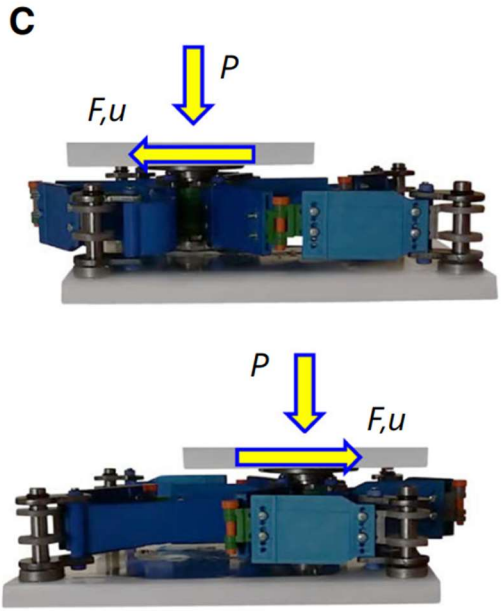

Figure 5 (continued) (C) Prototype #2 with stretchable tendons and metallic posts under testing

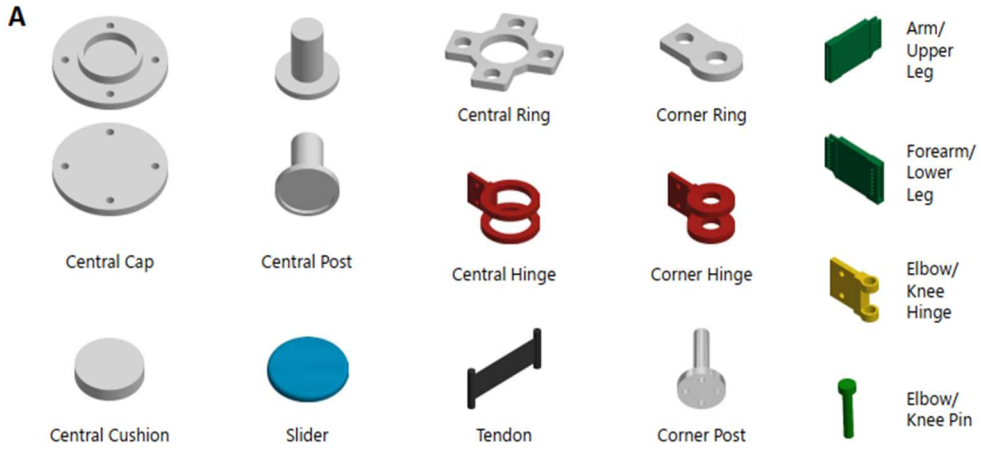

Figure 6 Different parts of the isolators. (A) List of components.

Figure 6 (continued) (B) Structural parts fabricated in S235 steel.

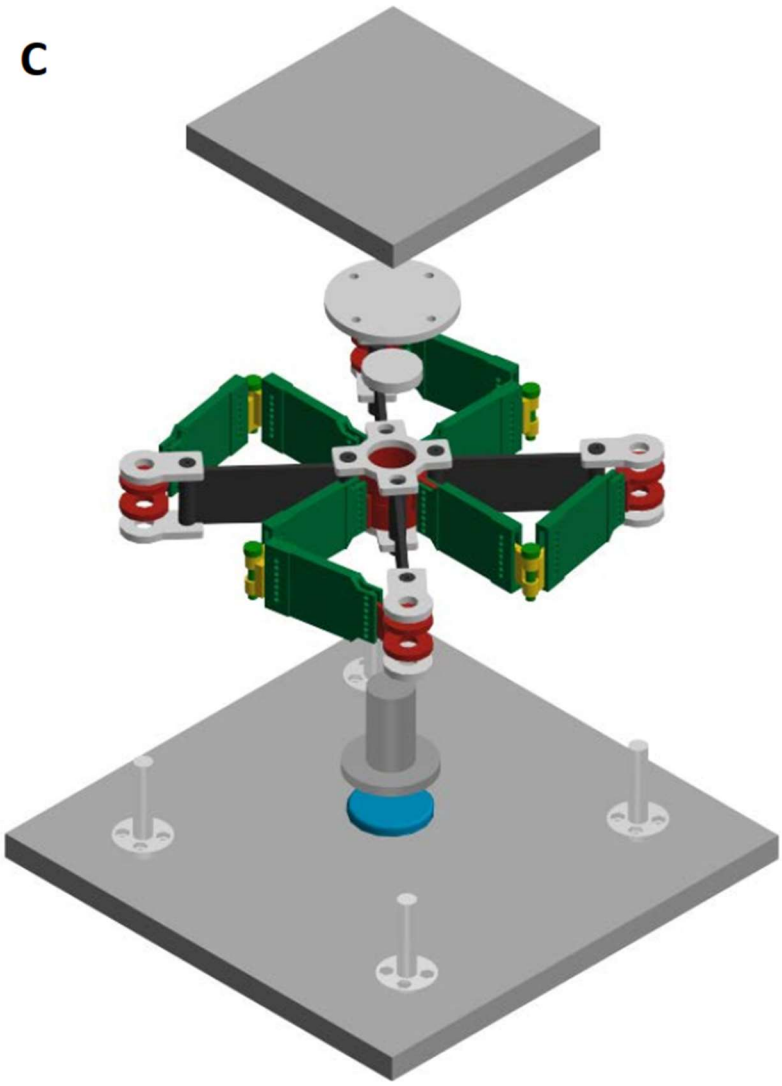

Figure 6 (continued) (C) Exploded view of the unit cell featuring a rest angle β = -10 deg.

An SSI prototype without tendons (hereafter referred to as sample #1) and a prototype equipped with thermoplastic polyurethane (TPU) membranes (sample #2) were

assembled at the Rapid Prototyping Laboratory of the Department of Civil Engineering of the University of Salerno. Figure 6 A illustrates the bill of materials of these prototypes, while Figure 6 C shows an exploded view of the unit cell. The fabricated SSI samples show lower limb length a_1=97.0 mm, upper limb length a_2=100.5 mm; and overall height of the unit cell equal to 95 mm (including the terminal plates). The limb members are composed of prismatic solid plates with a 40-mm maximum height, 80-mm total length, and a thickness variable of 5 to 6 mm. The central post has a cylindrical core with a 25-mm diameter.

It is fitted with a cap of 70 mm diameter, for a total height (including the cap and the slider) of 65 mm. The sliders are circular discs with 30-mm diameters and 5-mm thickness made of polytetrafluoroethylene (PTFE). The corner posts have a 10-mm diameter cylindrical core, a 26-mm diameter base enlargement with a 6-mm height, and a total height of 50 mm. The SSI prototypes are confined between a top square plate with a 150-mm edge and 15-mm thickness and a bottom square plate with a 250-mm edge and 15-mm thickness. The tendons forming sample #2 have a prismatic central region with a 31.6-mm height and a 1.9-mm thickness, which terminates with two terminal cylindrical rods with a 9-mm diameter and measuring 47.6 mm at the extremities. These rods are inserted into the corner rings and encase M3 steel bolts (3-mm diameter and 50-mm length) acting as stiffeners.

Table 1 key 3D printing parameters

Parameters	TPU
Print plane tilt	No
Heated printed plate	Yes
First layer height	0.15mm
First layer extrusion speed	50%
Surrounding temperature	23^0C
Print speed	25mm/s
Humidity	Absent
Layer thickness	0.3 mm
Nozzle diameter	0.4 mm
Filament diameter	1.75 mm
Extrusion temperature	230^0C
Activating cooling fan	Immediate
Cooling fan slow down	N/A
Retraction	N/A
Skirt height	N/A
Object skirt distance	5 mm
Brim	N/A
Infill (percentage)	50 %
Infill speed	35mm/s
Perimeter printing speed	35mm/s
Bridge	N/A
Print time and weight	
Print time/part	Weight/part
1h 30 min	18.86g

The 3D-printed parts of the SSI prototypes were manufactured using standard 3D printers based on the fused deposition modeling (FDM) technology. Polylactic acid (PLA) filaments commercially produced by Fillamentum® were used to build the components shown in Figure 6 A, except for the membrane/tendons, which were 3D printed using a TPU filament by Sunlu®. The PLA material employed has a mass density of 1.24 g/cm^3, a tensile strength at a yield of about 50 MPa, and a tensile elastic modulus of 3600 MPa.

Table 1 illustrates the key 3D printing settings used for the manufacture of a fully 3D-printed unit cell, together with the print times and weights of the different components (see Figure 6 A). Table 2 gives the cost analysis of the two prototypes, assuming a unit cost of €15.44 /kg for PLA Extrafill filaments by Fillamentum® (€38.6 for a 2.5 kg spool), and a unit cost of €43.98 /kg for TPU filaments by Sunlu® (€21.99 for a 0.5 kg spool). The cost analysis presented in Table 2 assumes that corner posts, corner rings, and the central ring of prototype #1 are 3D printed in PLA. The S235 structural steel parts were manufactured using a parallel lathe machine (Grazioli Fortuna 150, available at the partner metal framing company Carpenterie Morinelli srl [54], which also provided the up-to-date cost list.

The confinement plates were manufactured in the aluminum 7075-T651 alloy (Ergal) and were purchased from an online metal parts supplier (Acciai e Metalli) [59]. The sliders are high-strength polytetrafluoroethylene (PTFE) discs with 30 mm diameter and

5.0 mm thickness cut out of 1.25 m × 1.25m plates. These elements feature a maximum compressive strength in the range of 30 - 40 MPa, and a cost per slider of about €5.00 (including lubricant: silicon grease applied on the slider according to EN 1337-248 (*EN 1337-2*, 2003) [56]. The overall manufacturing cost for prototypes #1 and #2 is €120.72 and €392.53, respectively (not including labor costs for 3D printing).

Table 2 Print times and weights of the different parts of a fully 3d printed unit cell

Part name	Qty	Print time/part	Total print time	Weight/part	Weight
central cap	1	1h 38 min	1h 38 min	22 g	22 g
cap cushion	1	12 min	12 min	3 g	3 g
central hinge	4	41 min	2h 44 min	8 g	32 g
central post	1	2 h 39 min	2 h 39 min	39 g	39 g
central ring	2	31 min	1h 2 min	7 g	14 g
corner ring	8	16 min	2h 8 min	4 g	32 g
corner hinge	4	37 min	2h 28 min	8 g	32 g
corner post	4	1h 20 min	5h 20 min	8.50 g	34 g
Tendon	4	1h 25 min	5h 40 min	12 g	48 g
arm/upper leg	4	1h 28 min	5h 52 min	17. 5 g	70 g
forearm/lower leg	4	1h 28 min	5h 52 min	17. 5 g	70 g
elbow/knee hinge	8	26 min	3h 28 min	3 g	24 g
elbow/knee pin	4	21 min	1h 24 min	2 g	8 g

Overall weights of prototypes #1 and #2			
Prototype #	Unit cell weight	Top plate weight	Bottom plate weight	Weight
1	0.716 kg	0.948 kg	2.634 kg	4.299 kg
2	1.314 kg	0.948 kg	2.634 kg	4.897 kg

Cost analysis of prototypes #1 and #2 (Euro)						
Prototype #	PLA	TPU	Steel	Slider	Plates	Total cost
1	5.71	0.11	70.00	5.00	39.90	120.72
2	4.19	3.43	340.00	5.00	39.90	392.53

CHAPTER 4

EXPERIMENTAL VALIDATION PROCEDURE

Experimental validation tests were designed ‘ad hoc’ in collaboration with FIP MEC srl [55], a leading company in the field of anti-seismic devices based in Padova (Italy). A loading frame equipped with vertical and horizontal hydraulic actuators (Figure 7) was employed to apply unidirectional displacement histories to the bottom plate while subjecting the top plate to a fixed vertical load ‘P’. The testing activities led to the execution of 1 training cycle and 4 additional cycles of a sinusoidal displacement time-history with a frequency of 0.40 Hz and amplitude $d = \pm 50$ mm.

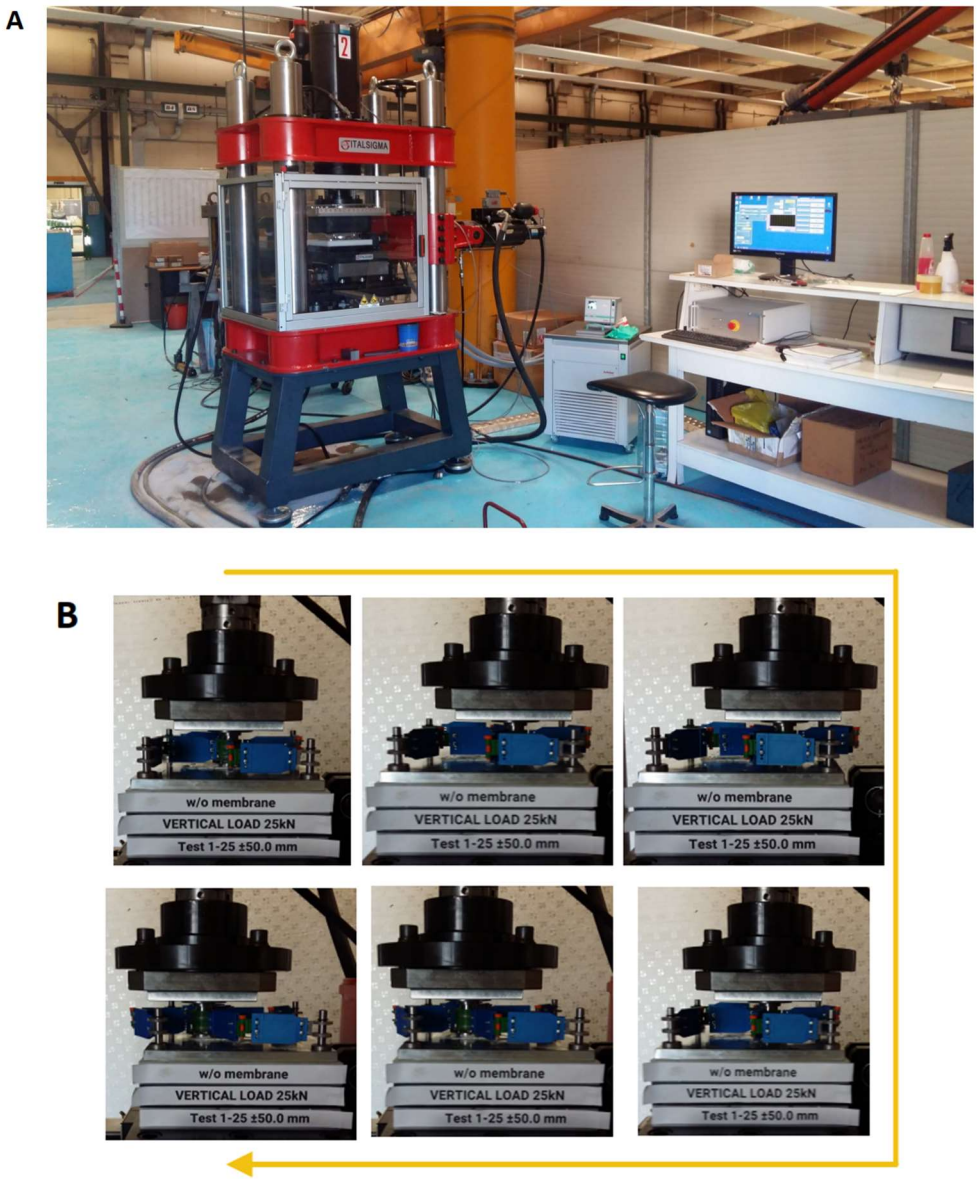

Figure 7 Employed experimental setup. (A) Experimental setup. (B) Snapshots extracted from the video recordings of the tests run on prototype # 1 under vertical load P= 25 kN and maximum lateral displacement d=±50mm

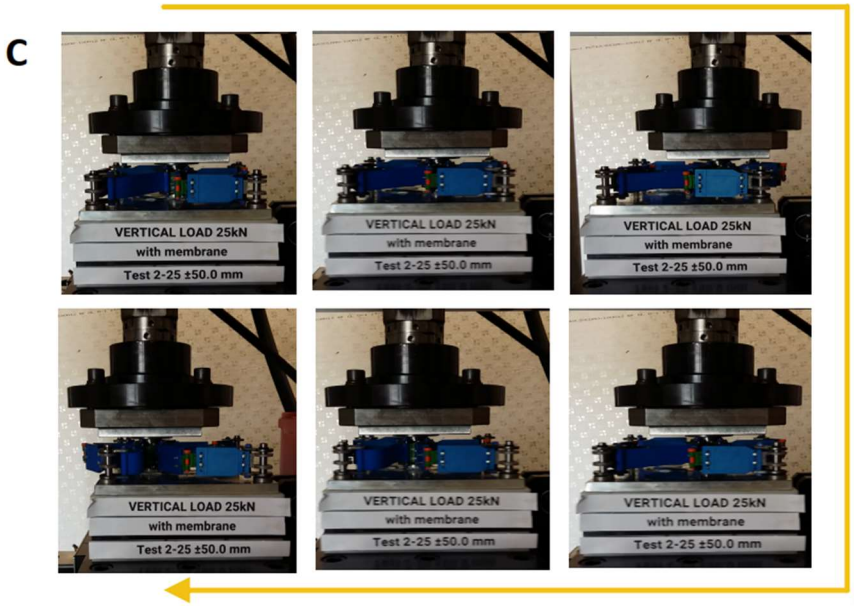

Figure 7 (continued) Employed experimental setup (C) Snapshots of the test run on prototype#2

Additional tests were run by applying one training cycle and 4 additional cycles of triangular displacement histories with a frequency of 0.50 Hz and amplitude d = ±25 mm. Three different values of the vertical load were applied to the top plate (P = 5, 15, 25 kN). Two sets of tendons were analyzed (sample #2): unconditioned tendons, and tendons subject to preliminary stretching through a few percent axial strains, leading such members to a state of pretension when the device was in the rest configuration. This pre-conditioning prevented the occurrence of significant residual strains after the training cycle.

For P = 5 kN, two pre-conditioned tendons were placed on opposite edges with respect to the loading direction, while the remaining two tendons were mounted as unconditioned (so that there was always one pre-conditioned tendon active for positive and negative lateral displacements). For P = 15 kN, three pre-conditioned tendons were mounted, while for P = 25 kN, all the tendons were pre-conditioned. The maximum engineering strain suffered by the tendons was estimated to reach values as high as 28% under testing, while the engineering strain rate suffered by the tendons was estimated to reach a peak value of 0.65/s.

The applied load frequencies are consistent with the typical frequency range of seismically isolated buildings [2][3]. To subject the tested specimens to similar sliding conditions, sample #1 was obtained by cutting and removing the membranes from sample #2, after all the tests on this sample were completed.

CHAPTER 5

EXPERIMENTAL CHARACTERIZATION OF THE RESPONSE OF THE TENDONS

The membrane/tendons of the SSI were 3D-printed, using a TPU filament with a mass density of 1.19 g/cm3 [58]. The mechanical characterization of these members was carried out via monotonic and cyclic uniaxial tension tests on 200 mm × 34 mm ×1:5 mm samples with gauge length L0 = 145 mm (Figure 8, A-I). The engineering axial strain of the sample is computed as follows: $\in = (l - L_0)=L_0$, with ‘ denoting the current length of the portion of the member used to measure the elongation (‘deformed gauge length’). Monotonic tests estimated a tensile modulus of 40 MPa; nominal stress at 35 % axial strain equal to 5 MPa; maximum nominal stress at the failure of 14 MPa; and 296 % failure strain Figure 8 A .

(Five series of cyclic, loading, and unloading tests were conducted at the displacement rate of 1,000 mm/min (0.11/s average strain rate) up to 35 % maximum strain, for a total of 20 cycles, the results of which are shown in Figure 8 B-F. The cyclic tests estimated maximum nominal stress of 5.4 MPa and a last cycle peak stress of 4.5 MPa. The average

stress-strain response after pre-conditioning can be easily fitted to the rate-independent, pseudo-elastic (PE) models by Dorfmann and Ogden [63] (Figure 8A, I).

The first of these models (hereafter referred to as 'model 1') assumes that the Mullins effect and residual strains have been removed through pre-conditioning and account for a hysteretic response during cyclic loading [63]. Let l_0 denote the deformed gauge length measured in the configuration at the end of the preconditioning phase. The nominal stress in the tendons ($\hat{\sigma}_t$) is related to the stretch ratio $\lambda = l/l_0$ (measured after pre-conditioning) through the following equations:

$$\hat{\sigma}_t^{(l)} = \frac{d\,\widetilde{W}\lambda}{d\lambda} \tag{1}$$

$$\hat{\sigma}_t^{(u,l)} = \hat{\sigma}_t^{(l)}\left[1 - \frac{1}{r}tanh\left(\frac{W_m - \widetilde{W}(\lambda)}{m}\right)\right] \tag{2}$$

where $\hat{\sigma}_t^{(l)}$ and $\hat{\sigma}_t^{(u)}$ respectively denote the nominal stress on the loading path and the unloading path; $\widetilde{W}(\lambda)$ denotes the strain energy function accounting for the incompressibility constraint, Here, w_m indicates the value of $\widetilde{w}$ at the maximum stretch λ_m during loading, while 'm' and 'r' are material parameters. The second hysteretic model generalizes the previous one to account for additional residual strains during

cyclic loading [63], after pre-conditioning ('model 2'). The unloading branch is now described through the following equation:

$$\sigma_t^{(u,2)} = \hat{\sigma}_t^{(u,1)} + \left[1 - \frac{1}{r} tanh\left(\left(\frac{W_m \widetilde{W}(\lambda)}{W_m}\right)^{\alpha_2}\right) / tanh(1)\right] (v_1 \lambda - v_2 \lambda^{-2}) \quad (3)$$

$\mathcal{V}_1$, $\mathcal{V}_2$ and α_2 are additional constitutive parameters. We use the Yeoh hyper-elastic model defined by

$$\widetilde{w} = \frac{(\lambda^3 - 3\lambda + 2)}{\lambda^3}\left(\lambda\left(c_{10}\lambda + c_{20}(\lambda^3 - 3\lambda + 2)\right) + c_{30}\,(\lambda + 2)^2(\lambda - 1)^4\right) \quad (4)$$

which is often employed to model the response of elastomeric isolators [64], and the Fit function of Mathematica®, to obtain: C_1 = 4:19579 MPa, C_2 = -4:85976 MPa, and C_3 = 9:67521 MPa for both hysteretic models by Dorfmann and Ogden. For the model without permanent deformation, we further obtain $r = r_1$ = 1:37159, and $m = m_1$ = 0:63206 MPa (see the solid curve in Figure 8, I). With reference to the second model by Dorfmann and Ogden [63], we instead estimate: $r = r_2$ = 0:571226; $m = m_2$ = 0:203351 MPa; $\mathcal{V}_1$ = 8:2281 MPa; $\mathcal{V}_2$ = 8:58084 MPa, α_2 = 6.25557 (dashed curve in Figure 8, I).

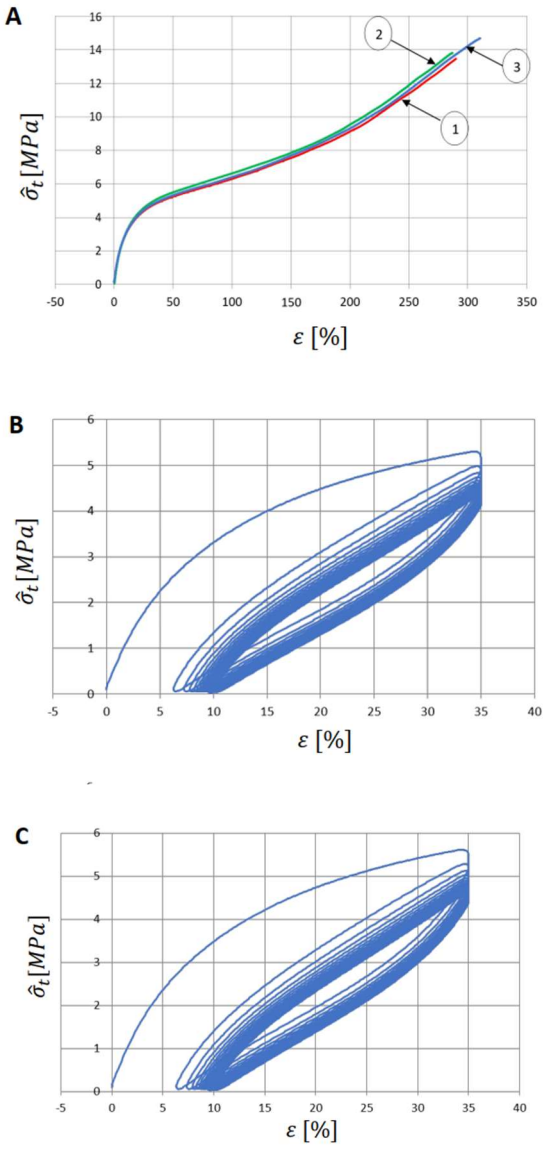

Figure. 8 Results of mechanical tests on TPU tendons. (A) Quasi-static tension tests conducted at the displacement rate of 1 mm/min to determine the tensile modulus and the displacement rate of 100 mm/min for failure analysis. (B-C) First two cyclic tests with 20 cycles up to 35 % axial strain at a displacement rate of 1,000 mm/min, up to 0.1 MPa stress at unloading.

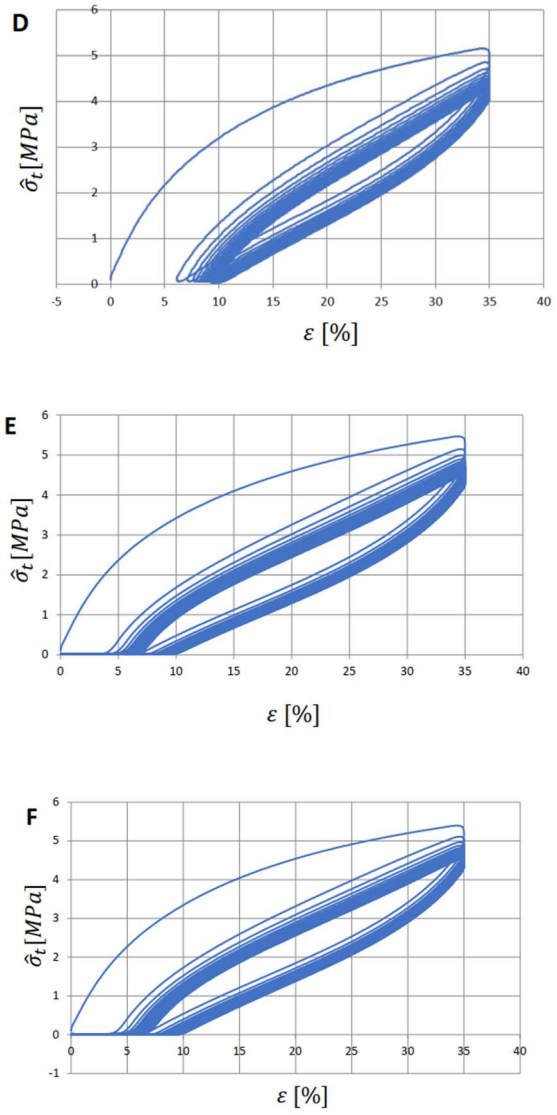

Figure. 8 (continued) (D) Third cyclic tests with 20 cycles up to 35 % axial strain at a displacement rate of 1,000 mm/min, up to 0.1 MPa stress at unloading. (E-F) Cyclic tests 4-5 with 20 cycles up to 35 % axial strain at a displacement rate of 1,000 mm/min, up to zero strain at unloading.

G

(h)

Figure 8 (continued) (G) Illustration of the deformed configuration at 35% strain of a tested specimen. (H) Undeformed and post-failure configuration of a specimen subjected to a monotonic tension test.

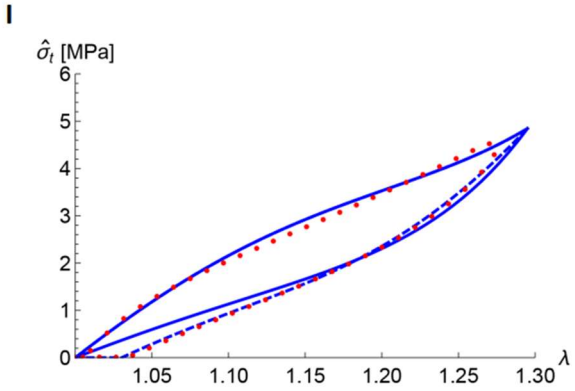

Figure 8 (continued) (I) Fit of a representative experimental stress-strain response after 15 cycles of pre-conditioning (test of panel F: circle marks) to a hysteretic model without permanent deformation (10) (model 1: solid line) and a hysteretic model accounting for a nonzero residual strain at the end of the unloading phase (11) (model 2: dashed line).

CHAPTER 6

RESULTS AND DISCUSSION

Let $F = F_r + F_s$ denote the overall shear force acting on the top plate of the SSI (base shear of the superstructure). The experimental and theoretical results obtained for the shear force F vs. lateral displacement u response of prototype #1 and #2 are illustrated in Figure 9 and Figure 10 respectively, in correspondence with the examined values of the vertical load (P = 5, 15, 25 kN).

The overall restoring force F_r transmitted from the tendons to the central post (Figure 3, C) is computed through the equation:

$$F_r = A_t \left(\sum_j (1 + \psi) \quad \widehat{\sigma}_t \left(\lambda_{t,j} \right) \widehat{\boldsymbol{k}}_{t,j} \right) \cdot \widehat{\boldsymbol{k}}^v \tag{5}$$

$$F_f = \mu P sign(\dot{v}) \tag{6}$$

$$= \mu_{s0} e^{-\frac{P}{P_{ref}}} \left(\gamma + (1-\gamma) e^{-\frac{|\dot{v}|}{\dot{v}_{ref}}} \right) \quad (7)$$

A trial-and-error procedure was employed to obtain the best-fit parameters of the friction model described by Equations ((*6*(*7*), and the constitutive model given by Equation (5) with respect to the experimental results for prototypes #1 and #2, respectively (after the training cycles). We estimated P_{ref} = 42.35 kN, μ_{s0} = 0.47%, γ = 4.00, v_{ref} = 2.50 mm/s and ψ = 0.19. The accuracy of the employed mechanical models for F_f and F_r is demonstrated by the good theory vs. experiment matching observed in Figure 9, Figure 10. For the tests run on prototype #1, we note the following theory vs. experiment differences in terms of the average energy dissipated per cycle (sinusoidal tests): -5.27 % for P = 5 kN (theory: 16.61 J; experiment: 17.54 J); 11.07 % for P = 15 kN (theory: 39.36 J; experiment: 35.44 J); and 7.86% for P = 25 kN (theory: 51.81 J; experiment: 48.03 J).

These values of *E DC* correspond to average values of μ_{eff} varying from 1.66% (P = 5 kN) to 1.04% (P = 25 kN). The oscillations of the experimental results visible in Figure 9 are explained by accuracy measurement errors due to the low values of the shear forces recorded during the tests (0.1–0.3kN), which are close to zero on the scale range of the horizontal actuator (0–100 kN), and the experimentally measured variability of the

vertical load P. Passing to examine the sinusoidal test on sample #2 under $P = 5$ kN, we note that the loading branches of the experimental F - u response exhibit low-slope segments in proximity to the points with $u = 0$ (see Figure 10).

Such portions of the F - u curve is caused by the fact the unconditioned tendons are initially 'slack' due to the residual strains accumulated in the training cycle. In the tests with $P = 15$ kN, the initial slope of the F - u curve (near $u = 0$) is smaller for $u > 0$ than for $u < 0$, thanks to the insertion of two preconditioned tendons working for $u < 0$ and only one working for $u > 0$ (see Figure 10). Finally, for $P = 25$ kN all the loading branches of the F -u curve exhibit considerably high slope near $u = 0$, because all the tendons were pre-conditioned in correspondence to such a value of P (Figure 10 *G*). As a result, the overall matching between theoretical predictions and experimental observations of the force-displacement response is appreciably more accurate for $P = 25$ kN than for the previous cases (cf. Figure 10 *C,E,G*).

Let us now compare the results of sinusoidal tests, affected by material- and friction-dependent nonlinearities (due to the time-variation of the sliding-velocity of the central post), with those of triangular input tests, where the sliding velocity is constant (see Figure 9, Figure 10). A comparative analysis of the response laws given in Figure 9 and Figure 10 reveals that the nonlinearity of the $F – u$ curve of prototype #2 is essentially due to the nonlinear behavior of the tendons and pre-conditioning effects. The hysteretic

response of the tendons determines the different shapes of the loading and unloading branches shown in Figure 10 *D,F,H* [43][44][45].

Referring to the theoretical model for prototype #2, we record ξ_{eff} = 17.05%, 24.72%, 27.84% for P = 5kN, 15 kN and 25 kN, respectively. Similarly, we estimate T_{eff} of prototype #2, respectively, equal to 1.32 s, 2.09 s and 2.51 s for P = 5kN, 15 kN and 25 kN. For P = 25 kN, the employed mechanical model estimates T_{eff} = 1.94 s (ξ_{eff} = 20.87%) when setting the cross-section area of the tendons to twice the value At_0 corresponding to prototype #2 (cf. Figure 5 E). Which are close to zero on the scale range of the horizontal actuator (0–100 kN), and the experimentally measured variability of the vertical load P. Passing to examine the sinusoidal test on sample #2 under P = 5 kN, we note that the loading branches of the experimental F - u response exhibit low-slope segments in proximity to the points with u = 0 (see Figure 10 C).

Such portions of the F - u curves are caused by the fact the unconditioned tendons are initially 'slack' due to the residual strains accumulated in the training cycle. In the tests with P = 15 kN, the initial slope of the F - u curve (near u = 0) is smaller from $u > 0$ than for $u < 0$, thanks to the insertion of two preconditioned tendons working for $u < 0$ and only one working for $u > 0$ (Figure 10 E). Finally, for P = 25 kN all the loading branches of the F -u curve exhibit a considerably high slope near u = 0 since all the tendons were pre-conditioned in correspondence to such a value of P (see Figure 10 G).

As a result, the overall matching between theoretical predictions and experimental observations of the force-displacement response is appreciably more accurate for P = 25 kN than for the previous cases (cf. Figure 10 *C,E,G*).

Let us now compare the results of sinusoidal tests, affected by material- and friction-dependent nonlinearities (due to the time-variation of the sliding-velocity of the central post), with those of triangular input tests, where the sliding velocity is constant (see Figure 9 and Figure 10). A comparative analysis of the response laws given in Figure 9 and Figure 10 reveals that the nonlinearity of the F – u curve of prototype #2 is essentially due to the nonlinear behavior of the tendons and pre-conditioning effects. The hysteretic response of the tendons determines the different shapes of the loading and unloading branches shown in Figure 10 *D,F,H* [43][44][45]. Referring to the theoretical model for prototype #2, we record ξ_{eff} = 17.05%, 24.72%, 27.84% for P = 5kN, 15 kN and 25 kN, respectively.

Similarly, we estimate T_{eff} of prototype #2, respectively, equal to 1.32 s, 2.09 s, and 2.51 s for P = 5kN, 15 kN, and 25 kN. For P = 25 kN, the employed mechanical model estimates T_{eff} = 1.94 s (ξ_{eff} = 20.87%) when setting the cross-section area of the tendons A_t to twice the value A_{t_0} corresponding to prototype #2 (cf. Figure 5 E).

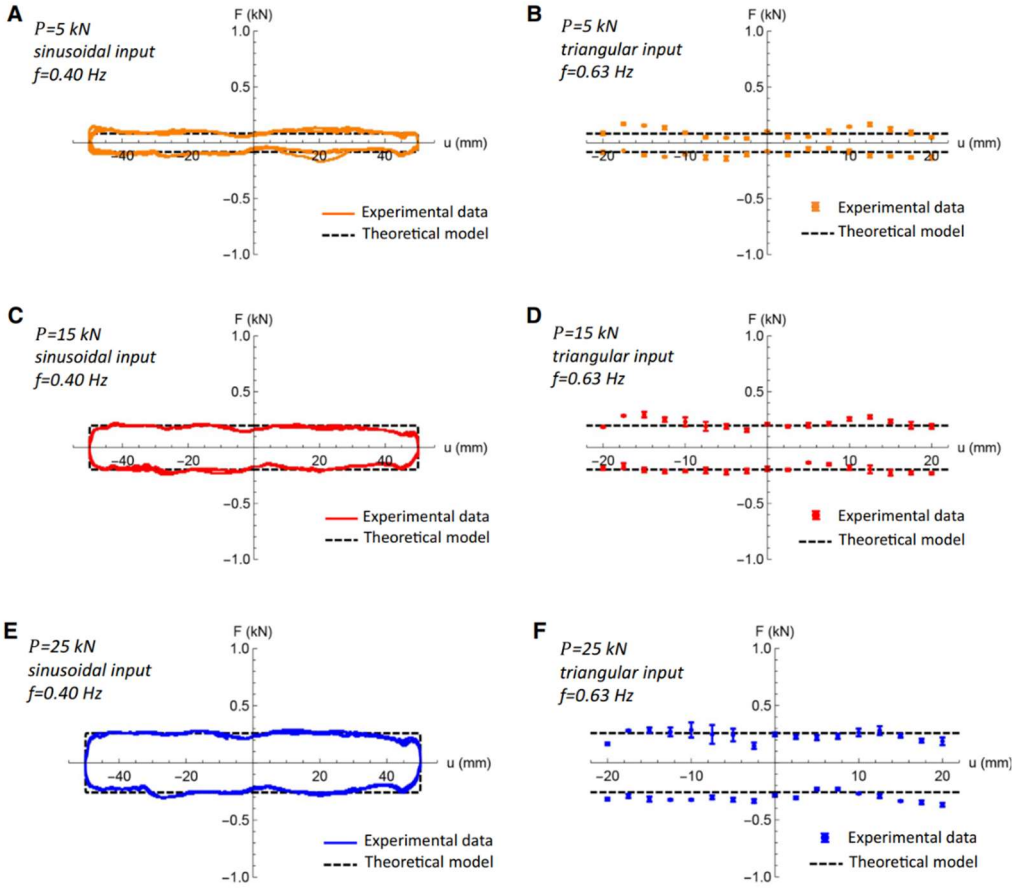

Figure 9 Shear force F versus lateral displacement u response of the SSI prototype #1. Comparison of experimental results and theoretical predictions under fixed vertical load P and cyclic displacement histories with amplitude d = ±50 mm, for P = 5 kN (A,B); P = 15 kN (C,D); and P = 25 kN (E,F). The displacement window of triangular loading tests has been restricted to 85% of the maximum value to exclude disturbance effects related to load reversal. Error bars refer to deviations of the shear force from the mean value under cyclic loading.

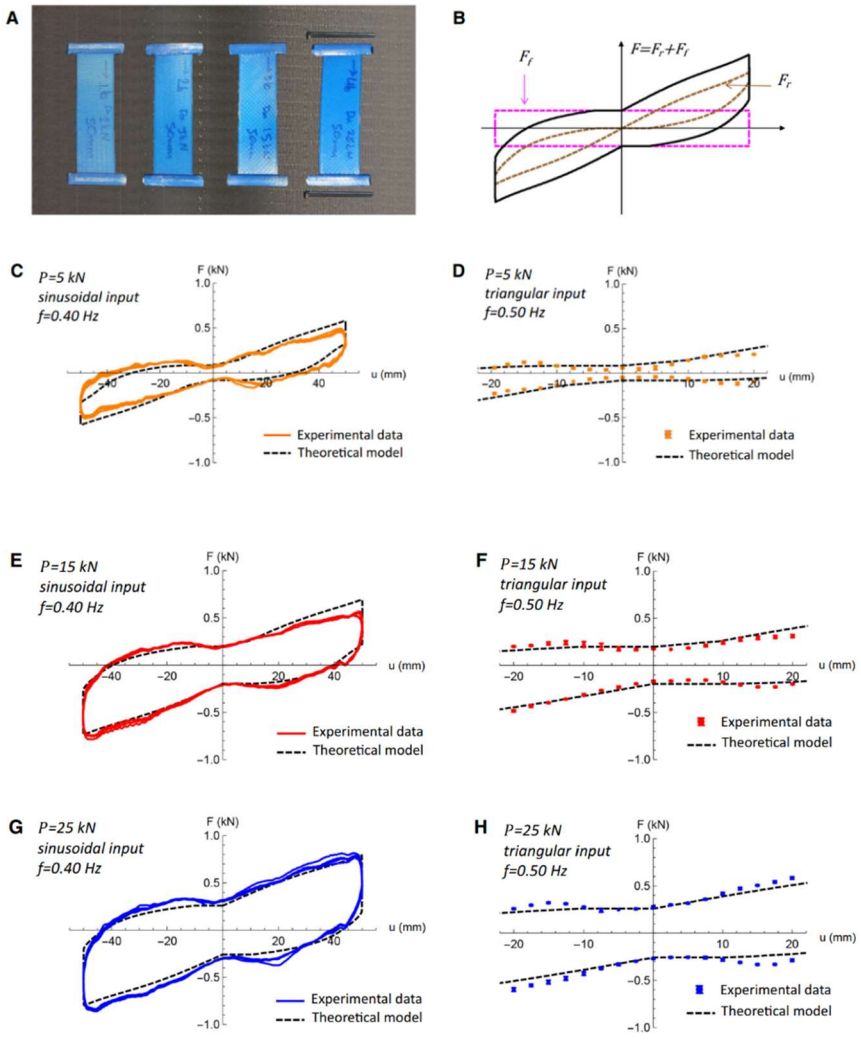

Figure 10 Shear force F versus lateral displacement u response of the SSI prototype #2. A) Images of the tendons reinforced with M3 bolts at the extremities. B) Components of the adopted mechanical model (sinusoidal loading with P = 25 kN). C–H) F - u curves for P = 5 kN (C, D); P = 15 kN (E-F); and P = 25 kN (G–H). The displacement window of triangular loading tests has been restricted to 85% of the maximum value to exclude disturbance effects related to load reversal

CHAPTER 7

SCALING LAWS

The sizing of the prototypes illustrated in the previous section can be extrapolated to SSIs of different sizes and load-displacement capacities. This extrapolation assumes that the materials used for the different parts, as well as the overall height H and the thickness t of the confinement plates, remain the same as for prototypes #1 and #2 (H=95 mm; t=15 mm). Since the locking displacement of the unit cell depends linearly on the limb lengths a_1 and a_2, we design the geometric variables for a SSI with lateral displacement capacity d in such a way that it results in: $a_1/a_1^{(1,2)} = d/d^{(1,2)}$ and $a_2/a_2^{(1,2)} = d/d^{(1,2)}$, where $d^{(i)}$ denotes the displacement capacity the prototype #i.

By prescribing a rest angle β = -10 deg, and making use of the chart given in Figure 2b of [66], we set $d^{(1)} = d^{(2)}$ = 70 mm. The vertical load capacity of prototypes #1 and #2 is $P^{(1)} = P^{(2)}$ = 25 kN, which induces a pressure of about 35 MPa in the PTFE slider. The maximum admissible force $P_y^{(1,2)}$ that the central post of prototypes #1 and #2 can carry without yielding (fully elastic regime) is estimated as 92 kN, utilizing an admissible

elastic stress $\sigma_{sa} = f_{yk}/1.25 = 188$ MPa for S235 steel ($f_{yk} = 235$ MPa denoting the characteristic yielding stress, see *EN 10025*).

6.1 SSI1 systems

We start by extrapolating the cost of prototype #1 to SSIs not equipped with tendons (SSI1 systems), which feature various (vertical) load and (lateral) displacement capacities. Such systems show the central post and cap made of S235 steel and the other parts of the unit cell 3D printed in TPU (cap cushion) or PLA (all the remaining parts). Hereafter, we will denote $C_i^{(j)}$ the cost of the component #i of the prototype #j, and C_i the cost of the same component in the current system.

The first component that we examine is the bottom plate, which rests on the foundation and has a non-structural function. The cost of such a plate that corresponds to a given displacement capacity d can be computed as follows:

$$C_1(d) = C_1^{(1)} \frac{d}{d^{(1)}} \tag{8}$$

Assuming that the quotation systems provided by the metal parts supplier give prices for metallic plates that scale linearly with the edge length (and the thickness) of the plate. The second group of components is formed by limb members; corner rings, posts,

and hinges; and elbow/knee pins and hinges. The longitudinal size of such members linearly scales with $a = max(a_1,a_2)$, i.e., with d. On assuming that their thickness also scales with d, we estimate the cost of the current group of components through the following formulae,

$$C_2(d) = C_2^{(1)}\left(\frac{d}{d^{(1)}}\right)^2 \tag{9}$$

The third group of parts collects the central post and cap, and the top plate. Such parts transfer the vertical load 'P' to the foundation. The cost of these components that corresponds to a given load-carrying capacity P can be estimated as it follows:

$$C_3(P) = C_3^{(1)}\mathcal{F}\left(\frac{P}{P_y^{(1,2)}}\right) \tag{10}$$

where:

$$\mathcal{F}(\mathrm{x}) := \begin{cases} 1, for\ x \leq 1 \\ x, for\ x > 1 \end{cases} \tag{11}$$

since we assume that the size of the parts under examination cannot be lower than that taken in correspondence with the base prototypes. The use of Eqn. (9) for estimating the cost of the central post is explained by the observation that the cross-section area of such a member can be designed to scale with 'P', by adopting the design formula of the structural members under axial loading [69] (remember that we are keeping the height

of the SSI constant). For what concerns the central cap, we assume a 2.8 constant ratio between the diameter of such a member and that of the central post, which scales with $P^{1/2}$. The thickness of such a member scale with the square root of the bending moment M_{cap} produced by the applied vertical load over the section of attack of the central post, i.e., with $P^{1/2}$. Similarly, we assume that the edge length of the top plate is 9 times larger than the diameter of the central post.

The thickness of this part is scaled with the square root of the bending moment M_{plate} over the section of attack of the central cap. Overall, we conclude that both the volume of the central cap and that of the top plate can be assumed to scale with '*P'*. The fourth group is the slider and the central cushion. To calculate their cost, we assume:

$$C_4(P) = C_4^{(1)} \frac{P}{P^{(1)}} \tag{12}$$

Finally, for what concerns the central ring and hinge, we observe that the diameter of such members linearly scales with the diameter of the central post. We can therefore estimate the cost of the current set of parts through the following formula:

$$C_5\,(P) = C_5^{(1)} \sqrt{\mathcal{F}\left(\frac{P}{P_y^{(1,2)}}\right)} \tag{13}$$

6.2 SSI2 systems

We can now extrapolate the cost of prototype #2 to SSIs equipped with tendons for which not only the central post and cap (as in SSI1 systems) but also the central ring, corner posts, and corner rings are made of S235 steel (SSI2 systems). The main difference between these devices and the SSI1 systems lies in the fact that the presence of the tendons now gives a structural role to the corner posts, whose function is to transfer the recentring forces carried by the tendons to the foundation. As for SSI1 systems, we can again categorize most of the parts into five groups, with the difference that group two will not include corner rings and posts. The scaling laws for the costs of these groups of parts are identical to those for SSI1 systems, with the replacement of the apex (1) with (2) where necessary. The cost estimation of the remaining parts of SSI2 systems is as follows. To match the requirements of the standards for seismic isolation, we set:

$$F_{r_d}(P) = \chi P \tag{14}$$

where F_{r_d} indicates the design value of tendons' restoring force, and χ denotes a dimensionless parameter [50]. We, therefore, design the cross-section area A_t of these members using the equation:

$$A_t(P)\, f_{r_d} = \chi P \tag{15}$$

Regarding the corner posts, each tendon transfers two shear forces to the competent corner post, which are each equal to one-half of the overall axial force carried by the tendon. The first force is applied at a height H_{ring} from the base of the core of the post, while the second one is applied at the base of prototype #2. Considering that the motion at 45 degrees of the unit cell almost stresses one single tendon (see the animations provided as Supplementary Materials), we assume that the above forces are each equal to $F_{rd}/2$. The corresponding bending moment at the base of the post is $M_p \approx F_{rd}H_{ring}/2$. We design the diameter d_p and the cross-section area A_p of the corner posts according to the following standard formulas for structural members loaded in bending [69]:

$$d_p(p) = \left(\frac{32M_p(\mathrm{P})}{\pi\sigma_{sa}z}\right)^{3/2}, \quad A_p(P) = \frac{\pi d_p^2}{4} \tag{16}$$

Finally, regarding the corner rings, we assume that the outer diameter of these members is equal to $m_f\, d_p$ where m_f is a magnification factor that we assign equal to 2.5. The members are loaded in tension under the forces transmitted from the tendons to the corner posts. To be on the safe side, we assign a force F_{r_d} to each ring, and we design the thickness t_r and the volume V_r of these members via the equations:

$$t_r(p) = \frac{F_{r_d}(P)}{\sigma_{sa} d_p (m_f - 1)}, \tag{17}$$

$$v_r(p) = \frac{\pi d_p^2(P)}{4}\left(m_f^2 - 1\right) t_r(p) \tag{18}$$

The extrapolation laws of the costs of tendons, corner posts, and corner rings, respectively, are:

$$C_6(P) = C_6^{(2)} \mathcal{F}\left(\frac{A_t}{A_t^{(2)}}\right), \tag{19}$$

$$C_7(P) = C_7^{(2)}\left[\xi + (1-\xi)\mathcal{F}\left(\frac{A_P}{A_P^{(1,2)}}\right)\right], \tag{20}$$

$$C_8(P) = C_8^{(2)} \mathcal{F}\left(\frac{V_r}{V_r^{(1,2)}}\right), \tag{21}$$

where ξ indicates a percentage of fixed costs due to the fine threading and machining of the corner posts.

6.3 Cost comparison

Let us now compare the costs of the scalable SSI systems, obtained through the cost analysis procedure outlined above, with those of commercial seismic isolators currently available on the market. The analyzed commercial devices are FP systems (single- and double-dish devices), and rubber bearings (RB), with the latter comprising high-damping rubber bearings (HDRB) and lead rubber bearings (LRB). These systems show displacement capacity in the range 100-300 mm and load-carrying capacity in the range 1000-1500 kN. The costs of commercial devices have been obtained by using the dimensions and mechanical properties provided in the catalogs of two internationally renowned manufacturing companies: FIP Industriale srl, and Freyssinet Italia.

Their price was roughly estimated by averaging the unit costs for seismic isolation devices from those of the public works price lists of the Italian regions of Abruzzo, Campania, and Sicily. Labor costs for the installation of the devices are not included in the calculations. As for the SSIs, we have focused on systems with 100 mm $\leq d \leq$ 300 mm and 250 kN $\leq P \leq$ 1500 kN. The costs of these systems have been roughly estimated using the cost-extrapolation procedure described in the previous sections, assuming: $f_{r_d} = F_{r_d}/A_t \approx$ 12 MPa; $\chi = 0.025$ (according to AASHTO, 2000 [52]); and $\xi = 0.40$.

The average costs of commercial RB and FP systems with d = 150 mm and P ranging between 1000 kN and 1500 kN is priced at 1.24 k€ and 2.32 k€, respectively. Those of

FP and RB devices with d = 250 and $P \in$ [1000,1500] kN are 3.04 k€ and 2.69 k€, respectively. SSI1 systems with d = 150 mm, $P \in$ [1000,1500] exhibit an average cost C = 1.49 k€, while analogous systems with d = 250 mm, $P \in$ [1000,1500] kN) show an average cost C = 1.56 k€. Finally, SSI2 systems with d = 150 mm, $P \in$ [1000,1500] kN and d = 250 mm, $P \in$ [1000,1500] kN) respectively exhibit average costs C = 3.37 k€, and C = 3.44 k€.

Cost savings can be obtained by employing low-cost metal 3D printers for the manufacture of the metallic parts of the SSI systems. One observes that the costs of SSI1 and SSI2 devices exhibit a small cost increase with d. A similar trend is exhibited by the FP systems, while the cost of rubber bearings instead shows a significantly high rate of growth with d. The costs of SSI1 and SSI2 systems appreciably increase with P. Such a feature is also exhibited by RB devices, while FP systems conversely feature a slight cost increase with P. SSI1 and SSI2 systems become particularly cost-effective in the case of medium- and small-scale isolation systems. The costs of a SSI1 systems with d = 150 mm, P = 500 kN and d = 250 mm, P = 500 kN amount to 0.64 k€ and 0.72 k€, respectively. Those of SSI2 systems with d = 150 mm, P = 500 kN and d = 250 mm, P = 500 kN are instead respectively equal to 1.50 k€ and 1.56 k€. By further decreasing P down to 250 kN and setting d = 150 mm, one finally obtains C = 0.36 k€ and C = 0.88 k€ for SSI1 and SSI2 systems, respectively.

CHAPTER 8

CONCLUSION AND FUTURE WORK

The work presented in this thesis let us conclude that the analyzed biomimetic isolators help us to forge a novel path to seismic isolation. Such devices with an anthropomorphic character are classified as highly tunable seismic isolators that can be manufactured with customized properties using optimal geometries and sustainable materials easily available around the world. Some key advantages enjoyed by these systems over their current state-of-the-art counterparts are derived from the possibility to tune the displacement capacity acting only on the internal architecture of the unit cell; the uniaxial tension regime of the tendons, up to 40%-55% maximum axial strains, which is suitable for a class of materials much larger than the elastomeric products employed in rubber bearings [53]; and the possibility of creating periodic 'metaisolators'.

In addition, the SSI does not require heavy industry and is easily repaired by replacing the tendons after an extreme seismic event. It is worth noting that the level of preliminary training of the tendons can be employed as a peculiar design variable of the SSI.

We have observed that the reduced slope at the origin of the hysteretic loops of the device indicates a prevalent contribution of the frictional component to the base shear. By adjusting the amplitude of the pre-conditioning of the tendons one can suitably design the extension of this region of reduced reaction force. With such design flexibility the building movement can be facilitated at the onset of the earthquake excitation, preventing the experience of significant levels of acceleration transferred to the structure, while providing higher stiffness for larger displacements.

The design and testing of architectured seismic isolators that feature an independently tunable antiseismic performance against horizontal and vertical ground motions will be addressed in future work, employing, e.g., linkages that mimic the knee articulation of the human leg in the vertical plane. Such a nonconventional performance is highly desirable in the case of high-risk industrial installations and power plants [5].

BIBLIOGRAPHY

[1] Naeim, F., Kelly, J.M., *Design of Seismic Isolated Structures: From Theory to Practice*. Wiley, New York (1999).

[2] Clemente, P., Martelli, A., *Seismically isolated buildings in Italy: state-of-the-art review and applications.* Soil Dyn. Earth. Eng. *119*, 471–487 (2019). https://doi.org/10.1016/j. soildyn.2017.12.029

[3] De Luca, A., Guidi, L.G., *State of the art in the worldwide evolution of base isolation design.* Soil Dyn. Earthq. Eng. (2019). https://doi.org/10.1016/j.soildyn.2019.105722

[4] Morales, E., Filiatrault, A., Aref, A., *Seismic floor isolation using recycled tires for essential buildings in developing countries*. B Earthq. Eng. *16*, 6299–6333 (2018). https:// doi.org/10.1007/s10518-018-0416-7

[5] Najafijozani, M., Becker, T.C., Konstantinidis, D., *Evaluating adaptive vertical seismic isolation for equipment in nuclear power plants*. Nucl. Eng. Des. *358*, 110399(2020). https://doi.org/10.1016/j.nucengdes.2019.110399

[6] Venanzi, I., Ierimonti, L., Materazzi, A.L., *Active base isolation of museum artifacts under seismic excitation.* J. Earthq. Eng. *24*, 506–527 (2020). https://doi.org/10.1080/ 13632469.2018.1453410

[7] Kelly, J.M., *Earthquake-Resistant Design with Rubber*. Springer, London (1993)

[8] Lomiento, G., Bonessio, N., Benzoni, G., *Friction model for sliding bearings under seismic excitation.* J. Earthq. Eng. *17*, 1162–1191 (2013). https://doi.org/10.1080/13632469.2013.814611

[9] Rathje, E.M., Abrahamson, N.A., Bray, J.D., *Simplified frequency content estimates of earthquake ground motions.* J. Geotech. Geoenviron. *124*, 150–158 (1998). https://doi.org/10.1061/(ASCE)1090-0241(1998)124:2(150)

[10] EN 15129. *Anti-seismic devices*. European committee for standardization (2009)

[11] Hamaguchi, H., Aizawa, S., Samejima, Y., Kikuchi, T., Suzuki, S., Yoshizawa, T., *A study of aging effect on a rubber bearing after about twenty years in use.* AIJ J. Technol. Des. *15*(30), 393–398 (2009). https://doi.org/10.3130/aijt.15.393

[12] Liu, W., Ren, Y., He, W., Feng, D., *Aging and creep properties of LRB isolators used in building*. World Inf. Earthq. Eng. *28*(4), 131–136 (2012)

[13] Calabrese, A., Losanno, D., Barjani, A., Spizzuoco, M., Strano, S., *Effects of the long-term aging of glass-fiber reinforced bearings (FRBs) on the seismic response of a baseisolated residential building.* Eng. Struct. (2020). https://doi. org/10.1016/j.engstruct.2020.110735

[14] Higashino, M., Hamaguchi, H.I., Minewaki, S., Aizawa, S., *Basic characteristics and durability of low-friction sliding bearings for base isolation*. J. Earthq. Eng. Seism. *4*, 95–105 (2003)

[15] Nakamura, Y., Okada, K., *Review on seismic isolation and response control methods of buildings in Japan*. Geoenviron Disasters (2019). https://doi.org/10.1186/s40677-019-0123-y

[16] Sierra, I.E.M., Losanno, D., Strano, S., Marulanda, J., Thomson, P., *Development and experimental behavior of HDR seismic isolators for low-rise residential buildings.* Eng. Struct. *183*, 894–906 (2019). https://doi.org/10.1016/j.engstruct.2019.01.037

[17] Spizzuoco, M., Calabrese, A., Serino, G., *Innovative low cost recycled rubber-fiber reinforced isolator: experimental tests and finite element analyses*. Eng. Struct. *76*, 99–111(2014). https://doi.org/10.1016/j.engstruct.2014.07.001

[18] Tsiavos, A., Alexander, N.A., Diambra, A., Ibraim, E., Vardanega, P.J., Gonzalez-Buelga, A., Sextos, A., *A sandrubber deformable granular layer as a low-cost seismic isolation strategy in developing countries: experimental investigation.* Soil Dyn. Earthq. Eng. *125*, 105731 (2019). https://doi.org/10.1016/j.soildyn.2019.105731

[19] Losanno, D., Palumbo, F., Calabrese, A., Barrasso, T., Vaiana, N., *Preliminary investigation of aging effects on recycled rubber fiber reinforced bearings (RR-FRBs).* J. Earthq. Eng. (2021). https://doi.org/10.1080/13632469.2021.1871683

[20] Barthelat, F., *Architectured materials in engineering and biology: fabrication, structure, mechanics and performance.* Int. Mater. Rev. *60*(8), 413–430 (2015). https://doi.org/10.1179/1743280415Y.0000000008

[21] Kadic, M., Milton, G.W., van Hecke, M., Wegener, M., *3D metamaterials*. Nat. Rev. Phys. *1*, 198–210 (2019). https://doi.org/10.1038/s42254-018-0018-y

[22] Rafsanjani, A., Bertoldi, K., Studart, A.R., *Programming soft robots with flexible mechanical metamaterials.* Sci. Robot. *29*, eaav7874 (2019). https://doi.org/10.1126/scirobotics.aav7874

[23] Kotikian, A., McMahan, C., Davidson, E.C., Muhammad, J.M., Weeks, R.D., Daraio, C., Lewis, J.A., *Untethered soft robotic matter with passive control of shape morphing and propulsion.* Sci. Robot. *4*(33), eaax7044 (2019). https://doi.org/10.1126/scirobotics.aax7044

[24] Milton, G.W., *New metamaterials with macroscopic behavior outside that of continuum elastodynamics.* New J. Phys. (2007). https://doi.org/10.1088/1367-2630/9/10/359

[25] Cummer, S.A., Christensen, J., Alu, A., *Controlling sound with acoustic metamaterials.* Nat. Rev. Mater. *1*, 16001(2016). https://doi.org/10.1038/natrevmats.2016.1

[26] Lepidi, M., Bacigalupo, A., *Wave propagation properties of one-dimensional acoustic metamaterials with nonlinear diatomic microstructure.* Nonlinear Dyn. *98*, 2711–2735 (2019). https://doi.org/10.1007/s11071-019-05032-3

[27] Bukhari, M., Barry, O., *Spectro-spatial analyses of a nonlinear metamaterial with multiple nonlinear local resonators.* Nonlinear Dyn. *99*, 1539–1560 (2020). https://doi.org/10.1007/s11071-019-05373-z

[28] Frenzel, T., Kadic, M., Wegener, M., *Three-dimensional mechanical metamaterials with a twist.* Science *358*(6366), 1072–1074 (2017). https://doi.org/10.1126/science.aao4640

[29] Falahati, M., Ahmadvand, P., Safaee, S., Chang, Y.-C., Lyu, Z., Chen, R., Li, L., Lin, Y., *Smart polymers and nanocomposites for 3D and 4D printing.* Mater. Today *40*, 215–245 (2020). https://doi.org/10.1016/j.mattod.2020.06.001

[30] Cruz Sanchez, F.A., Boudaoud, H., Camargo, M., Pearce, J.M., *Plastic recycling in additive manufacturing: A systematic literature review and opportunities for the circular economy.* J Clean. Prod. *264*, 121602 (2020). https://doi.org/10.1016/j.jclepro.2020.121602

[31] Colombi, A., Colquitt, D., Roux, P., Guenneau, S., Craster, R.V., *A seismic metamaterial: the resonant meta wedge.* Sci. Rep. *6*, 27717 (2016). https://doi.org/10.1038/srep27717

[32] Palermo, A., Krödel, S., Marzani, A., Daraio, C., *Engineered metabarrier as shield from seismic surface waves.* Sci. Rep. (2016). https://doi.org/10.1038/srep39356

[33] Du, Q., Zeng, Y., Huang, G., Yang, H., *Elastic metamaterial based seismic shield for both lamb and surface waves*. AIP Adv. *7*, 075015 (2017). https://doi.org/10.1063/1.4996716

[34] Brûlé, S., Ungureanu, B., Achaoui, Y., Diatta, A., Aznavourian, R., Antonakakis, T., Craster, R., Enoch, S., Guenneau, S., *Metamaterial-like transformed urbanism.* Innov. Infrastruct. Solut. *2*(1), 20 (2017)

[35] Brûlé, S., Enoch, S., Guenneau, S., *Emergence of seismic metamaterials: current state and future perspectives.* Phys. Lett. A *384*(1), 1–11 (2020)

[36] Krasnok, A., Vellucci, S., Miniaci, M., Kherraz, N., Croënne, C., Mazzotti, M., Morvaridi, M., Gliozzi, A.S., Onorato, M., Bosia, F., Pugno, N.M., *Hierarchical largescale elastic metamaterials for passive seismic wave mitigation*. EPJ Appl. Metamater. (2021). https://doi.org/10.1051/ epjam/2021009

[37] Fraternali, F., Amendola, A., *Mechanical modeling of innovative metamaterials alternating pentamode lattices and confinement plates*. J. Mech. Phys. Solids *99*, 259–271 (2017). https://doi.org/10.1016/j.jmps.2016.11.010

[38] Clayton, M., Philo, R., *Leonardo Da Vinci: anatomist. Royal Collection Trust (*2012). ISBN 978 1 909741 03 4. (https://www.rct.uk/collection/themes/publications/leonardo-da-vinci-anatomisthttps://www.rct.uk)

[39] Ahlborn, B.K., Blake, R.W., Megill, W.M., *Frequency tuning in animal locomotion*. Zoology *109*, 43–53 (2006). https://doi.org/10.1016/j.zool.2005.11.001

[40] Alexander, R.M., *Mechanics of skeleton and tendons.* In: Prakash Y.S. (ed.) Comprehensive Physiology (2011)

[41] Feng, X., Jing, X., Xu, Z., Guo, Y., *Bio-inspired antivibration with nonlinear inertia coupling.* Mech. Syst. Signal. Pr. *124*, 562–595 (2019). https://doi.org/10.1016/j.ymssp.2019.02.001

[42] Chen, J., Liao, W.H., *Design and control of a magnetorheological actuator for leg exoskeleton.* Proc. IEEE Int.Conf. ROBIO, Sanya, China 1388-1393 (2007). https://ieeexplore.ieee.org/document/4522367https://doi.org/10.1109/ROBIO.2007.4522367

[43] Dorfmann, A., Ogden, R.W., *A pseudo-elastic model for loading, partial unloading and reloading of particle reinforced rubber.* Int. J. Solids Struct. *40*, 2699–2714(2003). https://doi.org/10.1016/S0020-7683(03)00089-1

[44] Dorfmann, A., Ogden, R.W., *A constitutive model for the Mullins effect with permanent set in particle-reinforced rubber.* Int. J. Solids Struct. *42*, 2699–2714 (2003). https://doi.org/10.1016/j.ijsolstr.2003.11.014

[45] Qi, H.J., Boyce, M.C., *Stress-strain behavior of thermoplastic polyurethanes.* Mech. Mater. *37*(8), 817–839 (2005). https://doi.org/10.1016/j.mechmat.2004.08.001

[46] Chen, H., Trivedi, A.R., Siviour, C.R., *Application of linear viscoelastic continuum damage theory to the low and high strain rate response of thermoplastic polyurethane.* Exp. Mech. *60*(7), 925–936 (2020)

[47] Mohotti, D., Ali, M., Ngo, T., Lu, J., Mendis, P., *Strain rate dependent constitutive model for predicting the material behaviour of polyurea under high strain rate tensile loading.* Mater. Des. *53*, 830–837 (2014). https://doi.org/10.1016/j.matdes.2013.07.020

[48] Eurocode 8: *Design of structures for earthquake resistance EN1998-2*. European Committee for Standardization, Bruxelles, Belgium (2005)

[49] Beer, F.P., Johnston, E.R., DeWolf, J.T., Mazurek, D.F., *Mechanics of Materials,* 9th edn. McGraw-Hill, New York (2020)
[50] Cardone, D., Gesualdi, G., Brancato, P., *Restoring capability of friction pendulum seismic isolation systems.* Bull. Earthq. Eng. *13*, 2449–2480 (2015). https://doi.org/10.1007/s10518-014-9719-5
[51] CBSC: California Building Code. California Buildings Standards Commission, Sacramento (2001)
[52] AASHTO: Guide Specifications for Seismic Isolation Design. American Association of State Highways and Transportation Officials, Washington (2000)
[53] Nishi, T., Suzuki, S., Aoki, M., Sawada, T., Fukuda, S.: International investigation of shear displacement capacity of various elastomeric seismic-protection isolators for buildings. J. Rubber Res. *22*, 33–41 (2019). https://doi.org/10.1007/s42464-019-00006
[54] Carpenterie Metalliche Morinelli s.r.l. http://www.morinellicarpenterie.com
[55] FIP MEC s.r.l. https://www.fipmec.it
[56] EN 1337-2.Structural bearings - Part 2: Sliding elements. European Committee for Standardization (2003).
[57] Fillamentum Extrafill PLA filament. https://fillamentum.com
[58] Sunlu TPU flexible filament. https://www.sunlu.com
[59] Acciai e Metalli. https://acciaiemetalli.it.
[60] Kircher, C.A., *Seismically isolated structures.* in FEMA P-751, NEHRP Recommended Provisions Design Examples: Chapter 12, 12-17 (2012).
[61] Iqbal, A., Soft first story with seismic isolation system, Proceedings 2006 NZSEE Conference 363 (2006).
[62] X. Feng, X. Jing, Z. Xu, Y. Guo, *Bio-inspired anti-vibration with nonlinear inertia coupling.* Mech. Syst. Signal. Pr. 124, 562-595 (2019). doi:10.1016/j.ymssp.2019.02.001.
[63] Dorfmann, A., and R. W. Ogden., *A pseudo-elastic model for loading, partial unloading and reloading of particle-reinforced rubber.* Int. J. Solids Struct 40, no. 11 (2003): 2699-2714.
[64] Dorfmann, A., and Ray W. Ogden., A constitutive model for the Mullins effect with permanent set in particle-reinforced rubber. Int. J. Solids Struct 41, no. 7 (2004): 1855-1878.
[65] Saedniya, M., Talaeitaba, S. B., *Numerical modeling of elastomeric seismic isolators for determining force-displacement curve from cyclic loading. Int. J. Adv. Struct. Eng.* **11**, 361-376 (2019). doi:10.1007/s40091-019-00238-6

[66] Fraternali, F., Singh, N., Amendola, A., Benzoni, G., & Milton, G. W. (2021a). *A biomimetic sliding–stretching approach to seismic isolation.* Nonlinear Dynamics, **106**(4), 3147-3159.
[67] Fraternali, F., Singh, N., Amendola, A., Benzoni, G., & Milton, G. W. (2021b). *The 3D print job that keeps quake damage at bay.* Nature **600**(7887), 10.
[68] Fraternali, F. (2021c). *Kinematics of 3D printed anti earthquake system that mimics human bones.* Mathematica© notebook, Wolfram Community, Accessed at <https://community.wolfram.com/groups/-/m/t/2415323>.
[69] Beer, F. P., Johnston, E. R., DeWolf, J. T., & Mazurek, D. F. (1992). *Mechanics of materials.* In SI Units, McGraw-Hill, UK, App.

APPENDICES

APPENDIX A

MATHEMATICA® CODE FOR THE ANALYTIC FORMULATION OF THE KINEMATICS OF THE SSI

Appendix A: *Mathematica*® code for the analytic formulation of the kinematics of the SSI

Analytic form of the kinematics for arbitrary rest configuration

Notation
n[i] =nundef[i]=nbeta[i]=nundefbeta[i] denote the undeformed node coordinates
ndef[i] = ndefbeta[i] denote the deformed node coordinates
v denotes the lateral displacement of the SSI (denoted u in the main Article and the Methods section)

General data

In[1]:=
```
Clear[adata, vdata]
adata = {};
vdata = {vact → v, anglealpha → (alphav)};
cdata = {C[1] → 0, C[2] → 0};
kloadata = {Cos[anglealpha], Sin[anglealpha], 0} /. vdata
```

Out[5]=
```
{Cos[alphav], Sin[alphav], 0}
```

Undeformed node coordinates

In[6]:=
```
nnodes = 9;
```

In[7]:=
```
n[1] = {a2 + a1 * Sin[beta], a1 * Cos[beta], 0} /. adata;
n[2] = {a2, 0, 0} /. adata;
n[3] = {a1 * Cos[beta], -a2 - a1 * Sin[beta], 0} /. adata;

n[4] = {0, a2, 0} /. adata;
n[5] = {0, 0, 0} /. adata;
n[6] = {0, -a2, 0} /. adata;

n[7] = {-a1 * Cos[beta], a2 + a1 * Sin[beta], 0} /. adata;
n[8] = {-a2, 0, 0} /. adata;
n[9] = {-a2 - a1 * Sin[beta], -a1 * Cos[beta], 0} /. adata;
```

In[16]:=
```
Do[nundef[i] = n[i], {i, 1, nnodes}];
```

In[17]:=
```
a89 = a1 /. adata;
a58 = a2 /. adata;
a63 = a1 /. adata;
a56 = a2 /. adata;
a12 = a1 /. adata;
a52 = a2 /. adata;
a54 = a2 /. adata;
a74 = a1 /. adata;
```

In[25]:=
```
Do[nbeta[i] = n[i]; nundefbeta[i] = nbeta[i], {i, 1, nnodes}];
```

Solve the analytic form of the unit-cell kinematics (see Methods) for a1, a2 angles (a1=alpha1, a2=alpha2 with the notation of Fig. S2 A)

In[26]:=
```
n8xdefa = (n[9][[1]] + a89 * Sin[anglea1]) /. vdata;
n8xdefb = ((n[5][[1]] + vact * Cos[anglealpha]) - a58 * Cos[anglea2]) /. vdata;
n8ydefa = (n[9][[2]] + a89 * Cos[anglea1]) /. vdata;
n8ydefb = ((n[5][[2]] + vact * Sin[anglealpha]) - a58 * Sin[anglea2]) /. vdata;
eq8x = n8xdefa == n8xdefb;
eq8y = n8ydefa == n8ydefb;
angleasol = Solve[{eq8x, eq8y}, {anglea1, anglea2}] /. cdata // Simplify;
isol = 1;
angleasol[[isol]]
n8xdefa /. angleasol;
n8xdefb /. angleasol;
n8ydefa /. angleasol;
n8ydefb /. angleasol;
n[8];
```

Out[34]=
$$\{\text{anglea1} \to \text{ArcTan}\Big[\Big(2\,a1^2\,a2\,v\,\text{Cos}[\text{alphav}-\text{beta}]+2\,a1^4\,\text{Cos}[\text{beta}]+2\,a1^2\,v^2\,\text{Cos}[\text{beta}]-a1^2\,v^2\,\text{Cos}[2\,\text{alphav}+\text{beta}]+3\,a1^3\,v\,\text{Sin}[\text{alphav}]+a1\,v^3\,\text{Sin}[\text{alphav}]+a1\,a2\,v^2\,\text{Sin}[2\,\text{alphav}]+a1^3\,a2\,\text{Sin}[2\,\text{beta}]-\sqrt{\left(a1^2\,(a2+v\,\text{Cos}[\text{alphav}]+a1\,\text{Sin}[\text{beta}])^2\left(2\,a1^2\,a2^2-2\,a1^2\,v^2-2\,a2^2\,v^2-v^4-4\,a2\,v\left(a1^2+v^2\right)\text{Cos}[\text{alphav}]-2\,a2^2\,v^2\,\text{Cos}[2\,\text{alphav}]+2\,a1^2\,a2^2\,\text{Cos}[2\,\text{beta}]+2\,a1^2\,v^2\,\text{Cos}[2\,(\text{alphav}+\text{beta})]+4\,a1^2\,a2\,v\,\text{Cos}[\text{alphav}+2\,\text{beta}]+4\,a1\,a2^2\,v\,\text{Sin}[\text{alphav}-\text{beta}]-8\,a1\,a2\,v^2\,\text{Sin}[\text{beta}]-4\,a1\,a2^2\,v\,\text{Sin}[\text{alphav}+\text{beta}]-4\,a1\,v^3\,\text{Sin}[\text{alphav}+\text{beta}]-4\,a1\,a2\,v^2\,\text{Sin}[2\,\text{alphav}+\text{beta}]\right)\right)}+a1^3\,v\,\text{Sin}[\text{alphav}+2\,\text{beta}]\Big)\Big/\Big(a1^2\left(a1^2+a2^2+v^2+2\,a2\,v\,\text{Cos}[\text{alphav}]+2\,a1\,a2\,\text{Sin}[\text{beta}]+2\,a1\,v\,\text{Sin}[\text{alphav}+\text{beta}]\right)\Big),$$
$$\Big(2\,a1^5+8\,a1^3\,a2^2+5\,a1^3\,v^2+6\,a1\,a2^2\,v^2+a1\,v^4+a1\,a2\,v\left(18\,a1^2+4\,a2^2+7\,v^2\right)\text{Cos}[\text{alphav}]+a1\,v^2\left(4\,a1^2+4\,a2^2+v^2\right)\text{Cos}[2\,\text{alphav}]+a1\,a2\,v^3\,\text{Cos}[3\,\text{alphav}]-3\,a1^3\,a2\,v\,\text{Cos}[\text{alphav}-2\,\text{beta}]-2\,a1^5\,\text{Cos}[2\,\text{beta}]-4\,a1^3\,a2^2\,\text{Cos}[2\,\text{beta}]-3\,a1^3\,v^2\,\text{Cos}[2\,\text{beta}]-2\,a1^3\,v^2\,\text{Cos}[2\,(\text{alphav}+\text{beta})]-7\,a1^3\,a2\,v\,\text{Cos}[\text{alphav}+2\,\text{beta}]-5\,a1^4\,v\,\text{Sin}[\text{alphav}-\text{beta}]-8\,a1^2\,a2^2\,v\,\text{Sin}[\text{alphav}-\text{beta}]-3\,a1^2\,v^3\,\text{Sin}[\text{alphav}-\text{beta}]-3\,a1^2\,a2\,v^2\,\text{Sin}[2\,\text{alphav}-\text{beta}]+11\,a1^4\,a2\,\text{Sin}[\text{beta}]+4\,a1^2\,a2^3\,\text{Sin}[\text{beta}]+14\,a1^2\,a2\,v^2\,\text{Sin}[\text{beta}]-a1^4\,a2\,\text{Sin}[3\,\text{beta}]+6\,a1^4\,v\,\text{Sin}[\text{alphav}+\text{beta}]+12\,a1^2\,a2^2\,v\,\text{Sin}[\text{alphav}+\text{beta}]+4\,a1^2\,v^3\,\text{Sin}[\text{alphav}+\text{beta}]+7\,a1^2\,a2\,v^2\,\text{Sin}[2\,\text{alphav}+\text{beta}]+2\,a1\,\text{Cos}[\text{beta}]\sqrt{\left(a1^2\,(a2+v\,\text{Cos}[\text{alphav}]+a1\,\text{Sin}[\text{beta}])^2\left(2\,a1^2\,a2^2-2\,a1^2\,v^2-2\,a2^2\,v^2-v^4-4\,a2\,v\left(a1^2+v^2\right)\text{Cos}[\text{alphav}]-2\,a2^2\,v^2\,\text{Cos}[2\,\text{alphav}]+2\,a1^2\,a2^2\,\text{Cos}[2\,\text{beta}]+2\,a1^2\,v^2\,\text{Cos}[2\,(\text{alphav}+\text{beta})]+4\,a1^2\,a2\,v\,\text{Cos}[\text{alphav}+2\,\text{beta}]+4\,a1\,a2^2\,v\,\text{Sin}[\text{alphav}-\text{beta}]-8\,a1\,a2\,v^2\,\text{Sin}[\text{beta}]-4\,a1\,a2^2\,v\,\text{Sin}[\text{alphav}+\text{beta}]-4\,a1\,v^3\,\text{Sin}[\text{alphav}+\text{beta}]-4\,a1\,a2\,v^2\,\text{Sin}[2\,\text{alphav}+\text{beta}]\right)\right)}+2\,v\,\text{Sin}[\text{alphav}]\sqrt{\left(-a1^2\,(a2+v\,\text{Cos}[\text{alphav}]+a1\,\text{Sin}[\text{beta}])^2\left(-2\,a1^2\,a2^2+2\,a1^2\,v^2+2\,a2^2\,v^2+v^4+4\,a2\,v\left(a1^2+v^2\right)\text{Cos}[\text{alphav}]+2\,a2^2\,v^2\,\text{Cos}[2\,\text{alphav}]-2\,a1^2\,a2^2\,\text{Cos}[2\,\text{beta}]-2\,a1^2\,v^2\,\text{Cos}[2\,(\text{alphav}+\text{beta})]-4\,a1^2\,a2\,v\,\text{Cos}[\text{alphav}+2\,\text{beta}]+4\,a1\,a2^2\,v\,\text{Sin}[\text{alphav}-\text{beta}]+8\,a1\,a2\,v^2\,\text{Sin}[\text{beta}]+4\,a1\,a2^2\,v\,\text{Sin}[\text{alphav}+\text{beta}]+4\,a1\,v^3\,\text{Sin}[\text{alphav}+\text{beta}]+4\,a1\,a2\,v^2\,\text{Sin}[2\,\text{alphav}+\text{beta}]\right)\right)}+a1^2\,v^3\,\text{Sin}[3\,\text{alphav}+\text{beta}]-a1^4\,v\,\text{Sin}[\text{alphav}+3\,\text{beta}]\Big)\Big/\Big(2\,a1^2\,(a2+v\,\text{Cos}[\text{alphav}]+a1\,\text{Sin}[\text{beta}])\left(a1^2+a2^2+v^2+2\,a2\,v\,\text{Cos}[\text{alphav}]+2\,a1\,a2\,\text{Sin}[\text{beta}]+2\,a1\,v\,\text{Sin}[\text{alphav}+\text{beta}]\right)\Big)\Big],$$
$$\text{anglea2} \to \text{ArcTan}\Big[\Big(6\,a1^3\,a2^2+4\,a1\,a2^4+3\,a1^3\,v^2+8\,a1\,a2^2\,v^2+a1\,v^4+a1\,a2\,v\left(10\,a1^2+12\,a2^2+7\,v^2\right)\text{Cos}[\text{alphav}]+a1\,v^2\left(2\,a1^2+6\,a2^2+v^2\right)\text{Cos}[2\,\text{alphav}]+a1\,a2\,v^3\,\text{Cos}[3\,\text{alphav}]-3\,a1^3\,a2\,v\,\text{Cos}[\text{alphav}-2\,\text{beta}]-6\,a1^3\,a2^2\,\text{Cos}[2\,\text{beta}]-3\,a1^3\,v^2\,\text{Cos}[2\,\text{beta}]-2\,a1^3\,v^2\,\text{Cos}[2\,(\text{alphav}+\text{beta})]-7\,a1^3\,a2\,v\,\text{Cos}[\text{alphav}+2\,\text{beta}]-a1^4\,v\,\text{Sin}[\text{alphav}-\text{beta}]-12\,a1^2\,a2^2\,v\,\text{Sin}[\text{alphav}-\text{beta}]-3\,a1^2\,v^3\,\text{Sin}[\text{alphav}-\text{beta}]-3\,a1^2\,a2\,v^2\,\text{Sin}[2\,\text{alphav}-\text{beta}]+3\,a1^4\,a2\,\text{Sin}[\text{beta}]+12\,a1^2\,a2^3\,\text{Sin}[\text{beta}]+14\,a1^2\,a2\,v^2\,\text{Sin}[\text{beta}]-a1^4\,a2\,\text{Sin}[3\,\text{beta}]+2\,a1^4\,v\,\text{Sin}[\text{alphav}+\text{beta}]+16\,a1^2\,a2^2\,v\,\text{Sin}[\text{alphav}+\text{beta}]+4\,a1^2\,v^3\,\text{Sin}[\text{alphav}+\text{beta}]+7\,a1^2\,a2\,v^2\,\text{Sin}[2\,\text{alphav}+\text{beta}]-2\,a1\,\text{Cos}[\text{beta}]\sqrt{\left(a1^2\,(a2+v\,\text{Cos}[\text{alphav}]+a1\,\text{Sin}[\text{beta}])^2\left(2\,a1^2\,a2^2-2\,a1^2\,v^2-2\,a2^2\,v^2-v^4-4\,a2\,v\left(a1^2+v^2\right)\text{Cos}[\text{alphav}]-2\,a2^2\,v^2\,\text{Cos}[2\,\text{alphav}]+2\,a1^2\,a2^2\,\text{Cos}[2\,\text{beta}]+2\,a1^2\,v^2\,\text{Cos}[2\,(\text{alphav}+\text{beta})]+4\,a1^2\,a2\,v\,\text{Cos}[\text{alphav}+2\,\text{beta}]+4\,a1\,a2^2\,v\,\text{Sin}[\text{alphav}-\text{beta}]-8\,a1\,a2\,v^2\,\text{Sin}[\text{beta}]-4\,a1\,a2^2\,v\,\text{Sin}[\text{alphav}+\text{beta}]-4\,a1\,v^3\,\text{Sin}[\text{alphav}+\text{beta}]-4\,a1\,a2\,v^2\,\text{Sin}[2\,\text{alphav}+\text{beta}]\right)\right)}-2\,v\,\text{Sin}[\text{alphav}]\sqrt{\left(-a1^2\,(a2+v\,\text{Cos}[\text{alphav}]+a1\,\text{Sin}[\text{beta}])^2\left(-2\,a1^2\,a2^2+2\,a1^2\,v^2+2\,a2^2\,v^2+v^4+4\,a2\,v\left(a1^2+v^2\right)\text{Cos}[\text{alphav}]+2\,a2^2\,v^2\,\text{Cos}[2\,\text{alphav}]-2\,a1^2\,a2^2\,\text{Cos}[2\,\text{beta}]-2\,a1^2\,v^2\,\text{Cos}[2\,(\text{alphav}+\text{beta})]-4\,a1^2\,a2\,v\,\text{Cos}[\text{alphav}+2\,\text{beta}]+4\,a1\,a2^2\,v\,\text{Sin}[\text{alphav}-\text{beta}]+8\,a1\,a2\,v^2\,\text{Sin}[\text{beta}]+4\,a1\,a2^2\,v\,\text{Sin}[\text{alphav}+\text{beta}]+4\,a1\,v^3\,\text{Sin}[\text{alphav}+\text{beta}]+4\,a1\,a2\,v^2\,\text{Sin}[2\,\text{alphav}+\text{beta}]\right)\right)}+a1^2\,v^3\,\text{Sin}[3\,\text{alphav}+\text{beta}]-a1^4\,v\,\text{Sin}[\text{alphav}+3\,\text{beta}]\Big)\Big/\Big(2\,a1\,a2\,(a2+v\,\text{Cos}[\text{alphav}]+a1\,\text{Sin}[\text{beta}])\left(a1^2+a2^2+v^2+2\,a2\,v\,\text{Cos}[\text{alphav}]+2\,a1\,a2\,\text{Sin}[\text{beta}]+2\,a1\,v\,\text{Sin}[\text{alphav}+\text{beta}]\right)\Big)\Big],$$
$$\Big(2\,a1^2\,a2\,v\,\text{Cos}[\text{alphav}-\text{beta}]+2\,a1^2\left(a2^2+v^2\right)\text{Cos}[\text{beta}]-a1^2\,v^2\,\text{Cos}[2\,\text{alphav}+\text{beta}]+a1^3\,v\,\text{Sin}[\text{alphav}]+2\,a1\,a2^2\,v\,\text{Sin}[\text{alphav}]+a1\,v^3\,\text{Sin}[\text{alphav}]+a1\,a2\,v^2\,\text{Sin}[2\,\text{alphav}]+a1^3\,a2\,\text{Sin}[2\,\text{beta}]+\sqrt{\left(a1^2\,(a2+v\,\text{Cos}[\text{alphav}]+a1\,\text{Sin}[\text{beta}])^2\left(2\,a1^2\,a2^2-2\,a1^2\,v^2-2\,a2^2\,v^2-v^4-4\,a2\,v\left(a1^2+v^2\right)\text{Cos}[\text{alphav}]-2\,a2^2\,v^2\,\text{Cos}[2\,\text{alphav}]+2\,a1^2\,a2^2\,\text{Cos}[2\,\text{beta}]+2\,a1^2\,v^2\,\text{Cos}[2\,(\text{alphav}+\text{beta})]+4\,a1^2\,a2\,v\,\text{Cos}[\text{alphav}+2\,\text{beta}]+4\,a1\,a2^2\,v\,\text{Sin}[\text{alphav}-\text{beta}]-8\,a1\,a2\,v^2\,\text{Sin}[\text{beta}]-4\,a1\,a2^2\,v\,\text{Sin}[\text{alphav}+\text{beta}]-4\,a1\,v^3\,\text{Sin}[\text{alphav}+\text{beta}]-4\,a1\,a2\,v^2\,\text{Sin}[2\,\text{alphav}+\text{beta}]\right)\right)}+a1^3\,v\,\text{Sin}[\text{alphav}+2\,\text{beta}]\Big)\Big/\Big(a1\,a2\left(a1^2+a2^2+v^2+2\,a2\,v\,\text{Cos}[\text{alphav}]+2\,a1\,a2\,\text{Sin}[\text{beta}]+2\,a1\,v\,\text{Sin}[\text{alphav}+\text{beta}]\right)\Big)\Big]\}$$

Solve the analytic form of the unit-cell kinematics for b1, b2 angles (b1=beta1, b2=beta2 with the notation of Fig. S2, A)

In[40]:=
```
n6xdefa = (n[3][[1]] - a63 * Cos[angleb1]) /. vdata;
n6xdefb = ((n[5][[1]] + vact * Cos[anglealpha]) - a56 * Sin[angleb2]) /. vdata;
n6ydefa = (n[3][[2]] + a63 * Sin[angleb1]) /. vdata;
n6ydefb = ((n[5][[2]] + vact * Sin[anglealpha]) - a56 * Cos[angleb2]) /. vdata;
eq6x = n6xdefa == n6xdefb;
eq6y = n6ydefa == n6ydefb;
anglebsol = Solve[{eq6x, eq6y}, {angleb1, angleb2}] /. cdata // Simplify;
isol = 1;
anglebsol[[isol]]
n6xdefa /. anglebsol;
n6xdefb /. anglebsol;
n6ydefa /. anglebsol;
n6ydefb /. anglebsol;
n[6];
```

Out[48]=
$$\{\text{angleb1} \to \text{ArcTan}\left[-\left(\left(a1\, v\left(3\, a1^2+v^2\right)\text{Cos}[\text{alphav}]-2\, a1^2\left(a1^2+v^2\right)\text{Cos}[\text{beta}]-a1^2\, v^2\,\text{Cos}[2\,\text{alphav}+\text{beta}]+a1^3\, v\,\text{Cos}[\text{alphav}+2\,\text{beta}]+a1\, a2\, v^2\,\text{Sin}[2\,\text{alphav}]-2\, a1^2\, a2\, v\,\text{Sin}[\text{alphav}-\text{beta}]-a1^3\, a2\,\text{Sin}[2\,\text{beta}]+\sqrt{\left(-a1^2\left(a2+v\,\text{Sin}[\text{alphav}]+a1\,\text{Sin}[\text{beta}]\right)^2\left(-2\, a1^2\, a2^2+2\, a1^2\, v^2+2\, a2^2\, v^2+v^4-2\, a2^2\, v^2\,\text{Cos}[2\,\text{alphav}]+4\, a1\, a2^2\, v\,\text{Cos}[\text{alphav}-\text{beta}]-2\, a1^2\, a2^2\,\text{Cos}[2\,\text{beta}]-4\, a1\, a2^2\, v\,\text{Cos}[\text{alphav}+\text{beta}]-4\, a1\, v^3\,\text{Cos}[\text{alphav}+\text{beta}]+2\, a1^2\, v^2\,\text{Cos}[2\left(\text{alphav}+\text{beta}\right)]+4\, a1^2\, a2\, v\,\text{Sin}[\text{alphav}]+4\, a2\, v^3\,\text{Sin}[\text{alphav}]+8\, a1\, a2\, v^2\,\text{Sin}[\text{beta}]-4\, a1\, a2\, v^2\,\text{Sin}[2\,\text{alphav}+\text{beta}]-4\, a1^2\, a2\, v\,\text{Sin}[\text{alphav}+2\,\text{beta}]\right)\right)}\right)\Big/\left(a1^2\left(a1^2+a2^2+v^2-2\, a1\, v\,\text{Cos}[\text{alphav}+\text{beta}]+2\, a2\, v\,\text{Sin}[\text{alphav}]+2\, a1\, a2\,\text{Sin}[\text{beta}]\right)\right)\right)\right],$$
$$\left(2\, a1^5+8\, a1^3\, a2^2+5\, a1^3\, v^2+6\, a1\, a2^2\, v^2+a1\, v^4-a1\, v^2\left(4\, a1^2+4\, a2^2+v^2\right)\text{Cos}[2\,\text{alphav}]+a1^2\, v\left(5\, a1^2+8\, a2^2+3\, v^2\right)\text{Cos}[\text{alphav}-\text{beta}]-2\, a1^5\,\text{Cos}[2\,\text{beta}]-4\, a1^3\, a2^2\,\text{Cos}[2\,\text{beta}]-3\, a1^3\, v^2\,\text{Cos}[2\,\text{beta}]-6\, a1^4\, v\,\text{Cos}[\text{alphav}+\text{beta}]-12\, a1^2\, a2^2\, v\,\text{Cos}[\text{alphav}+\text{beta}]-4\, a1^2\, v^3\,\text{Cos}[\text{alphav}+\text{beta}]+2\, a1^3\, v^2\,\text{Cos}[2\left(\text{alphav}+\text{beta}\right)]+a1^2\, v^3\,\text{Cos}[3\,\text{alphav}+\text{beta}]+a1^4\, v\,\text{Cos}[\text{alphav}+3\,\text{beta}]+18\, a1^3\, a2\, v\,\text{Sin}[\text{alphav}]+4\, a1\, a2^3\, v\,\text{Sin}[\text{alphav}]+7\, a1\, a2\, v^3\,\text{Sin}[\text{alphav}]-a1\, a2\, v^3\,\text{Sin}[3\,\text{alphav}]-3\, a1^3\, a2\, v\,\text{Sin}[\text{alphav}-2\,\text{beta}]+3\, a1^2\, a2\, v^2\,\text{Sin}[2\,\text{alphav}-\text{beta}]+11\, a1^4\, a2\,\text{Sin}[\text{beta}]+4\, a1^2\, a2^3\,\text{Sin}[\text{beta}]+14\, a1^2\, a2\, v^2\,\text{Sin}[\text{beta}]-a1^4\, a2\,\text{Sin}[3\,\text{beta}]-7\, a1^2\, a2\, v^2\,\text{Sin}[2\,\text{alphav}+\text{beta}]-7\, a1^3\, a2\, v\,\text{Sin}[\text{alphav}+2\,\text{beta}]-2\, v\,\text{Cos}[\text{alphav}]\sqrt{\left(-a1^2\left(a2+v\,\text{Sin}[\text{alphav}]+a1\,\text{Sin}[\text{beta}]\right)^2\left(-2\, a1^2\, a2^2+2\, a1^2\, v^2+2\, a2^2\, v^2+v^4-2\, a2^2\, v^2\,\text{Cos}[2\,\text{alphav}]+4\, a1\, a2^2\, v\,\text{Cos}[\text{alphav}-\text{beta}]-2\, a1^2\, a2^2\,\text{Cos}[2\,\text{beta}]-4\, a1\, a2^2\, v\,\text{Cos}[\text{alphav}+\text{beta}]-4\, a1\, v^3\,\text{Cos}[\text{alphav}+\text{beta}]+2\, a1^2\, v^2\,\text{Cos}[2\left(\text{alphav}+\text{beta}\right)]+4\, a1^2\, a2\, v\,\text{Sin}[\text{alphav}]+4\, a2\, v^3\,\text{Sin}[\text{alphav}]+8\, a1\, a2\, v^2\,\text{Sin}[\text{beta}]-4\, a1\, a2\, v^2\,\text{Sin}[2\,\text{alphav}+\text{beta}]-4\, a1^2\, a2\, v\,\text{Sin}[\text{alphav}+2\,\text{beta}]\right)\right)}+2\, a1\,\text{Cos}[\text{beta}]\sqrt{\left(a1^2\left(a2+v\,\text{Sin}[\text{alphav}]+a1\,\text{Sin}[\text{beta}]\right)^2\left(2\, a1^2\, a2^2-2\, a1^2\, v^2-2\, a2^2\, v^2-v^4+2\, a2^2\, v^2\,\text{Cos}[2\,\text{alphav}]-4\, a1\, a2^2\, v\,\text{Cos}[\text{alphav}-\text{beta}]+2\, a1^2\, a2^2\,\text{Cos}[2\,\text{beta}]+4\, a1\, a2^2\, v\,\text{Cos}[\text{alphav}+\text{beta}]+4\, a1\, v^3\,\text{Cos}[\text{alphav}+\text{beta}]-2\, a1^2\, v^2\,\text{Cos}[2\left(\text{alphav}+\text{beta}\right)]-4\, a1^2\, a2\, v\,\text{Sin}[\text{alphav}]-4\, a2\, v^3\,\text{Sin}[\text{alphav}]-8\, a1\, a2\, v^2\,\text{Sin}[\text{beta}]+4\, a1\, a2\, v^2\,\text{Sin}[2\,\text{alphav}+\text{beta}]+4\, a1^2\, a2\, v\,\text{Sin}[\text{alphav}+2\,\text{beta}]\right)\right)}\Big/\left(2\, a1^2\left(a2+v\,\text{Sin}[\text{alphav}]+a1\,\text{Sin}[\text{beta}]\right)\left(a1^2+a2^2+v^2-2\, a1\, v\,\text{Cos}[\text{alphav}+\text{beta}]+2\, a2\, v\,\text{Sin}[\text{alphav}]+2\, a1\, a2\,\text{Sin}[\text{beta}]\right)\right)\right],$$
$$\text{angleb2} \to \text{ArcTan}\left[\left(6\, a1^3\, a2^2+4\, a1\, a2^4+3\, a1^3\, v^2+8\, a1\, a2^2\, v^2+a1\, v^4-a1\, v^2\left(2\, a1^2+6\, a2^2+v^2\right)\text{Cos}[2\,\text{alphav}]+a1^2\, v\left(a1^2+12\, a2^2+3\, v^2\right)\text{Cos}[\text{alphav}-\text{beta}]-6\, a1^3\, a2^2\,\text{Cos}[2\,\text{beta}]-3\, a1^3\, v^2\,\text{Cos}[2\,\text{beta}]-2\, a1^4\, v\,\text{Cos}[\text{alphav}+\text{beta}]-16\, a1^2\, a2^2\, v\,\text{Cos}[\text{alphav}+\text{beta}]-4\, a1^2\, v^3\,\text{Cos}[\text{alphav}+\text{beta}]+2\, a1^3\, v^2\,\text{Cos}[2\left(\text{alphav}+\text{beta}\right)]+a1^2\, v^3\,\text{Cos}[3\,\text{alphav}+\text{beta}]+a1^4\, v\,\text{Cos}[\text{alphav}+3\,\text{beta}]+10\, a1^3\, a2\, v\,\text{Sin}[\text{alphav}]+12\, a1\, a2^3\, v\,\text{Sin}[\text{alphav}]+7\, a1\, a2\, v^3\,\text{Sin}[\text{alphav}]-a1\, a2\, v^3\,\text{Sin}[3\,\text{alphav}]-3\, a1^3\, a2\, v\,\text{Sin}[\text{alphav}-2\,\text{beta}]+3\, a1^2\, a2\, v^2\,\text{Sin}[2\,\text{alphav}-\text{beta}]+3\, a1^4\, a2\,\text{Sin}[\text{beta}]+12\, a1^2\, a2^3\,\text{Sin}[\text{beta}]+14\, a1^2\, a2\, v^2\,\text{Sin}[\text{beta}]-a1^4\, a2\,\text{Sin}[3\,\text{beta}]-7\, a1^2\, a2\, v^2\,\text{Sin}[2\,\text{alphav}+\text{beta}]-7\, a1^3\, a2\, v\,\text{Sin}[\text{alphav}+2\,\text{beta}]+2\, v\,\text{Cos}[\text{alphav}]\sqrt{\left(-a1^2\left(a2+v\,\text{Sin}[\text{alphav}]+a1\,\text{Sin}[\text{beta}]\right)^2\left(-2\, a1^2\, a2^2+2\, a1^2\, v^2+2\, a2^2\, v^2+v^4-2\, a2^2\, v^2\,\text{Cos}[2\,\text{alphav}]+4\, a1\, a2^2\, v\,\text{Cos}[\text{alphav}-\text{beta}]-2\, a1^2\, a2^2\,\text{Cos}[2\,\text{beta}]-4\, a1\, a2^2\, v\,\text{Cos}[\text{alphav}+\text{beta}]-4\, a1\, v^3\,\text{Cos}[\text{alphav}+\text{beta}]+2\, a1^2\, v^2\,\text{Cos}[2\left(\text{alphav}+\text{beta}\right)]+4\, a1^2\, a2\, v\,\text{Sin}[\text{alphav}]+4\, a2\, v^3\,\text{Sin}[\text{alphav}]+8\, a1\, a2\, v^2\,\text{Sin}[\text{beta}]-4\, a1\, a2\, v^2\,\text{Sin}[2\,\text{alphav}+\text{beta}]-4\, a1^2\, a2\, v\,\text{Sin}[\text{alphav}+2\,\text{beta}]\right)\right)}-2\, a1\,\text{Cos}[\text{beta}]\sqrt{\left(a1^2\left(a2+v\,\text{Sin}[\text{alphav}]+a1\,\text{Sin}[\text{beta}]\right)^2\left(2\, a1^2\, a2^2-2\, a1^2\, v^2-2\, a2^2\, v^2-v^4+2\, a2^2\, v^2\,\text{Cos}[2\,\text{alphav}]-4\, a1\, a2^2\, v\,\text{Cos}[\text{alphav}-\text{beta}]+2\, a1^2\, a2^2\,\text{Cos}[2\,\text{beta}]+4\, a1\, a2^2\, v\,\text{Cos}[\text{alphav}+\text{beta}]+4\, a1\, v^3\,\text{Cos}[\text{alphav}+\text{beta}]-2\, a1^2\, v^2\,\text{Cos}[2\left(\text{alphav}+\text{beta}\right)]-4\, a1^2\, a2\, v\,\text{Sin}[\text{alphav}]-4\, a2\, v^3\,\text{Sin}[\text{alphav}]-8\, a1\, a2\, v^2\,\text{Sin}[\text{beta}]+4\, a1\, a2\, v^2\,\text{Sin}[2\,\text{alphav}+\text{beta}]+4\, a1^2\, a2\, v\,\text{Sin}[\text{alphav}+2\,\text{beta}]\right)\right)}\Big/\left(2\, a1\, a2\left(a2+v\,\text{Sin}[\text{alphav}]+a1\,\text{Sin}[\text{beta}]\right)\left(a1^2+a2^2+v^2-2\, a1\, v\,\text{Cos}[\text{alphav}+\text{beta}]+2\, a2\, v\,\text{Sin}[\text{alphav}]+2\, a1\, a2\,\text{Sin}[\text{beta}]\right)\right),$$
$$-\left(\left(-a1\, v\left(a1^2+2\, a2^2+v^2\right)\text{Cos}[\text{alphav}]+2\, a1^2\left(a2^2+v^2\right)\text{Cos}[\text{beta}]+a1^2\, v^2\,\text{Cos}[2\,\text{alphav}+\text{beta}]-a1^3\, v\,\text{Cos}[\text{alphav}+2\,\text{beta}]-a1\, a2\, v^2\,\text{Sin}[2\,\text{alphav}]+2\, a1^2\, a2\, v\,\text{Sin}[\text{alphav}-\text{beta}]+a1^3\, a2\,\text{Sin}[2\,\text{beta}]+\sqrt{\left(-a1^2\left(a2+v\,\text{Sin}[\text{alphav}]+a1\,\text{Sin}[\text{beta}]\right)^2\left(-2\, a1^2\, a2^2+2\, a1^2\, v^2+2\, a2^2\, v^2+v^4-2\, a2^2\, v^2\,\text{Cos}[2\,\text{alphav}]+4\, a1\, a2^2\, v\,\text{Cos}[\text{alphav}-\text{beta}]-2\, a1^2\, a2^2\,\text{Cos}[2\,\text{beta}]-4\, a1\, a2^2\, v\,\text{Cos}[\text{alphav}+\text{beta}]-4\, a1\, v^3\,\text{Cos}[\text{alphav}+\text{beta}]+2\, a1^2\, v^2\,\text{Cos}[2\left(\text{alphav}+\text{beta}\right)]+4\, a1^2\, a2\, v\,\text{Sin}[\text{alphav}]+4\, a2\, v^3\,\text{Sin}[\text{alphav}]+8\, a1\, a2\, v^2\,\text{Sin}[\text{beta}]-4\, a1\, a2\, v^2\,\text{Sin}[2\,\text{alphav}+\text{beta}]-4\, a1^2\, a2\, v\,\text{Sin}[\text{alphav}+2\,\text{beta}]\right)\right)}\Big/\left(a1\, a2\left(a1^2+a2^2+v^2-2\, a1\, v\,\text{Cos}[\text{alphav}+\text{beta}]+2\, a2\, v\,\text{Sin}[\text{alphav}]+2\, a1\, a2\,\text{Sin}[\text{beta}]\right)\right)\right)\right]\}$$

Solve the analytic form of the unit-cell kinematics for c1, c2 angles (c1=gamma1, c2=gamma2 with the notation of Fig. S2, A)

In[54]:=
```
n2xdefa = (n[1][[1]] + a12 * Sin[anglec1]) /. vdata;
n2xdefb = ((n[5][[1]] + vact * Cos[anglealpha]) + a52 * Cos[anglec2]) /. vdata;
n2ydefa = (n[1][[2]] - a12 * Cos[anglec1]) /. vdata;
n2ydefb = ((n[5][[2]] + vact * Sin[anglealpha]) - a52 * Sin[anglec2]) /. vdata;
eq2x = n2xdefa == n2xdefb;
eq2y = n2ydefa == n2ydefb;
anglecsol = Solve[{eq2x, eq2y}, {anglec1, anglec2}] /. cdata // Simplify;
isol = 1;
anglecsol[[isol]]
n2xdefa /. anglecsol;
n2xdefb /. anglecsol;
n2ydefa /. anglecsol;
n2ydefb /. anglecsol;
n[2];
```

Out[62]=
$$\{\text{anglec1} \to \text{ArcTan}\Big[-\Big(\big(2\,a1^2\,a2\,v\,\text{Cos}[\text{alphav}-\text{beta}] - 2\,a1^2\,\left(a1^2+v^2\right)\text{Cos}[\text{beta}] + a1^2\,v^2\,\text{Cos}[2\,\text{alphav}+\text{beta}] + 3\,a1^3\,v\,\text{Sin}[\text{alphav}] + a1\,v^3\,\text{Sin}[\text{alphav}] - a1\,a2\,v^2\,\text{Sin}[2\,\text{alphav}] - a1^3\,a2\,\text{Sin}[2\,\text{beta}] + \sqrt{\left(a1^2\,(a2 - v\,\text{Cos}[\text{alphav}] + a1\,\text{Sin}[\text{beta}]\right)^2\left(2\,a1^2\,a2^2 - 2\,a1^2\,v^2 - 2\,a2^2\,v^2 - v^4 + 4\,a2\,v\,\left(a1^2+v^2\right)\text{Cos}[\text{alphav}] - 2\,a2^2\,v^2\,\text{Cos}[2\,\text{alphav}] + 2\,a1^2\,a2^2\,\text{Cos}[2\,\text{beta}] + 2\,a1^2\,v^2\,\text{Cos}[2\,(\text{alphav}+\text{beta})] - 4\,a1^2\,a2\,v\,\text{Cos}[\text{alphav}+2\,\text{beta}] - 4\,a1\,a2^2\,v\,\text{Sin}[\text{alphav}-\text{beta}] - 8\,a1\,a2\,v^2\,\text{Sin}[\text{beta}] + 4\,a1\,a2^2\,v\,\text{Sin}[\text{alphav}+\text{beta}] + 4\,a1\,v^3\,\text{Sin}[\text{alphav}+\text{beta}] - 4\,a1\,a2\,v^2\,\text{Sin}[2\,\text{alphav}+\text{beta}]\right)} + a1^3\,v\,\text{Sin}[\text{alphav}+2\,\text{beta}]\big)\Big/\left(a1^2\left(a1^2+a2^2+v^2-2\,a2\,v\,\text{Cos}[\text{alphav}] + 2\,a1\,a2\,\text{Sin}[\text{beta}] - 2\,a1\,v\,\text{Sin}[\text{alphav}+\text{beta}]\right)\right)\Big)\Big],$$

$$-\Big(\big(2\,a1^5 + 8\,a1^3\,a2^2 + 5\,a1^3\,v^2 + 6\,a1\,a2^2\,v^2 + a1\,v^4 - a1\,a2\,v\,\left(18\,a1^2 + 4\,a2^2 + 7\,v^2\right)\text{Cos}[\text{alphav}] + a1\,v^2\,\left(4\,a1^2 + 4\,a2^2 + v^2\right)\text{Cos}[2\,\text{alphav}] - a1\,a2\,v^3\,\text{Cos}[3\,\text{alphav}] + 3\,a1^3\,a2\,v\,\text{Cos}[\text{alphav}-2\,\text{beta}] - 2\,a1^5\,\text{Cos}[2\,\text{beta}] - 4\,a1^3\,a2^2\,\text{Cos}[2\,\text{beta}] - 3\,a1^3\,v^2\,\text{Cos}[2\,\text{beta}] - 2\,a1^3\,v^2\,\text{Cos}[2\,(\text{alphav}+\text{beta})] + 7\,a1^3\,a2\,v\,\text{Cos}[\text{alphav}+2\,\text{beta}] + 5\,a1^4\,v\,\text{Sin}[\text{alphav}-\text{beta}] + 8\,a1^2\,a2^2\,v\,\text{Sin}[\text{alphav}-\text{beta}] + 3\,a1^2\,v^3\,\text{Sin}[\text{alphav}-\text{beta}] - 3\,a1^2\,a2\,v^2\,\text{Sin}[2\,\text{alphav}-\text{beta}] + 11\,a1^4\,a2\,\text{Sin}[\text{beta}] + 4\,a1^2\,a2^3\,\text{Sin}[\text{beta}] + 14\,a1^2\,a2\,v^2\,\text{Sin}[\text{beta}] - a1^4\,a2\,\text{Sin}[3\,\text{beta}] - 6\,a1^4\,v\,\text{Sin}[\text{alphav}+\text{beta}] - 12\,a1^2\,a2^2\,v\,\text{Sin}[\text{alphav}+\text{beta}] - 4\,a1^2\,v^3\,\text{Sin}[\text{alphav}+\text{beta}] + 7\,a1^2\,a2\,v^2\,\text{Sin}[2\,\text{alphav}+\text{beta}] + 2\,a1\,\text{Cos}[\text{beta}]\,\sqrt{\left(a1^2\,(a2 - v\,\text{Cos}[\text{alphav}] + a1\,\text{Sin}[\text{beta}]\right)^2\left(2\,a1^2\,a2^2 - 2\,a1^2\,v^2 - 2\,a2^2\,v^2 - v^4 + 4\,a2\,v\,\left(a1^2+v^2\right)\text{Cos}[\text{alphav}] - 2\,a2^2\,v^2\,\text{Cos}[2\,\text{alphav}] + 2\,a1^2\,a2^2\,\text{Cos}[2\,\text{beta}] + 2\,a1^2\,v^2\,\text{Cos}[2\,(\text{alphav}+\text{beta})] - 4\,a1^2\,a2\,v\,\text{Cos}[\text{alphav}+2\,\text{beta}] - 4\,a1\,a2^2\,v\,\text{Sin}[\text{alphav}-\text{beta}] - 8\,a1\,a2\,v^2\,\text{Sin}[\text{beta}] + 4\,a1\,a2^2\,v\,\text{Sin}[\text{alphav}+\text{beta}] + 4\,a1\,v^3\,\text{Sin}[\text{alphav}+\text{beta}] - 4\,a1\,a2\,v^2\,\text{Sin}[2\,\text{alphav}+\text{beta}]\right)} - 2\,v\,\text{Sin}[\text{alphav}]\,\sqrt{\left(a1^2\,(a2 - v\,\text{Cos}[\text{alphav}] + a1\,\text{Sin}[\text{beta}]\right)^2\left(2\,a1^2\,a2^2 - 2\,a1^2\,v^2 - 2\,a2^2\,v^2 - v^4 + 4\,a2\,v\,\left(a1^2+v^2\right)\text{Cos}[\text{alphav}] - 2\,a2^2\,v^2\,\text{Cos}[2\,\text{alphav}] + 2\,a1^2\,a2^2\,\text{Cos}[2\,\text{beta}] + 2\,a1^2\,v^2\,\text{Cos}[2\,(\text{alphav}+\text{beta})] - 4\,a1^2\,a2\,v\,\text{Cos}[\text{alphav}+2\,\text{beta}] - 4\,a1\,a2^2\,v\,\text{Sin}[\text{alphav}-\text{beta}] - 8\,a1\,a2\,v^2\,\text{Sin}[\text{beta}] + 4\,a1\,a2^2\,v\,\text{Sin}[\text{alphav}+\text{beta}] + 4\,a1\,v^3\,\text{Sin}[\text{alphav}+\text{beta}] - 4\,a1\,a2\,v^2\,\text{Sin}[2\,\text{alphav}+\text{beta}]\right)} - a1^2\,v^3\,\text{Sin}[3\,\text{alphav}+\text{beta}] + a1^4\,v\,\text{Sin}[\text{alphav}+3\,\text{beta}]\big)\Big/\left(2\,a1^2\,(a2 - v\,\text{Cos}[\text{alphav}] + a1\,\text{Sin}[\text{beta}])\,\left(a1^2+a2^2+v^2-2\,a2\,v\,\text{Cos}[\text{alphav}] + 2\,a1\,a2\,\text{Sin}[\text{beta}] - 2\,a1\,v\,\text{Sin}[\text{alphav}+\text{beta}]\right)\right)\Big)\Big],$$

$$\text{anglec2} \to \text{ArcTan}\Big[\big(6\,a1^3\,a2^2 + 4\,a1\,a2^4 + 3\,a1^3\,v^2 + 8\,a1\,a2^2\,v^2 + a1\,v^4 - a1\,a2\,v\,\left(10\,a1^2 + 12\,a2^2 + 7\,v^2\right)\text{Cos}[\text{alphav}] + a1\,v^2\,\left(2\,a1^2 + 6\,a2^2 + v^2\right)\text{Cos}[2\,\text{alphav}] - a1\,a2\,v^3\,\text{Cos}[3\,\text{alphav}] + 3\,a1^3\,a2\,v\,\text{Cos}[\text{alphav}-2\,\text{beta}] - 6\,a1^3\,a2^2\,\text{Cos}[2\,\text{beta}] - 3\,a1^3\,v^2\,\text{Cos}[2\,\text{beta}] - 2\,a1^3\,v^2\,\text{Cos}[2\,(\text{alphav}+\text{beta})] + 7\,a1^3\,a2\,v\,\text{Cos}[\text{alphav}+2\,\text{beta}] + a1^4\,v\,\text{Sin}[\text{alphav}-\text{beta}] + 12\,a1^2\,a2^2\,v\,\text{Sin}[\text{alphav}-\text{beta}] + 3\,a1^2\,v^3\,\text{Sin}[\text{alphav}-\text{beta}] - 3\,a1^2\,a2\,v^2\,\text{Sin}[2\,\text{alphav}-\text{beta}] + 3\,a1^4\,a2\,\text{Sin}[\text{beta}] + 12\,a1^2\,a2^3\,\text{Sin}[\text{beta}] + 14\,a1^2\,a2\,v^2\,\text{Sin}[\text{beta}] - a1^4\,a2\,\text{Sin}[3\,\text{beta}] - 2\,a1^4\,v\,\text{Sin}[\text{alphav}+\text{beta}] - 16\,a1^2\,a2^2\,v\,\text{Sin}[\text{alphav}+\text{beta}] - 4\,a1^2\,v^3\,\text{Sin}[\text{alphav}+\text{beta}] + 7\,a1^2\,a2\,v^2\,\text{Sin}[2\,\text{alphav}+\text{beta}] - 2\,a1\,\text{Cos}[\text{beta}]\,\sqrt{\left(a1^2\,(a2 - v\,\text{Cos}[\text{alphav}] + a1\,\text{Sin}[\text{beta}]\right)^2\left(2\,a1^2\,a2^2 - 2\,a1^2\,v^2 - 2\,a2^2\,v^2 - v^4 + 4\,a2\,v\,\left(a1^2+v^2\right)\text{Cos}[\text{alphav}] - 2\,a2^2\,v^2\,\text{Cos}[2\,\text{alphav}] + 2\,a1^2\,a2^2\,\text{Cos}[2\,\text{beta}] + 2\,a1^2\,v^2\,\text{Cos}[2\,(\text{alphav}+\text{beta})] - 4\,a1^2\,a2\,v\,\text{Cos}[\text{alphav}+2\,\text{beta}] - 4\,a1\,a2^2\,v\,\text{Sin}[\text{alphav}-\text{beta}] - 8\,a1\,a2\,v^2\,\text{Sin}[\text{beta}] + 4\,a1\,a2^2\,v\,\text{Sin}[\text{alphav}+\text{beta}] + 4\,a1\,v^3\,\text{Sin}[\text{alphav}+\text{beta}] - 4\,a1\,a2\,v^2\,\text{Sin}[2\,\text{alphav}+\text{beta}]\right)} + 2\,v\,\text{Sin}[\text{alphav}]\,\sqrt{\left(a1^2\,(a2 - v\,\text{Cos}[\text{alphav}] + a1\,\text{Sin}[\text{beta}]\right)^2\left(2\,a1^2\,a2^2 - 2\,a1^2\,v^2 - 2\,a2^2\,v^2 - v^4 + 4\,a2\,v\,\left(a1^2+v^2\right)\text{Cos}[\text{alphav}] - 2\,a2^2\,v^2\,\text{Cos}[2\,\text{alphav}] + 2\,a1^2\,a2^2\,\text{Cos}[2\,\text{beta}] + 2\,a1^2\,v^2\,\text{Cos}[2\,(\text{alphav}+\text{beta})] - 4\,a1^2\,a2\,v\,\text{Cos}[\text{alphav}+2\,\text{beta}] - 4\,a1\,a2^2\,v\,\text{Sin}[\text{alphav}-\text{beta}] - 8\,a1\,a2\,v^2\,\text{Sin}[\text{beta}] + 4\,a1\,a2^2\,v\,\text{Sin}[\text{alphav}+\text{beta}] + 4\,a1\,v^3\,\text{Sin}[\text{alphav}+\text{beta}] - 4\,a1\,a2\,v^2\,\text{Sin}[2\,\text{alphav}+\text{beta}]\right)} - a1^2\,v^3\,\text{Sin}[3\,\text{alphav}+\text{beta}] + a1^4\,v\,\text{Sin}[\text{alphav}+3\,\text{beta}]\big)\Big/\left(2\,a1\,a2\,(a2 - v\,\text{Cos}[\text{alphav}] + a1\,\text{Sin}[\text{beta}])\,\left(a1^2+a2^2+v^2-2\,a2\,v\,\text{Cos}[\text{alphav}] + 2\,a1\,a2\,\text{Sin}[\text{beta}] - 2\,a1\,v\,\text{Sin}[\text{alphav}+\text{beta}]\right)\right),$$

$$\big(2\,a1^2\,a2\,v\,\text{Cos}[\text{alphav}-\text{beta}] - 2\,a1^2\,\left(a2^2+v^2\right)\text{Cos}[\text{beta}] + a1^2\,v^2\,\text{Cos}[2\,\text{alphav}+\text{beta}] + a1^3\,v\,\text{Sin}[\text{alphav}] + 2\,a1\,a2^2\,v\,\text{Sin}[\text{alphav}] + a1\,v^3\,\text{Sin}[\text{alphav}] - a1\,a2\,v^2\,\text{Sin}[2\,\text{alphav}] - a1^3\,a2\,\text{Sin}[2\,\text{beta}] - \sqrt{\left(a1^2\,(a2 - v\,\text{Cos}[\text{alphav}] + a1\,\text{Sin}[\text{beta}]\right)^2\left(2\,a1^2\,a2^2 - 2\,a1^2\,v^2 - 2\,a2^2\,v^2 - v^4 + 4\,a2\,v\,\left(a1^2+v^2\right)\text{Cos}[\text{alphav}] - 2\,a2^2\,v^2\,\text{Cos}[2\,\text{alphav}] + 2\,a1^2\,a2^2\,\text{Cos}[2\,\text{beta}] + 2\,a1^2\,v^2\,\text{Cos}[2\,(\text{alphav}+\text{beta})] - 4\,a1^2\,a2\,v\,\text{Cos}[\text{alphav}+2\,\text{beta}] - 4\,a1\,a2^2\,v\,\text{Sin}[\text{alphav}-\text{beta}] - 8\,a1\,a2\,v^2\,\text{Sin}[\text{beta}] + 4\,a1\,a2^2\,v\,\text{Sin}[\text{alphav}+\text{beta}] + 4\,a1\,v^3\,\text{Sin}[\text{alphav}+\text{beta}] - 4\,a1\,a2\,v^2\,\text{Sin}[2\,\text{alphav}+\text{beta}]\right)} + a1^3\,v\,\text{Sin}[\text{alphav}+2\,\text{beta}]\big)\Big/\left(a1\,a2\,\left(a1^2+a2^2+v^2-2\,a2\,v\,\text{Cos}[\text{alphav}] + 2\,a1\,a2\,\text{Sin}[\text{beta}] - 2\,a1\,v\,\text{Sin}[\text{alphav}+\text{beta}]\right)\right)\Big]\Big\}$$

Solve the analytic form of the unit-cell kinematics for d1, d2 angles (d1=delta1, d2=delta2 with the notation of Fig. S2, A)

In[68]:=
```
n4xdefa = (n[7][[1]] + a74 * Cos[angled1]) /. vdata;
n4xdefb = ((n[5][[1]] + vact * Cos[anglealpha]) - a54 * Sin[angled2]) /. vdata;
n4ydefa = (n[7][[2]] + a74 * Sin[angled1]) /. vdata;
n4ydefb = ((n[5][[2]] + vact * Sin[anglealpha]) + a54 * Cos[angled2]) /. vdata;
eq4x = n4xdefa == n4xdefb;
eq4y = n4ydefa == n4ydefb;
angledsol = Solve[{eq4x, eq4y}, {angled1, angled2}] /. cdata // Simplify;
isol = 1;
angledsol[[isol]]
n4xdefa /. angledsol;
n4xdefb /. angledsol;
n4ydefa /. angledsol;
n4ydefb /. angledsol;
n[4];
```

Out[76]=
```
{angled1 →
  ArcTan[ (a1 v (3 a1^2 + v^2) Cos[alphav] + 2 a1^2 (a1^2 + v^2) Cos[beta] + a1^2 v^2 Cos[2 alphav + beta] + a1^3 v Cos[alphav + 2 beta] - a1 a2 v^2
      Sin[2 alphav] - 2 a1^2 a2 v Sin[alphav - beta] + a1^3 a2 Sin[2 beta] - √(-a1^2 (a2 - v Sin[alphav] + a1 Sin[beta])^2 (-2 a1^2 a2^2 + 2 a1^2
        v^2 + 2 a2^2 v^2 + v^4 - 2 a2^2 v^2 Cos[2 alphav] - 4 a1 a2^2 v Cos[alphav - beta] - 2 a1^2 a2^2 Cos[2 beta] + 4 a1 a2^2 v Cos[alphav + beta] +
        4 a1 v^3 Cos[alphav + beta] + 2 a1^2 v^2 Cos[2 (alphav + beta)] - 4 a1^2 a2 v Sin[alphav] - 4 a2 v^3 Sin[alphav] +
        8 a1 a2 v^2 Sin[beta] - 4 a1 a2 v^2 Sin[2 alphav + beta] + 4 a1^2 a2 v Sin[alphav + 2 beta]))) /
    (a1^2 (a1^2 + a2^2 + v^2 + 2 a1 v Cos[alphav + beta] - 2 a2 v Sin[alphav] + 2 a1 a2 Sin[beta])),
  -((2 a1^5 + 8 a1^3 a2^2 + 5 a1^3 v^2 + 6 a1 a2^2 v^2 + a1 v^4 - a1 v^2 (4 a1^2 + 4 a2^2 + v^2) Cos[2 alphav] - a1^2 v (5 a1^2 + 8 a2^2 + 3 v^2) Cos[alphav - beta] -
      2 a1^5 Cos[2 beta] - 4 a1^3 a2^2 Cos[2 beta] - 3 a1^3 v^2 Cos[2 beta] + 6 a1^4 v Cos[alphav + beta] + 12 a1^2 a2^2 v Cos[alphav + beta] +
      4 a1^2 v^3 Cos[alphav + beta] + 2 a1^3 v^2 Cos[2 (alphav + beta)] - a1^2 v^3 Cos[3 alphav + beta] - a1^4 v Cos[alphav + 3 beta] -
      18 a1^3 a2 v Sin[alphav] - 4 a1 a2^3 v Sin[alphav] - 7 a1 a2 v^3 Sin[alphav] + a1 a2 v^3 Sin[3 alphav] + 3 a1^3 a2 v Sin[alphav - 2 beta] +
      3 a1^2 a2 v^2 Sin[2 alphav - beta] + 11 a1^4 a2 Sin[beta] + 4 a1^2 a2^3 Sin[beta] + 14 a1^2 a2 v^2 Sin[beta] - a1^4 a2 Sin[3 beta] -
      7 a1^2 a2 v^2 Sin[2 alphav + beta] + 7 a1^3 a2 v Sin[alphav + 2 beta] + 2 v Cos[alphav] √(a1^2 (a2 - v Sin[alphav] + a1 Sin[beta])^2
        (2 a1^2 a2^2 - 2 a1^2 v^2 - 2 a2^2 v^2 - v^4 + 2 a2^2 v^2 Cos[2 alphav] + 4 a1 a2^2 v Cos[alphav - beta] + 2 a1^2 a2^2 Cos[2 beta] -
          4 a1 a2^2 v Cos[alphav + beta] - 4 a1 v^3 Cos[alphav + beta] - 2 a1^2 v^2 Cos[2 (alphav + beta)] + 4 a1^2 a2 v Sin[alphav] +
          4 a2 v^3 Sin[alphav] - 8 a1 a2 v^2 Sin[beta] + 4 a1 a2 v^2 Sin[2 alphav + beta] - 4 a1^2 a2 v Sin[alphav + 2 beta])) +
      2 a1 Cos[beta] √(a1^2 (a2 - v Sin[alphav] + a1 Sin[beta])^2 (2 a1^2 a2^2 - 2 a1^2 v^2 - 2 a2^2 v^2 - v^4 + 2 a2^2 v^2 Cos[2 alphav] +
          4 a1 a2^2 v Cos[alphav - beta] + 2 a1^2 a2^2 Cos[2 beta] - 4 a1 a2^2 v Cos[alphav + beta] -
          4 a1 v^3 Cos[alphav + beta] - 2 a1^2 v^2 Cos[2 (alphav + beta)] + 4 a1^2 a2 v Sin[alphav] + 4 a2 v^3 Sin[alphav] -
          8 a1 a2 v^2 Sin[beta] + 4 a1 a2 v^2 Sin[2 alphav + beta] - 4 a1^2 a2 v Sin[alphav + 2 beta]))) /
    (2 a1^2 (a2 - v Sin[alphav] + a1 Sin[beta]) (a1^2 + a2^2 + v^2 + 2 a1 v Cos[alphav + beta] - 2 a2 v Sin[alphav] + 2 a1 a2 Sin[beta]))],
  angled2 → ArcTan[ (6 a1^3 a2^2 + 4 a1 a2^4 + 3 a1^3 v^2 + 8 a1 a2^2 v^2 + a1 v^4 - a1 v^2 (2 a1^2 + 6 a2^2 + v^2) Cos[2 alphav] -
      a1^2 v (a1^2 + 12 a2^2 + 3 v^2) Cos[alphav - beta] - 6 a1^3 a2^2 Cos[2 beta] -
      3 a1^3 v^2 Cos[2 beta] + 2 a1^4 v Cos[alphav + beta] + 16 a1^2 a2^2 v Cos[alphav + beta] +
      4 a1^2 v^3 Cos[alphav + beta] + 2 a1^3 v^2 Cos[2 (alphav + beta)] -
      a1^2 v^3 Cos[3 alphav + beta] - a1^4 v Cos[alphav + 3 beta] - 10 a1^3 a2 v Sin[alphav] -
      12 a1 a2^3 v Sin[alphav] - 7 a1 a2 v^3 Sin[alphav] + a1 a2 v^3 Sin[3 alphav] +
      3 a1^3 a2 v Sin[alphav - 2 beta] + 3 a1^2 a2 v^2 Sin[2 alphav - beta] + 3 a1^4 a2 Sin[beta] +
      12 a1^2 a2^3 Sin[beta] + 14 a1^2 a2 v^2 Sin[beta] - a1^4 a2 Sin[3 beta] -
      7 a1^2 a2 v^2 Sin[2 alphav + beta] + 7 a1^3 a2 v Sin[alphav + 2 beta] - 2 v Cos[alphav]
      √(a1^2 (a2 - v Sin[alphav] + a1 Sin[beta])^2 (2 a1^2 a2^2 - 2 a1^2 v^2 - 2 a2^2 v^2 - v^4 + 2 a2^2 v^2 Cos[2 alphav] + 4 a1 a2^2 v Cos[alphav - beta] +
          2 a1^2 a2^2 Cos[2 beta] - 4 a1 a2^2 v Cos[alphav + beta] - 4 a1 v^3 Cos[alphav + beta] - 2 a1^2 v^2 Cos[2 (alphav + beta)] + 4 a1^2 a2 v
          Sin[alphav] + 4 a2 v^3 Sin[alphav] - 8 a1 a2 v^2 Sin[beta] + 4 a1 a2 v^2 Sin[2 alphav + beta] - 4 a1^2 a2 v Sin[alphav + 2 beta])) -
      2 a1 Cos[beta] √(a1^2 (a2 - v Sin[alphav] + a1 Sin[beta])^2 (2 a1^2 a2^2 - 2 a1^2 v^2 - 2 a2^2 v^2 - v^4 + 2 a2^2 v^2 Cos[2 alphav] +
          4 a1 a2^2 v Cos[alphav - beta] + 2 a1^2 a2^2 Cos[2 beta] - 4 a1 a2^2 v Cos[alphav + beta] -
          4 a1 v^3 Cos[alphav + beta] - 2 a1^2 v^2 Cos[2 (alphav + beta)] + 4 a1^2 a2 v Sin[alphav] + 4 a2 v^3 Sin[alphav] -
          8 a1 a2 v^2 Sin[beta] + 4 a1 a2 v^2 Sin[2 alphav + beta] - 4 a1^2 a2 v Sin[alphav + 2 beta]))) /
    (2 a1 a2 (a2 - v Sin[alphav] + a1 Sin[beta]) (a1^2 + a2^2 + v^2 + 2 a1 v Cos[alphav + beta] - 2 a2 v Sin[alphav] + 2 a1 a2 Sin[beta])),
  (a1 v (a1^2 + 2 a2^2 + v^2) Cos[alphav] + 2 a1^2 (a2^2 + v^2) Cos[beta] + a1^2 v^2 Cos[2 alphav + beta] +
    a1^3 v Cos[alphav + 2 beta] - a1 a2 v^2 Sin[2 alphav] - 2 a1^2 a2 v Sin[alphav - beta] +
    a1^3 a2 Sin[2 beta] + √(-a1^2 (a2 - v Sin[alphav] + a1 Sin[beta])^2
      (-2 a1^2 a2^2 + 2 a1^2 v^2 + 2 a2^2 v^2 + v^4 - 2 a2^2 v^2 Cos[2 alphav] - 4 a1 a2^2 v Cos[alphav - beta] - 2 a1^2 a2^2 Cos[2 beta] +
        4 a1 a2^2 v Cos[alphav + beta] + 4 a1 v^3 Cos[alphav + beta] + 2 a1^2 v^2 Cos[2 (alphav + beta)] - 4 a1^2 a2 v Sin[alphav] -
        4 a2 v^3 Sin[alphav] + 8 a1 a2 v^2 Sin[beta] - 4 a1 a2 v^2 Sin[2 alphav + beta] + 4 a1^2 a2 v Sin[alphav + 2 beta]))) /
    (a1 a2 (a1^2 + a2^2 + v^2 + 2 a1 v Cos[alphav + beta] - 2 a2 v Sin[alphav] + 2 a1 a2 Sin[beta]))]}
```

Node coordinates in the deformed configuration

In[82]:=
```
Do[ndef[i] = nundef[i], {i, 1, nnodes}];
ndef[5] = n[5] + {vact * Cos[anglealpha], vact * Sin[anglealpha], 0} /. vdata
ndef[8] = {(n8xdefa /. angleasol[[isol]]), (n8ydefa /. angleasol[[isol]]), 0};
ndef[6] = {(n6xdefa /. anglebsol[[isol]]), (n6ydefa /. anglebsol[[isol]]), 0};
ndef[2] = {(n2xdefa /. anglecsol[[isol]]), (n2ydefa /. anglecsol[[isol]]), 0};
ndef[4] = {(n4xdefa /. angledsol[[isol]]), (n4ydefa /. angledsol[[isol]]), 0};
```

Out[83]=
```
{v Cos[alphav], v Sin[alphav], 0}
```

In[88]:=
```
Do[ndefbeta[i] = nundefbeta[i], {i, 1, nnodes}];
isol = 1;
ndefbeta[5] = ndef[5];
ndefbeta[8] = ndef[8];
ndefbeta[6] = ndef[6];
ndefbeta[2] = ndef[2];
ndefbeta[4] = ndef[4];
```

Analytic computation of the locking geometry for arbitrary rest configuration

In[95]:=
```
cdata = {C[1] → 0, C[2] → 0};
```

First locking condition for the alignment of the limb members 5-8 and 8-9 (Fig. S2, A)

In[96]:=
```
data = {};
Clear[alpha]
```

In[98]:=
```
eq1a = v Sin[alpha] + a1 Cos[beta] == (a1 + a2) Sin[phi];
eq2a = v Cos[alpha] + a2 + a1 Sin[beta] == (a1 + a2) Cos[phi];

eq1dataa = eq1a /. data;
eq2dataa = eq2a /. data;

solnewa = Solve[{eq1dataa, eq2dataa}, {v, phi}] // Simplify;
```

In[103]:=
```
vsol1a = (v /. solnewa[[1]]) /. {alpha → (alphadeg * Pi / 180)} // Simplify;
vsol2a = (v /. solnewa[[2]]) /. {alpha → (alphadeg * Pi / 180)} // Simplify;
```

Second locking condition for the alignment of the limb members 5-6 and 6-3 (Fig. S2, A)

In[105]:=
```
data = {};
Clear[alpha]
```

In[107]:=
```
eq1b = v Sin[alpha] + a2 + a1 Sin[beta] == a1 Cos[phi] + a2 Cos[phi];
eq2b = v Cos[alpha] + a2 Sin[phi] + a1 Sin[phi] == a1 Cos[beta] ;

eq1datab = eq1b /. data;
eq2datab = eq2b /. data;

solnewb = Solve[{eq1datab, eq2datab}, {v, phi}] // Simplify;
```

In[112]:=
```
vsol1b = (v /. solnewb[[1]]) /. {alpha → (alphadeg * Pi / 180)} // Simplify;
vsol2b = (v /. solnewb[[2]]) /. {alpha → (alphadeg * Pi / 180)} // Simplify;
```

Third locking condition for the alignment of the limb members 5-2 and 2-1 (Fig. S2, A)

In[114]:=
```
data = {};
Clear[alpha]
```

In[116]:=
```
eq1c = v Sin[alpha - Pi] + a1 Cos[beta] == a1 Sin[phi] + a2 Sin[phi];
eq2c = v Cos[alpha - Pi] + a2 + a1 Sin[beta] == a1 Cos[phi] + a2 Cos[phi] ;

eq1datac = eq1c /. data;
eq2datac = eq2c /. data;

solnewc = Solve[{eq1datac, eq2datac}, {v, phi}] // Simplify;
```

In[121]:=
```
vsol1c = (v /. solnewc[[1]]) /. {alpha → (alphadeg * Pi / 180)} // Simplify;
vsol2c = (v /. solnewc[[2]]) /. {alpha → (alphadeg * Pi / 180)} // Simplify;
```

Fourth locking condition for the alignment of the limb members 5-4 and 4-7 (Fig. S2, A)

In[123]:=
```
data = {};
Clear[alpha]
```

In[125]:=
```
eq1d = v Sin[2 * Pi - alpha] + a2 + a1 Sin[beta] == a1 Cos[phi] + a2 Cos[phi];
eq2d = v Cos[2 * Pi - alpha] + a1 Cos[beta] == a1 Sin[phi] + a2 Sin[phi] ;

eq1datad = eq1d /. data;
eq2datad = eq2d /. data;

solnewd = Solve[{eq1datad, eq2datad}, {v, phi}] // Simplify;
```

In[130]:=
```
vsol1d = (v /. solnewd[[1]]) /. {alpha → (alphadeg * Pi / 180)} // Simplify;
vsol2d = (v /. solnewd[[2]]) /. {alpha → (alphadeg * Pi / 180)} // Simplify;
```

Find vmax vs alpha law for beta = 0 deg (vmax=u_{lock} with the notation of the main text)

Analytic expression of vbarlock (vbarlock={\bar u}_{lock} with the notation of the main text)

In[132]:=
```
vbarlock = (vsol1a /. {a1 → a, a2 → a, beta → 0, alphadeg → (α * 180 / Pi)}) / a // Simplify
vbarlock1 = vbarlock /. {a -> 1}
```

Out[132]=
$$-\text{Cos}[\alpha] - \text{Sin}[\alpha] + \left(\text{Sec}[\alpha]\sqrt{\left(a^4\,\text{Cos}[\alpha]^2\,(3+\text{Sin}[2\alpha])\right)}\right)/a^2$$

Out[133]=
$$-\text{Cos}[\alpha] - \text{Sin}[\alpha] + \text{Sec}[\alpha]\sqrt{\left(\text{Cos}[\alpha]^2\,(3+\text{Sin}[2\alpha])\right)}$$

Plot of vbarlock for varying alpha

In[134]:=
```
dataplot = {a → 100., a1 → 100., a2 → 100., beta → (0)}
```

Out[134]=
$$\{a \to 100.,\ a1 \to 100.,\ a2 \to 100.,\ \text{beta} \to 0\}$$

In[135]:=
```
vplotabcd = Min[vsol1a /. dataplot, vsol1b /. dataplot];
vgraphabcd = Plot[{vplotabcd}, {alphadeg, 0, 89.99}, PlotStyle → {Thick, Red},
  AxesLabel → {"α (deg)", "v [mm]"}, (*PlotRange→{vplotmin,vplotmax}*) PlotRange → All, PlotPoints → 100]
eps = 1 * 10^{-9};
vplot0abcd = vplotabcd /. {alphadeg → 0 + eps}
vplot45abcd = vplotabcd /. {alphadeg → 45}
vplot90abcd = vplotabcd /. {alphadeg → 90 - eps}
vplotbeta0deg = Plot[{vplotabcd / {a /. dataplot}}, {alphadeg, 0, 90}, PlotStyle → {Thick, Red},
   AxesLabel → {"α (deg)", "v [mm]"}, PlotRange → All, PlotPoints → 100, Frame → {{True, True}, {True, False}}];
```

Out[136]=

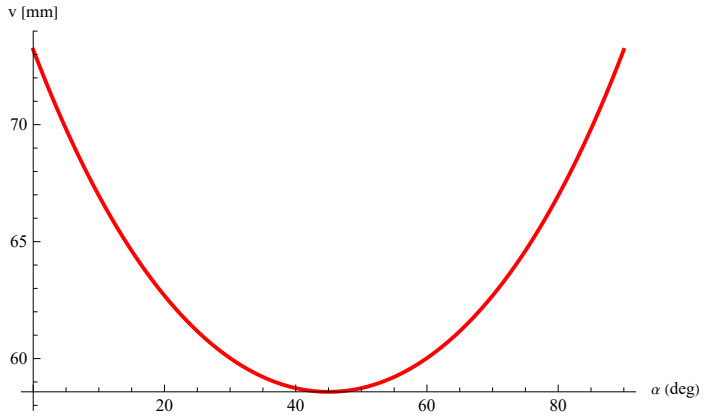

Out[138]= 73.2051

Out[139]= 58.5786

Out[140]= 73.2051

In[142]:=
```
v1 = vsol1a /. dataplot;
Dv1 = D[v1, alphadeg];
solDv1 = FindRoot[{Dv1 == 0}, {alphadeg, 45}]
vbarlockmin0 = (v1 /. solDv1) / a /. dataplot
```

Out[144]= {alphadeg → 45.}

Out[145]= 0.585786

Engineering axial strains of the tendons

In[146]:=
```
Clear[a]
data = {a → a, a1 → a, a2 → a, beta → 0, v → (vbar a), alphav → α};
vdes = vbarlock1
```

Out[148]= $-\text{Cos}[\alpha] - \text{Sin}[\alpha] + \text{Sec}[\alpha] \sqrt{\left(\text{Cos}[\alpha]^2 \ (3 + \text{Sin}[2\,\alpha])\right)}$

```
ibar = 5;
jbar = 9;
adef2act = (ndef[ibar] - ndef[jbar]).(ndef[ibar] - ndef[jbar]) /. data;
aundef2act = (nundef[ibar] - nundef[jbar]).(nundef[ibar] - nundef[jbar]) /. data;
epsact = (Sqrt[adef2act] - Sqrt[aundef2act]) / Sqrt[aundef2act] /. data;
eps59 = epsact
eps59 /. {a → aplot} // Simplify
k59 = (ndef[ibar] - ndef[jbar]) / Sqrt[adef2act] /. data
k59 /. {a → aplot} // Simplify
eps59lock = eps59 /. {vbar → vdes} // Simplify
```

$$\left(-\sqrt{2}\,\sqrt{a^2}+\sqrt{\left((a+a\,\text{vbar}\,\text{Cos}[\alpha])^2+(a+a\,\text{vbar}\,\text{Sin}[\alpha])^2\right)}\right)\Big/\left(\sqrt{2}\,\sqrt{a^2}\right)$$

$$\frac{1}{2}\left(-2+\left(\sqrt{2}\,\sqrt{\left(\text{aplot}^2\left(2+\text{vbar}^2+2\,\text{vbar}\,\text{Cos}[\alpha]+2\,\text{vbar}\,\text{Sin}[\alpha]\right)\right)}\right)\Big/\left(\sqrt{\text{aplot}^2}\right)\right)$$

$$\left\{(a+a\,\text{vbar}\,\text{Cos}[\alpha])\Big/\left(\sqrt{\left((a+a\,\text{vbar}\,\text{Cos}[\alpha])^2+(a+a\,\text{vbar}\,\text{Sin}[\alpha])^2\right)}\right),\right.$$
$$\left.(a+a\,\text{vbar}\,\text{Sin}[\alpha])\Big/\left(\sqrt{\left((a+a\,\text{vbar}\,\text{Cos}[\alpha])^2+(a+a\,\text{vbar}\,\text{Sin}[\alpha])^2\right)}\right),\,0\right\}$$

$$\left\{(\text{aplot}\,(1+\text{vbar}\,\text{Cos}[\alpha]))\Big/\left(\sqrt{\left(\text{aplot}^2\left(2+\text{vbar}^2+2\,\text{vbar}\,\text{Cos}[\alpha]+2\,\text{vbar}\,\text{Sin}[\alpha]\right)\right)}\right),\right.$$
$$\left.(\text{aplot}\,(1+\text{vbar}\,\text{Sin}[\alpha]))\Big/\left(\sqrt{\left(\text{aplot}^2\left(2+\text{vbar}^2+2\,\text{vbar}\,\text{Cos}[\alpha]+2\,\text{vbar}\,\text{Sin}[\alpha]\right)\right)}\right),\,0\right\}$$

$$-1+\sqrt{2}$$

```
ibar = 5;
jbar = 7;
adef2act = (ndef[ibar] - ndef[jbar]).(ndef[ibar] - ndef[jbar]) /. data;
aundef2act = (nundef[ibar] - nundef[jbar]).(nundef[ibar] - nundef[jbar]) /. data;
epsact = (Sqrt[adef2act] - Sqrt[aundef2act]) / Sqrt[aundef2act] /. data;
eps57 = epsact
eps57 /. {a → aplot} // Simplify
k57 = (ndef[ibar] - ndef[jbar]) / Sqrt[adef2act] /. data
k57 /. {a → aplot} // Simplify
eps57lock = eps57 /. {vbar → vdes} // Simplify
```

$$\left(-\sqrt{2}\,\sqrt{a^2}+\sqrt{\left((a+a\,\text{vbar}\,\text{Cos}[\alpha])^2+(-a+a\,\text{vbar}\,\text{Sin}[\alpha])^2\right)}\right)\Big/\left(\sqrt{2}\,\sqrt{a^2}\right)$$

$$\frac{1}{2}\left(-2+\left(\sqrt{2}\,\sqrt{\left(\text{aplot}^2\left(2+\text{vbar}^2+2\,\text{vbar}\,\text{Cos}[\alpha]-2\,\text{vbar}\,\text{Sin}[\alpha]\right)\right)}\right)\Big/\left(\sqrt{\text{aplot}^2}\right)\right)$$

$$\left\{(a+a\,\text{vbar}\,\text{Cos}[\alpha])\Big/\left(\sqrt{\left((a+a\,\text{vbar}\,\text{Cos}[\alpha])^2+(-a+a\,\text{vbar}\,\text{Sin}[\alpha])^2\right)}\right),\right.$$
$$\left.(-a+a\,\text{vbar}\,\text{Sin}[\alpha])\Big/\left(\sqrt{\left((a+a\,\text{vbar}\,\text{Cos}[\alpha])^2+(-a+a\,\text{vbar}\,\text{Sin}[\alpha])^2\right)}\right),\,0\right\}$$

$$\left\{(\text{aplot}\,(1+\text{vbar}\,\text{Cos}[\alpha]))\Big/\left(\sqrt{\left(\text{aplot}^2\left(2+\text{vbar}^2+2\,\text{vbar}\,\text{Cos}[\alpha]-2\,\text{vbar}\,\text{Sin}[\alpha]\right)\right)}\right),\right.$$
$$\left.(\text{aplot}\,(-1+\text{vbar}\,\text{Sin}[\alpha]))\Big/\left(\sqrt{\left(\text{aplot}^2\left(2+\text{vbar}^2+2\,\text{vbar}\,\text{Cos}[\alpha]-2\,\text{vbar}\,\text{Sin}[\alpha]\right)\right)}\right),\,0\right\}$$

$$\frac{1}{2}\left(-2+\left(\sqrt{2}\,\sqrt{\left(-a^2\left(-5+\text{Cos}[3\,\alpha]\,\text{Sec}[\alpha]-\text{Sec}[\alpha]\,\text{Sin}[3\,\alpha]-\text{Tan}[\alpha]+4\sqrt{\left(\text{Cos}[\alpha]^2\,(3+\text{Sin}[2\,\alpha])\right)}\,\text{Tan}[\alpha]\right)\right)}\right)\Big/\left(\sqrt{a^2}\right)\right)$$

```
ibar = 5;
jbar = 3;
adef2act = (ndef[ibar] - ndef[jbar]).(ndef[ibar] - ndef[jbar]) /. data;
aundef2act = (nundef[ibar] - nundef[jbar]).(nundef[ibar] - nundef[jbar]) /. data;
epsact = (Sqrt[adef2act] - Sqrt[aundef2act]) / Sqrt[aundef2act] /. data;
eps53 = epsact
eps53 /. {a → aplot} // Simplify
k53 = (ndef[ibar] - ndef[jbar]) / Sqrt[adef2act] /. data
k53 /. {a → aplot} // Simplify
eps53lock = eps53 /. {vbar → vdes} // Simplify
```

$$\left(-\sqrt{2}\,\sqrt{a^2}+\sqrt{\left((-a+a\,\text{vbar}\,\text{Cos}[\alpha])^2+(a+a\,\text{vbar}\,\text{Sin}[\alpha])^2\right)}\right)\Big/\left(\sqrt{2}\,\sqrt{a^2}\right)$$

$$\frac{1}{2}\left(-2+\left(\sqrt{2}\,\sqrt{\left(\text{aplot}^2\left(2+\text{vbar}^2-2\,\text{vbar}\,\text{Cos}[\alpha]+2\,\text{vbar}\,\text{Sin}[\alpha]\right)\right)}\right)\Big/\left(\sqrt{\text{aplot}^2}\right)\right)$$

$$\left\{(-a+a\,\text{vbar}\,\text{Cos}[\alpha])\Big/\left(\sqrt{\left((-a+a\,\text{vbar}\,\text{Cos}[\alpha])^2+(a+a\,\text{vbar}\,\text{Sin}[\alpha])^2\right)}\right),\right.$$
$$\left.(a+a\,\text{vbar}\,\text{Sin}[\alpha])\Big/\left(\sqrt{\left((-a+a\,\text{vbar}\,\text{Cos}[\alpha])^2+(a+a\,\text{vbar}\,\text{Sin}[\alpha])^2\right)}\right),\,0\right\}$$

$$\left\{(\text{aplot}\,(-1+\text{vbar}\,\text{Cos}[\alpha]))\Big/\left(\sqrt{\left(\text{aplot}^2\left(2+\text{vbar}^2-2\,\text{vbar}\,\text{Cos}[\alpha]+2\,\text{vbar}\,\text{Sin}[\alpha]\right)\right)}\right),\right.$$
$$\left.(\text{aplot}\,(1+\text{vbar}\,\text{Sin}[\alpha]))\Big/\left(\sqrt{\left(\text{aplot}^2\left(2+\text{vbar}^2-2\,\text{vbar}\,\text{Cos}[\alpha]+2\,\text{vbar}\,\text{Sin}[\alpha]\right)\right)}\right),\,0\right\}$$

$$-1+\left(\sqrt{\left(-a^2\left(-3-\text{Cos}[2\,\alpha]-2\,\text{Cos}[\alpha]\,\text{Sin}[\alpha]+2\sqrt{\left(\text{Cos}[\alpha]^2\,(3+\text{Sin}[2\,\alpha])\right)}\right)\right)}\right)\Big/\left(\sqrt{a^2}\right)$$

[179]:=
```
ibar = 5;
jbar = 1;
adef2act = (ndef[ibar] - ndef[jbar]).(ndef[ibar] - ndef[jbar]) /. data;
aundef2act = (nundef[ibar] - nundef[jbar]).(nundef[ibar] - nundef[jbar]) /. data;
epsact = (Sqrt[adef2act] - Sqrt[aundef2act]) / Sqrt[aundef2act] /. data;
eps51 = epsact
eps51 /. {a → aplot} // Simplify
k51 = (ndef[ibar] - ndef[jbar]) / Sqrt[adef2act] /. data
k51 /. {a → aplot} // Simplify
eps51lock = eps51 /. {vbar → vdes} // Simplify
```

t[184]= $\left(-\sqrt{2}\,\sqrt{a^2+\sqrt{\left((-a+a\,\text{vbar}\,\text{Cos}[\alpha])^2+(-a+a\,\text{vbar}\,\text{Sin}[\alpha])^2\right)}}\right)\Big/\left(\sqrt{2}\,\sqrt{a^2}\right)$

t[185]= $\frac{1}{2}\left(-2+\left(\sqrt{2}\,\sqrt{\left(\text{aplot}^2\left(2+\text{vbar}^2-2\,\text{vbar}\,\text{Cos}[\alpha]-2\,\text{vbar}\,\text{Sin}[\alpha]\right)\right)}\right)\Big/\left(\sqrt{\text{aplot}^2}\right)\right)$

t[186]= $\left\{(-a+a\,\text{vbar}\,\text{Cos}[\alpha])\Big/\left(\sqrt{\left((-a+a\,\text{vbar}\,\text{Cos}[\alpha])^2+(-a+a\,\text{vbar}\,\text{Sin}[\alpha])^2\right)}\right),\right.$
$\left.(-a+a\,\text{vbar}\,\text{Sin}[\alpha])\Big/\left(\sqrt{\left((-a+a\,\text{vbar}\,\text{Cos}[\alpha])^2+(-a+a\,\text{vbar}\,\text{Sin}[\alpha])^2\right)}\right),0\right\}$

t[187]= $\left\{(\text{aplot}\,(-1+\text{vbar}\,\text{Cos}[\alpha]))\Big/\left(\sqrt{\left(\text{aplot}^2\left(2+\text{vbar}^2-2\,\text{vbar}\,\text{Cos}[\alpha]-2\,\text{vbar}\,\text{Sin}[\alpha]\right)\right)}\right),\right.$
$\left.(\text{aplot}\,(-1+\text{vbar}\,\text{Sin}[\alpha]))\Big/\left(\sqrt{\left(\text{aplot}^2\left(2+\text{vbar}^2-2\,\text{vbar}\,\text{Cos}[\alpha]-2\,\text{vbar}\,\text{Sin}[\alpha]\right)\right)}\right),0\right\}$

t[188]= $\left(-\sqrt{a^2+\sqrt{\left(a^2\left(4+3\,\text{Cos}[\alpha]\,\text{Sin}[\alpha]-2\sqrt{\left(\text{Cos}[\alpha]^2\,(3+\text{Sin}[2\alpha])\right)}-\left(-1+\text{Sin}[\alpha]^2+2\sqrt{\left(\text{Cos}[\alpha]^2\,(3+\text{Sin}[2\alpha])\right)}\right)\text{Tan}[\alpha]\right)\right)}}\right)\Big/\left(\sqrt{a^2}\right)$

- **Plot the locking strains vs loading angle alpha**

[189]:=
```
vmaxrule = {α → (alphadeg * Pi / 180), vbar → vdes};

eps59lockplot = eps59lock /. vmaxrule // Simplify;
eps57lockplot = eps57lock /. vmaxrule // Simplify;
eps53lockplot = eps53lock /. vmaxrule // Simplify;
eps51lockplot = eps51lock /. vmaxrule // Simplify;
```

[194]:=
```
epsfact = 1;
epsliminf = 1 - √2;
aplot = 1;
aplotrule = {a → aplot};
epsalphaplot = Plot[{eps59lockplot * epsfact /. aplotrule, eps57lockplot * epsfact /. aplotrule,
    eps53lockplot * epsfact /. aplotrule, eps51lockplot * epsfact /. aplotrule, epsliminf * epsfact}, {alphadeg, 0, 90},
  PlotStyle → {{Thick, Red}, {Thick, Orange}, {Thick, Magenta}, {Thick, Blue}, {Thick, Blue, Dashed}},
  AxesLabel → {"α (deg)", "ϵt,lock"}, PlotRange → {Automatic, Automatic},
  Ticks → {Automatic, {{-1 + √2, "√2-1"}, {1 - √2, "1-√2"}}}]
```

t[198]=

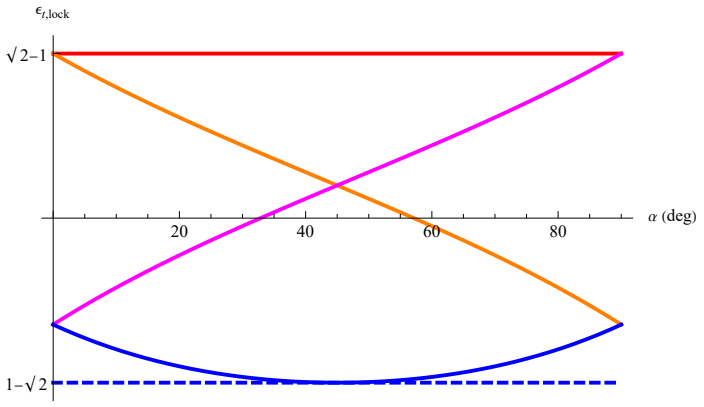

Find vmax vs alpha law for a1=a2=a, beta = 10 deg

[199]:=
```
dataplot = {a → 100., a1 → 100., a2 → 100., beta → (10. * Pi / 180)}
```

t[199]= {a → 100., a1 → 100., a2 → 100., beta → 0.174533}

[200]:=
```
vplotabcd = Min[vsol1a /. dataplot, vsol1b /. dataplot];
vgraphabcd = Plot[{vplotabcd}, {alphadeg, 0, 89.99}, PlotStyle → {Thick, Green},
   AxesLabel → {"α (deg)", "v [mm]"}, (*PlotRange→{vplotmin,vplotmax}*) PlotRange → All, PlotPoints → 100];
eps = 1 * 10^{-9};
vplot0abcd = vplotabcd /. {alphadeg → 0 + eps}
vplot45abcd = vplotabcd /. {alphadeg → 45}
vplot80abcd = vplotabcd /. {alphadeg → 80}
vplot85abcd = vplotabcd /. {alphadeg → 85}
vplot90abcd = vplotabcd /. {alphadeg → 90 - eps}
vplotbeta10deg = Plot[{vplotabcd / {a /. dataplot}}, {alphadeg, 0, 90}, PlotStyle → {Thick, RGBColor[0.1, 1, 0.5]},
  AxesLabel → {"α (deg)", "v [mm]"}, PlotRange → All, PlotPoints → 100, Frame → {{True, True}, {True, False}}]
```

[203]= 56.7085

[204]= 46.9279

[205]= 56.7085

[206]= 59.7825

[207]= 56.7085

[208]=

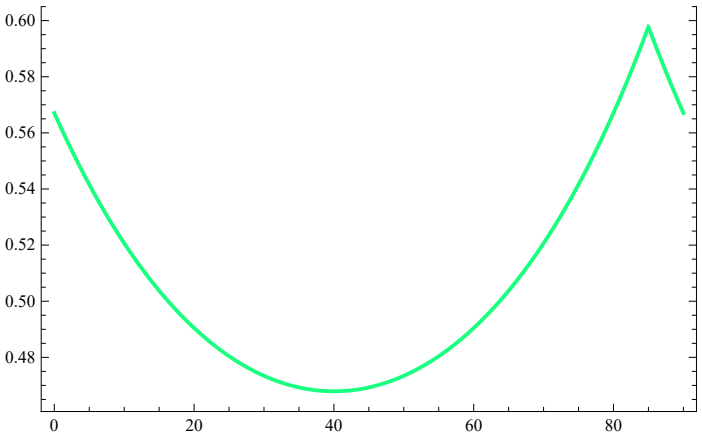

[209]:=
```
v1 = vsol1a /. dataplot;
Dv1 = D[v1, alphadeg];
solDv1 = FindRoot[{Dv1 == 0}, {alphadeg, 45}]
vbarlockminp10 = (v1 /. solDv1) / a /. dataplot
```

[211]= {alphadeg → 40.}

[212]= 0.467911

Find vmax vs alpha law for a1=a2=a, beta = 5 deg

[213]:=
```
dataplot = {a → 100., a1 → 100., a2 → 100., beta → (5. * Pi / 180)}
```

[213]= {a → 100., a1 → 100., a2 → 100., beta → 0.0872665}

[214]:=
```
vplotabcd = Min[vsol1a /. dataplot, vsol1b /. dataplot];
vgraphabcd = Plot[{vplotabcd}, {alphadeg, 0, 89.99}, PlotStyle → {Thick, Blue},
  AxesLabel → {"α (deg)", "v [mm]"}, (*PlotRange→{vplotmin,vplotmax}*) PlotRange → All, PlotPoints → 100]
eps = 1 * 10^{-9};
vplot0abcd = vplotabcd /. {alphadeg → 0 + eps}
vplot45abcd = vplotabcd /. {alphadeg → 45}
vplot85abcd = vplotabcd /. {alphadeg → 85}
vplot875abcd = vplotabcd /. {alphadeg → 87.5}
vplot90abcd = vplotabcd /. {alphadeg → 90 - eps}
vplotbeta5deg = Plot[{vplotabcd / {a /. dataplot}}, {alphadeg, 0, 90}, PlotStyle → {Thick, Blue},
   AxesLabel → {"α (deg)", "v [mm]"}, PlotRange → All, PlotPoints → 100, Frame → {{True, True}, {True, False}}];
```

[215]=

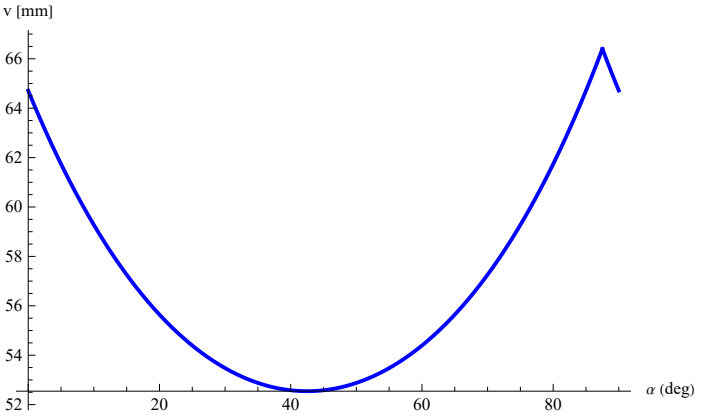

[217]= 64.7086

[218]= 52.5814

[219]= 64.7086

[220]= 66.4038

[221]= 64.7086

[223]:=
```
v1 = vsol1a /. dataplot;
Dv1 = D[v1, alphadeg];
solDv1 = FindRoot[{Dv1 == 0}, {alphadeg, 45}]
vbarlockminp5 = (v1 /. solDv1) / a /. dataplot
```

[225]= {alphadeg → 42.5}

[226]= 0.525445

Find vmax vs alpha law for a1=a2=a, beta = -5 deg

[227]:=
```
dataplot = {a → 100., a1 → 100., a2 → 100., beta → (-5. * Pi / 180)}
```

[227]= {a → 100., a1 → 100., a2 → 100., beta → -0.0872665}

[228]:=
```
vplotabcd = Min[vsol1a /. dataplot, vsol1b /. dataplot, vsol2d /. dataplot];
vgraphabcd = Plot[{vplotabcd}, {alphadeg, 0, 89.99}, PlotStyle → {Thick, Magenta},
  AxesLabel → {"α (deg)", "v [mm]"}, (*PlotRange→{vplotmin,vplotmax}*) PlotRange → All, PlotPoints → 100]
eps = 1 * 10^{-9};
vplot0abcd = vplotabcd /. {alphadeg → 0 + eps}
vplot25abcd = vplotabcd /. {alphadeg → 2.5}
vplot5abcd = vplotabcd /. {alphadeg → 5}
vplot45abcd = vplotabcd /. {alphadeg → 45}
vplot90abcd = vplotabcd /. {alphadeg → 90 - eps}
vplotbetam5deg = Plot[{vplotabcd / {a /. dataplot}}, {alphadeg, 0, 90}, PlotStyle → {Thick, Magenta},
   AxesLabel → {"α (deg)", "v [mm]"}, PlotRange → All, PlotPoints → 100, Frame → {{True, True}, {True, False}}];
```

[229]=

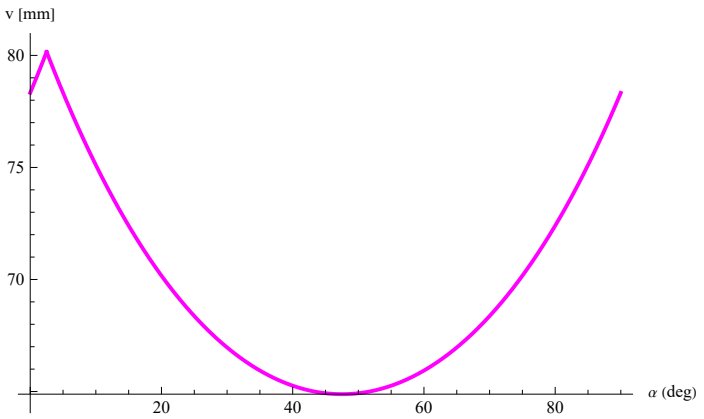

[231]= 78.3332

[232]= 80.1602

[233]= 78.3332

[234]= 64.9237

[235]= 78.3332

[237]:=
```
v1 = vsol1a /. dataplot;
Dv1 = D[v1, alphadeg];
solDv1 = FindRoot[{Dv1 == 0}, {alphadeg, 45}]
vbarlockminm5 = (v1 /. solDv1) / a /. dataplot
```

[239]= {alphadeg → 47.5}

[240]= 0.64882

Find vmax vs alpha law for a1=a2=a, beta = -10deg

[241]:=
```
dataplot = {a → 100., a1 → 100., a2 → 100., beta → (-10. * Pi / 180)}
```

[241]= {a → 100., a1 → 100., a2 → 100., beta → -0.174533}

```
vplotabcd = Min[vsol1a /. dataplot, vsol1b /. dataplot, vsol2d /. dataplot];
vgraphabcd = Plot[{vplotabcd}, {alphadeg, 0, 89.99}, PlotStyle → {Thick, Orange},
  AxesLabel → {"α (deg)", "v [mm]"}, (*PlotRange→{vplotmin,vplotmax}*) PlotRange → All, PlotPoints → 100]
eps = 1 * 10^{-9};
vplot0abcd = vplotabcd /. {alphadeg → 0 + eps}
vplot5abcd = vplotabcd /. {alphadeg → 5}
vplot10abcd = vplotabcd /. {alphadeg → 10}
vplot45abcd = vplotabcd /. {alphadeg → 45}
vplot90abcd = vplotabcd /. {alphadeg → 90 - eps}
vplotbetam10deg = Plot[{vplotabcd / {a /. dataplot}}, {alphadeg, 0, 90}, PlotStyle → {Thick, Orange},
   AxesLabel → {"α (deg)", "v [mm]"}, PlotRange → All, PlotPoints → 100, Frame → {{True, True}, {True, False}}];
```

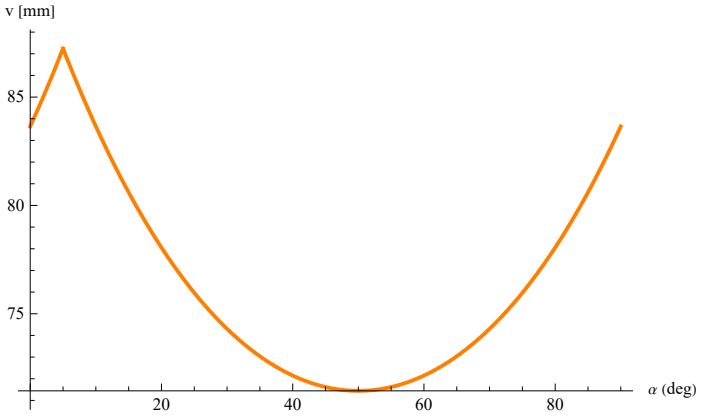


```
83.6495

87.2435

83.6495

71.6176

83.6495
```

```
v1 = vsol1a /. dataplot;
Dv1 = D[v1, alphadeg];
solDv1 = FindRoot[{Dv1 == 0}, {alphadeg, 45}]
vbarlockminm10 = (v1 /. solDv1) / a /. dataplot

vbarlockminp10
(vbarlockminm10 - vbarlockminp10) / vbarlockminp10 * 100
```

```
{alphadeg → 50.}

0.714425

0.467911

52.6839
```

Global vlock vs. alpha chart

[257]:=
```
vlockchart = Show[vplotbeta10deg, vplotbeta5deg, vplotbeta0deg, vplotbetam5deg, vplotbetam10deg]
(* SetDirectory[NotebookDirectory[]];
Export["vlock_chart.pdf",vlockchart] *)
```

t[257]=

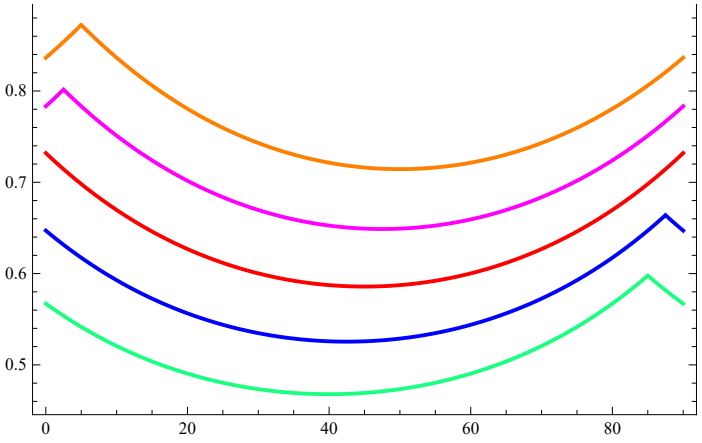

APPENDIX B

MATHEMATICA® CODE FOR THE SIMULATION OF THE FORCE-DISPLACEMENT RESPONSE OF PROTOTYPE #2 UNDER P=25 KN

Appendix B: *Mathematica*® code for the simulation of the force-displacement response of prototype #2 under P=25 kN

General data

General data

```
In[ ]:= Clear[adata, vdata]
        adata = {};
        vdata = {vact → v, anglealpha → (alphav)};
        cdata = {C[1] → 0, C[2] → 0};
        kloadata = {Cos[anglealpha], Sin[anglealpha], 0} /. vdata
Out[ ]= {Cos[alphav], Sin[alphav], 0}

In[ ]:= degbetacurr = 0.0;
        degalphacurr = 0.0;
        dataplot = {alphav → (degalphacurr * Pi / 180), alphadegload → (degalphacurr),
          a → 100.50, a1 → 97, a2 → 100.50, beta → (degbetacurr * Pi / 180 * 1),
          vamax → 50, epspredata → (0.0), epspreveresaldata -> (0.0)}
        dataplot2 = {a → (a /. dataplot), a1 → (a1 /. dataplot),
          a2 → (a2 /. dataplot), beta → (beta /. dataplot)}
Out[ ]= {alphav → 0., alphadegload → 0., a → 100.5, a1 → 97, a2 → 100.5,
         beta → 0., vamax → 50, epspredata → 0., epspreveresaldata → 0.}

Out[ ]= {a → 100.5, a1 → 97, a2 → 100.5, beta → 0.}
```

Theoretical and experimental F - v curves of sinusoidal tests

Velocity vs. time law of the tests

```
In[ ]:= Clear[loaddata0]

        Clear[mufrictactfriction0, mufrictactfriction1, mufrictactfriction2, mufrictactfriction3]

        loaddata = {loadfreq → (0.4), Pref → 42.352,
          gammaref → 4.0, vdotref → 2.5, mus0 → (0.004675661715740908`)}

        Fmaxplotall = 1000;
        Fminplotall = -Fmaxplotall;
Out[ ]= {loadfreq → 0.4, Pref → 42.352, gammaref → 4., vdotref → 2.5, mus0 → 0.00467566}

In[ ]:= vmax
        vlawtime = vmax * Sin[2 * Pi * loadfreq * time]
        vdotlawtime = D[vlawtime, time]
Out[ ]= 50

Out[ ]= 50 Sin[2 loadfreq π time]

Out[ ]= 100 loadfreq π Cos[2 loadfreq π time]
```

In[•]:=
```
Solve[vmax * Sin[2 * Pi * loadfreq * time] == v, {time}]
isol = 2;
soltime = Solve[vmax * Sin[2 * Pi * loadfreq * time] == v, {time}][[isol]] /. {C[1] → 0}
(time /. {soltime}) /. {v → 0}
(time /. {soltime}) /. {v → vmax}
```

Out[•]= $\left\{\left\{\text{time} \to \boxed{\frac{\pi - \text{ArcSin}\left[\frac{v}{50}\right] + 2\,\pi\,C_1}{2\,\text{loadfreq}\,\pi} \quad \text{if} \quad C_1 \in \mathbb{Z}}\right\}, \left\{\text{time} \to \boxed{\frac{\text{ArcSin}\left[\frac{v}{50}\right] + 2\,\pi\,C_1}{2\,\text{loadfreq}\,\pi} \quad \text{if} \quad C_1 \in \mathbb{Z}}\right\}\right\}$

Out[•]= $\left\{\text{time} \to \frac{\text{ArcSin}\left[\frac{v}{50}\right]}{2\,\text{loadfreq}\,\pi}\right\}$

Out[•]= $\{0\}$

Out[•]= $\left\{\frac{1}{4\,\text{loadfreq}}\right\}$

In[•]:=
```
vdotlawv = vdotlawtime /. soltime // Simplify
vdotlawvdata = vdotlawv /. loaddata
vdotlawvdata /. {v → 0}
vdotlawvdata /. {v → vmax}
```

Out[•]= $2\,\text{loadfreq}\,\pi\,\sqrt{2500 - v^2}$

Out[•]= $2.51327\,\sqrt{2500 - v^2}$

Out[•]= 125.664

Out[•]= 0.

Load case # 3 - 25 kN

In[•]:=
```
coloract = Black;
colorexp = Blue;
loadact = 3;
vmaxcurr = 50;
expdashed = Dashed;
expdashed = "";
thdashed = "";
thdashed = Dashed;
fontsize = 12;
r = 0.1;
numthickness = Thickness[r];
(* numthickness=AbsoluteThickness ;*)
numthickness = Thick;
```

In[ ]:=
```
Veffact = Veffactfriction3;
mufrictact = mus0 * Exp[-Veffactfriction3 / Pref] *
    (gammaref + (1 - gammaref) * Exp[-vdotlawv / vdotref]) /. loaddata;
VeffactN = Veffact * 1000; (* N *)
Floadact = Fload00;
Funloact = Funlo00;

Vnormact = VeffactN / (fact);
Floadactfriction = Floadact + mufrictact * Vnormact;
Funloactfriction = Funloact - mufrictact * Vnormact;

FFrictionp = +mufrictact * Vnormact;
FFrictionm = -mufrictact * Vnormact;

mufrictact * Vnormact /. {v → vmaxcurr };
Fmaxact = Floadactfriction /. {v → vmaxcurr };
Floadact /. {v → vmaxcurr };

mufrictact3 = mufrictact;
Floadactfriction3 = Floadactfriction;
Funloactfriction3 = Funloactfriction;
Fmaxact3 = Fmaxact
muW3 = mufrictact * Vnormact
Fmaxact = Max[Fmaxact1, Fmaxact2, Fmaxact3] // N
```

Out[ ]= 606.992

Out[ ]= $64.7773 \left(4. - 3. e^{-1.00531 \sqrt{2500-v^2}}\right)$

Out[ ]= Max[606.992, Fmaxact1, Fmaxact2]

Plot current load case

In[ ]:=
```
Fmaxplot = Fmaxact * 1.5;
Fminplot = -Fmaxplot;
```

In[ ]:=
```
vFmax = 0.995 * vmaxcurr
```

Out[ ]= 49.75

In[ ]:=
```
vfact = 1.;
Ffact = fact / 1000;
vdimrule = {v → (vdim / vfact)};
plotfrictionscaled =
 Plot[{Ffact * (Floadactfriction /. vdimrule), Ffact * (Funloactfriction /. vdimrule)},
  {vdim, 0, vmaxcurr * vfact}, PlotStyle → {{numthickness, coloract, thdashed}},
  TicksStyle → {{FontSize → 12, Black}, {FontSize → fontsize, Black}},
  LabelStyle → {FontSize → fontsize, Black}, AxesLabel → {"v (mm)", "F (kN)"},
  PlotRange → {{-vmaxcurr * vfact * 1.1, vmaxcurr * vfact * 1.1},
    {Ffact * Fminplotall, Ffact * Fmaxplotall}}, AxesOrigin → {0, 0}]

plotfrictionscaledadd1 =
 {{vmaxcurr * vfact, (Ffact * (Floadactfriction /. vdimrule)) /. {vdim -> vmaxcurr * vfact}},
  {vmaxcurr * vfact, (Ffact * (Funloactfriction /. vdimrule)) /. {vdim -> vmaxcurr * vfact}}}

Ffact = -fact / 1000;
vdimrule = {v → (-vdim / vfact)};
plotfrictionscaledinv =
  Plot[{Ffact * (Floadactfriction /. vdimrule), Ffact * (Funloactfriction /. vdimrule)},
   {vdim, -vmaxcurr * vfact, 0}, PlotStyle → {{numthickness, coloract, thdashed}},
   TicksStyle → {{FontSize → 12, Black}, {FontSize → fontsize, Black}},
   LabelStyle → {FontSize → fontsize, Black}, AxesLabel → {"v (mm)", "F (kN)"},
   PlotRange → {{-vmaxcurr * vfact * 1.1, vmaxcurr * vfact * 1.1},
     {Ffact * Fminplotall, Ffact * Fmaxplotall}}, AxesOrigin → {0, 0}];

plotfrictionscaledadd2 =
 {{-vmaxcurr * vfact, (Ffact * (Floadactfriction /. vdimrule)) /. {vdim → -vmaxcurr * vfact}},
  {-vmaxcurr * vfact, (Ffact * (Funloactfriction /. vdimrule)) /. {vdim → -vmaxcurr * vfact}}}

Listplotadd3 = ListPlot[{plotfrictionscaledadd1, plotfrictionscaledadd2}, Joined → True,
   PlotStyle → {{numthickness, coloract, thdashed}, {numthickness, coloract, thdashed}}];

theoryplot = Show[plotfrictionscaled, plotfrictionscaledinv, Listplotadd3]
```

Out[ ]=

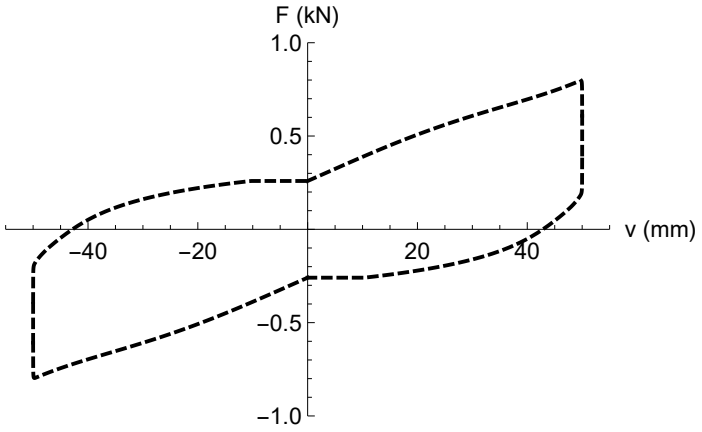

In[ ]:=
```
dispact = 2;
expcurvedataunscaled = FIPload[loadact, dispact];
nexp = Dimensions[expcurvedataunscaled][[1]];
expcurvedata =
  Table[{expcurvedataunscaled[[i, 1]], expcurvedataunscaled[[i, 2]] / 1000}, {i, 1, nexp}];
expcurve = ListPlot[{expcurvedata}, Joined → True, PlotStyle -> {{expdashed, colorexp}},
   TicksStyle → {{FontSize → fontsize, Black}, {FontSize → fontsize, Black}},
   LabelStyle → {FontSize → fontsize, Black}];

expcurve3 = expcurve;
expcurvedata3sinusOK = expcurvedata;

fig5g = Show[plotfrictionscaled, plotfrictionscaledinv, Listplotadd3, expcurve]
(* Export["Fig5g.pdf",fig5g]; *)
```

Out[ ]=

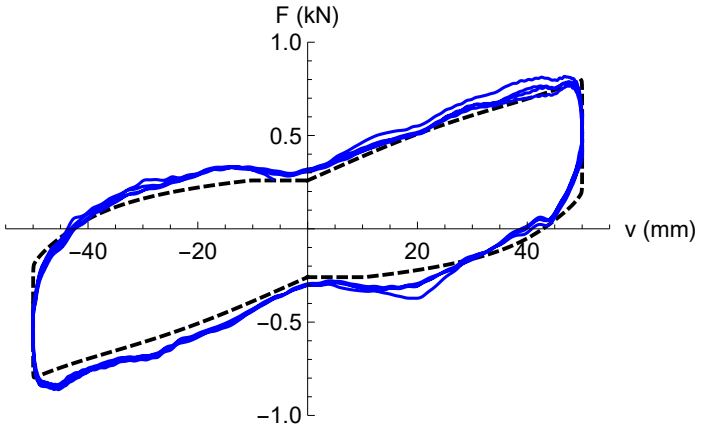

Estimate fundamental period current load case

In[ ]:=
```
Ffact = fact;
vdimrule = {v → (vdim / vfact)};
vmaxscaled = vmaxcurr * vfact

vFmax
Fmaxscaled = Ffact * (Floadactfriction /. vdimrule) /. {vdim → (vFmax)}
F0scaled = Ffact * (Floadactfriction /. vdimrule) /. {vdim → 0}
Kheffact = Fmaxscaled / vmaxscaled (* N/mm *)
masseffact = Veffact * 1000 / 9.81 (* 25 kN transformed into kg *)
KheffNmact = Kheffact * 1000 (* Keff from N/mm to N/m *)
Theffact = 2 * Pi * Sqrt[masseffact / KheffNmact]
```

Out[ ]= 50.

Out[ ]= 49.75

Out[ ]= 796.831

Out[ ]= 259.109

Out[ ]= 15.9366

Out[ ]= 2548.42

Out[ ]= 15 936.6

Out[ ]= 2.51256

In[ ]:=
```
vFmax = vmaxcurr;
force1 = Ffact * (Floadactfriction /. vdimrule);
force2 = Ffact * (Funloactfriction /. vdimrule);
Plot[{force1, force2}, {vdim, 0, vFmax * vfact},
 PlotStyle → {{coloract, Thick}}, AxesLabel → {"v (mm)", "F (N)"},
 PlotRange → {{-vmaxcurr * vfact * 1.1, vmaxcurr * vfact * 1.1}, {Ffact * Fminplot, Ffact * Fmaxplot}},
 AxesOrigin → {0, 0}]

EDC1Nmm = NIntegrate[force1, {vdim, 0, vFmax * vfact}];
EDC1 = EDC1Nmm / 1000
EDC2Nmm = NIntegrate[-force2, {vdim, 0, vFmax * vfact}];
EDC2 = EDC2Nmm / 1000
EDCTH = (EDC1 + EDC2) * 2
```

Out[ ]= 27.3055

Out[ ]= 7.54274

Out[ ]= 69.6964

In[ ]:=
```
EDCTH3 = EDCTH;
csieffact = EDCTH / (2 * Pi * KheffNmact * ((vmaxscaled / 1000) ^ 2))
```

Out[ ]= 0.278416

```
In[ ]:= mudynav = 1.0361291837657416` / 100;
        EDCfrictionavg = 4 * mudynav * Veffact * vmaxcurr
        EDCTH / EDCfrictionavg
```

```
Out[ ]= 51.8065
```

```
Out[ ]= 1.34532
```

```
In[ ]:= Theffload3 = Theffact
        csieff3 = csieffact
```

```
Out[ ]= 2.51256
```

```
Out[ ]= 0.278416
```

Plot the different contributions to the force-displacement model

```
In[ ]:= scaleAt = 1.0;
        Atdim2 = 1.9 * 31.6 * scaleAt (* mm2, rescaled cross-
          section area of the membranes of  the metaisolator in the rest configuration *)
        psiload = 1.19; (* 1.1918720852764824`; *)
        psiunlo = 1.0;
        Fmaxplotall0 = Fmaxplotall;
        Fmaxplotall = 1000 * (1 + scaleAt) / 2;
        Fminplotall = -Fmaxplotall;
```

```
Out[ ]= 60.04
```

```
In[ ]:= Frload0 = psiload * Atdim2 * fload0;
        Frunlo0 = psiunlo * Atdim2 * funlo0;
        Floadact = Frload0;
        Funloact = Frunlo0;
```

Friction term

```
In[ ]:= Floadactfriction = Floadact * 0 + mufrictact * Vnormact;
        Funloactfriction = Funloact * 0 - mufrictact * Vnormact;
        coloract = Magenta;
        thdashed = Thick;
        thdashed = Dashed;
```

```
In[ ]:= Fmaxplot = Fmaxact * 1.5;
        Fminplot = -Fmaxplot;
```

In[ ]:=
```
vfact = 1.;
Ffact = fact / 1000;
vdimrule = {v → (vdim / vfact)};
plotfrictionscaled =
  Plot[{Ffact * (Floadactfriction /. vdimrule), Ffact * (Funloactfriction /. vdimrule)},
   {vdim, 0, vmaxcurr * vfact}, PlotStyle → {{coloract, numthickness, thdashed}},
   TicksStyle → {{FontSize → 12, Black}, {FontSize → fontsize, Black}},
   LabelStyle → {FontSize → fontsize, Black}, AxesLabel → {"u", "F"},
   Ticks → None, PlotRange → {{-vmaxcurr * vfact * 1.1, vmaxcurr * vfact * 1.1},
     {Ffact * Fminplotall, Ffact * Fmaxplotall}}, AxesOrigin → {0, 0}];

plotfrictionscaledadd1 =
 {{vmaxcurr * vfact, (Ffact * (Floadactfriction /. vdimrule)) /. {vdim -> vmaxcurr * vfact}},
  {vmaxcurr * vfact, (Ffact * (Funloactfriction /. vdimrule)) /. {vdim -> vmaxcurr * vfact}}}

Ffact = -fact / 1000;
vdimrule = {v → (-vdim / vfact)};
plotfrictionscaledinv =
  Plot[{Ffact * (Floadactfriction /. vdimrule), Ffact * (Funloactfriction /. vdimrule)},
   {vdim, -vmaxcurr * vfact, 0}, PlotStyle → {{coloract, numthickness, thdashed}},
   TicksStyle → {{FontSize → 12, Black}, {FontSize → fontsize, Black}},
   LabelStyle → {FontSize → fontsize, Black}, AxesLabel → {"u", "F"},
   Ticks → None, PlotRange → {{-vmaxcurr * vfact * 1.1, vmaxcurr * vfact * 1.1},
     {Ffact * Fminplotall, Ffact * Fmaxplotall}}, AxesOrigin → {0, 0}];

plotfrictionscaledadd2 =
 {{-vmaxcurr * vfact, (Ffact * (Floadactfriction /. vdimrule)) /. {vdim → -vmaxcurr * vfact}},
  {-vmaxcurr * vfact, (Ffact * (Funloactfriction /. vdimrule)) /. {vdim → -vmaxcurr * vfact}}}

Listplotadd3 = ListPlot[{plotfrictionscaledadd1, plotfrictionscaledadd2}, Joined → True,
    PlotStyle → {{coloract, Thick, thdashed}, {coloract, numthickness, thdashed}}];

plotfriction = Show[plotfrictionscaled, plotfrictionscaledinv, Listplotadd3]
```

Out[ ]=
```
{{50., 0.0647773}, {50., -0.0647773}}
```

Out[ ]=
```
{{-50., -0.0647773}, {-50., 0.0647773}}
```

Out[ ]=

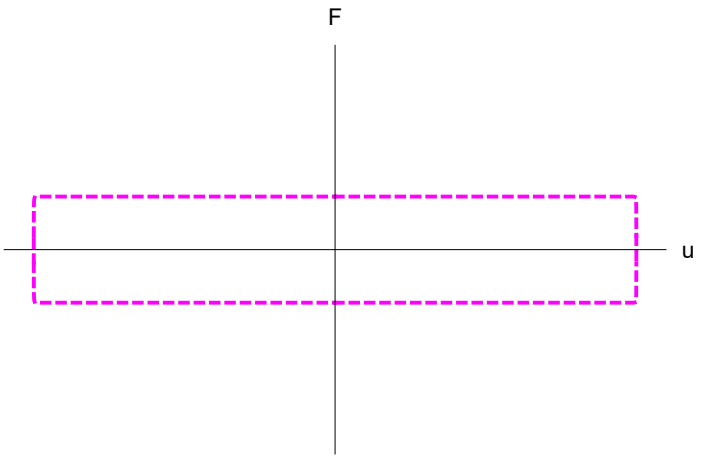

Recentering term

In[ ]:=
```
Floadactfriction = Floadact * 1 + mufrictact * Vnormact * 0;
Funloactfriction = Funloact * 1 - mufrictact * Vnormact * 0;
coloract = Brown;
thdashed = Thick;
thdashed = DotDashed;
thdashed = Dashed;
```

In[ ]:=
```
Fmaxplot = Fmaxact * 1.5;
Fminplot = -Fmaxplot;
```

In[ ]:=
```
vfact = 1.;
Ffact = fact / 1000;
vdimrule = {v → (vdim / vfact)};
plotfrictionscaled =
 Plot[{Ffact * (Floadactfriction /. vdimrule), Ffact * (Funloactfriction /. vdimrule)},
  {vdim, 0, vmaxcurr * vfact}, PlotStyle → {{coloract, numthickness, thdashed}},
  TicksStyle → {{FontSize → 12, Black}, {FontSize → fontsize, Black}},
  LabelStyle → {FontSize → fontsize, Black}, AxesLabel → {"u", "F"},
  Ticks → None, PlotRange → {{-vmaxcurr * vfact * 1.1, vmaxcurr * vfact * 1.1},
    {Ffact * Fminplotall, Ffact * Fmaxplotall}}, AxesOrigin → {0, 0}]

plotfrictionscaledadd1 =
 {{vmaxcurr * vfact, (Ffact * (Floadactfriction /. vdimrule)) /. {vdim -> vmaxcurr * vfact}},
  {vmaxcurr * vfact, (Ffact * (Funloactfriction /. vdimrule)) /. {vdim -> vmaxcurr * vfact}}}

Ffact = -fact / 1000;
vdimrule = {v → (-vdim / vfact)};
plotfrictionscaledinv =
 Plot[{Ffact * (Floadactfriction /. vdimrule), Ffact * (Funloactfriction /. vdimrule)},
  {vdim, -vmaxcurr * vfact, 0}, PlotStyle → {{coloract, numthickness, thdashed}},
  TicksStyle → {{FontSize → 12, Black}, {FontSize → fontsize, Black}},
  LabelStyle → {FontSize → fontsize, Black}, AxesLabel → {"u", "F"},
  Ticks → None, PlotRange → {{-vmaxcurr * vfact * 1.1, vmaxcurr * vfact * 1.1},
    {Ffact * Fminplotall, Ffact * Fmaxplotall}}, AxesOrigin → {0, 0}]

plotfrictionscaledadd2 =
 {{-vmaxcurr * vfact, (Ffact * (Floadactfriction /. vdimrule)) /. {vdim → -vmaxcurr * vfact}},
  {-vmaxcurr * vfact, (Ffact * (Funloactfriction /. vdimrule)) /. {vdim → -vmaxcurr * vfact}}}

Listplotadd3 = ListPlot[{plotfrictionscaledadd1, plotfrictionscaledadd2}, Joined → True,
  PlotStyle → {{coloract, Thick, thdashed}, {coloract, numthickness, thdashed}}]

plotrecentering = Show[plotfrictionscaled, plotfrictionscaledinv, Listplotadd3]
```

Out[ ]=
```
{{-50., -0.541364}, {-50., -0.454928}}
```

Out[ ]=

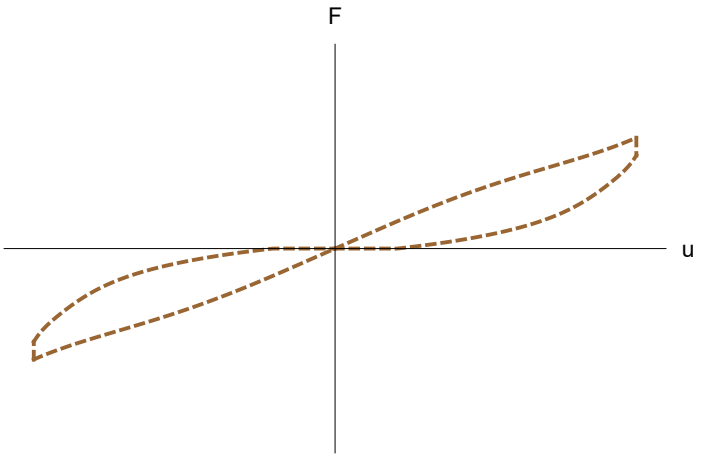

Combo plot

In[ ]:=
```
Fmaxplot = Fmaxact;
Fminplot = -Fmaxplot;
Floadactfriction = Floadact * 1 + mufrictact * Vnormact * 1;
Funloactfriction = Funloact * 1 - mufrictact * Vnormact * 1;
coloract = Black;
thdashed = Thick;
thdashed = DotDashed;
thdashed = Solid;
```

In[ ]:=
```
comboplot = Show[plotfriction, plotrecentering, theoryplot]
path = FileNameJoin[{NotebookDirectory[], "comboplot.pdf"}];
(* Export[path,comboplot]*)
```

Out[ ]=

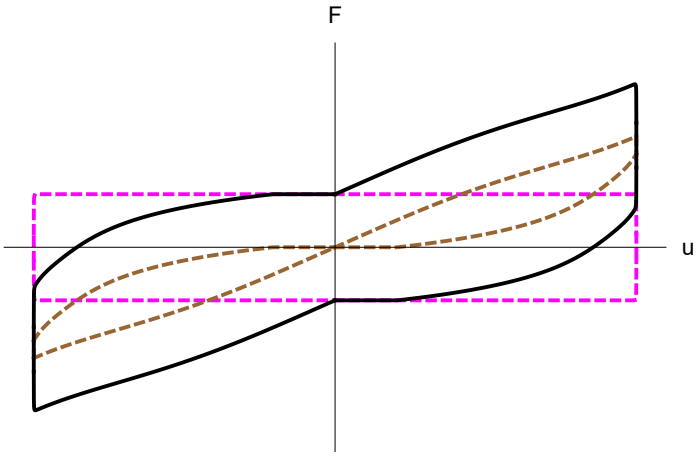

APPENDIX C

STL GRAPHIC/CAD FILES OF 3D PRINTED PARTS

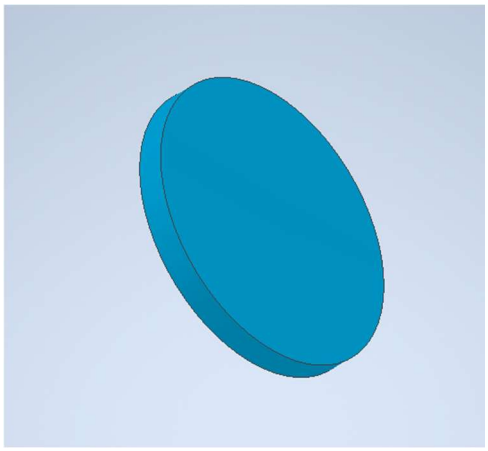

CAD design for Cap cushion

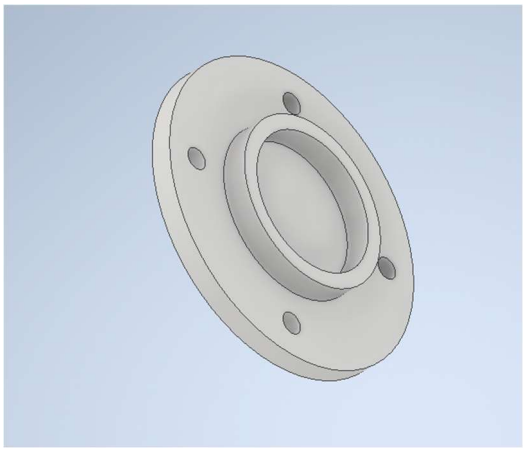

CAD design for Cap

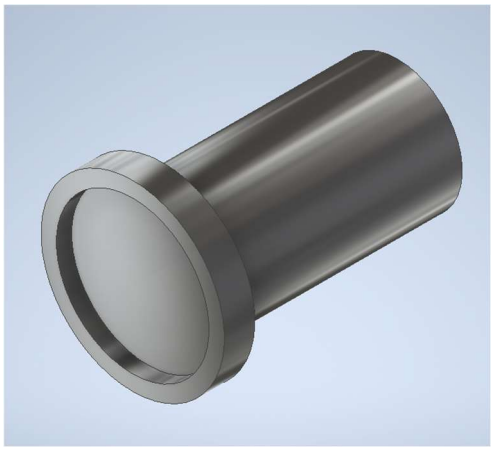

CAD design for Central post

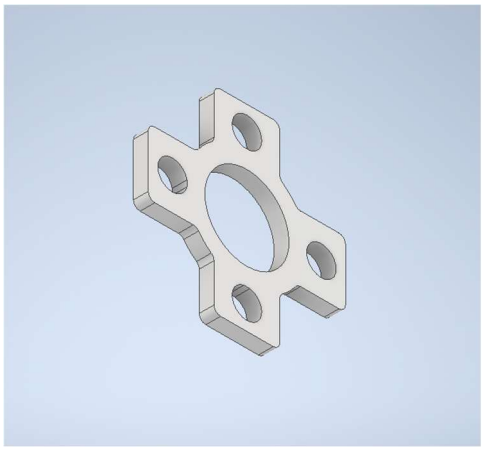

CAD design for Central ring

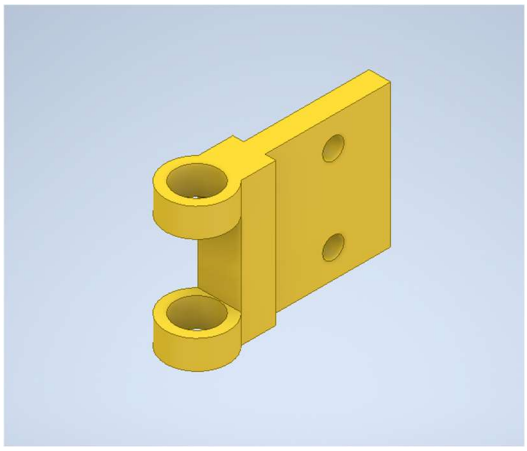

CAD design for Elbow hinge

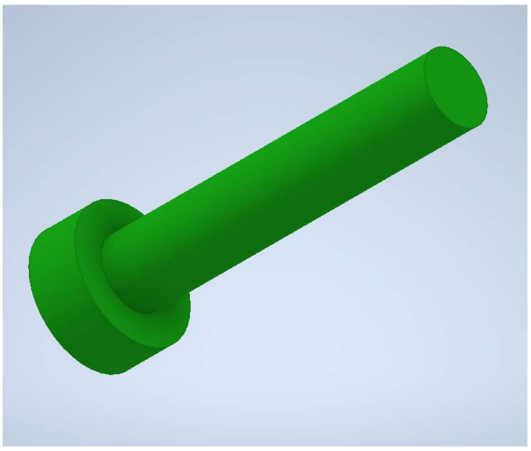

CAD design for Elbow pin

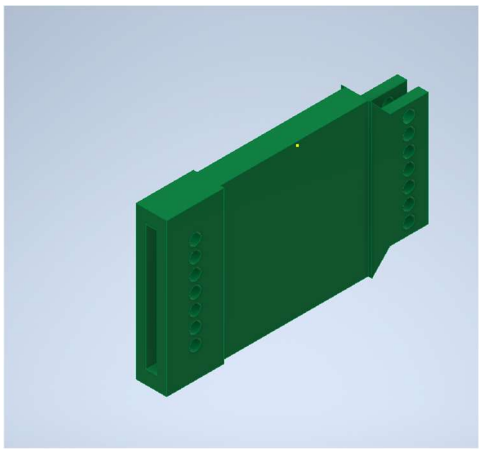

CAD design for Arm

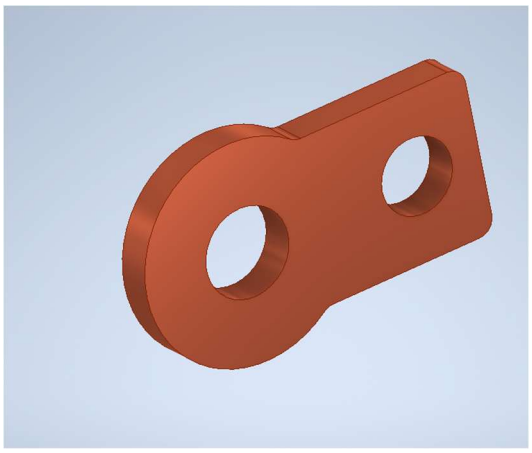

CAD design for short ring

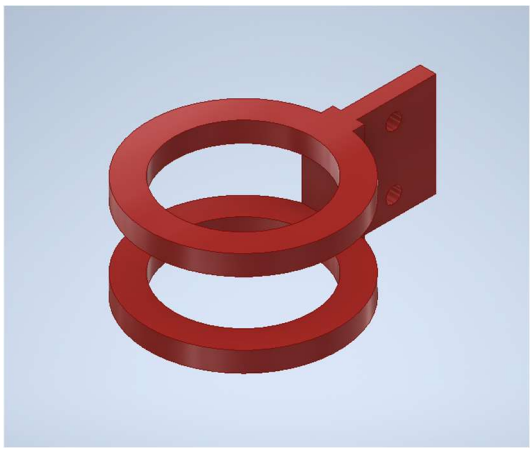

CAD design for Shoulder hinge

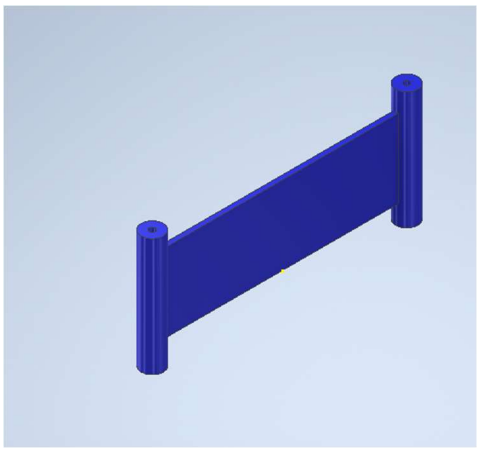

CAD design for Tendon

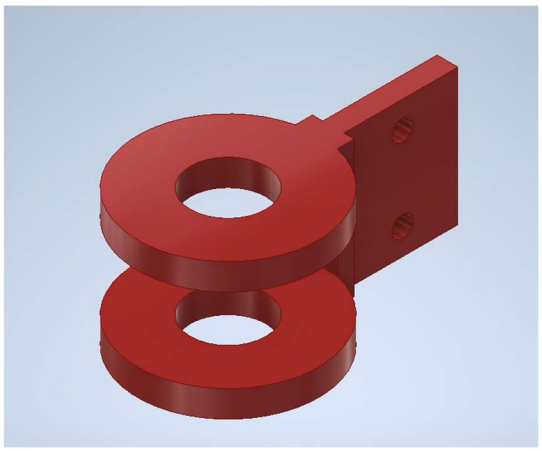

CAD design for Wrist hinge

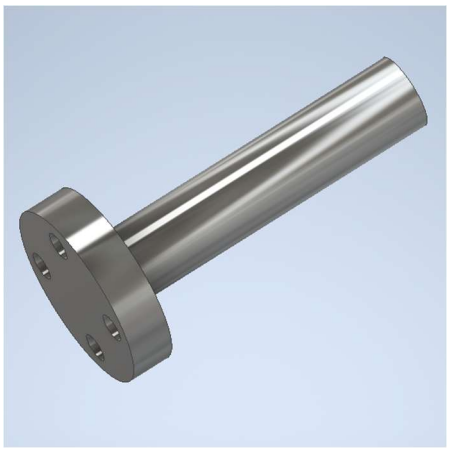

CAD design for Shoulder pin

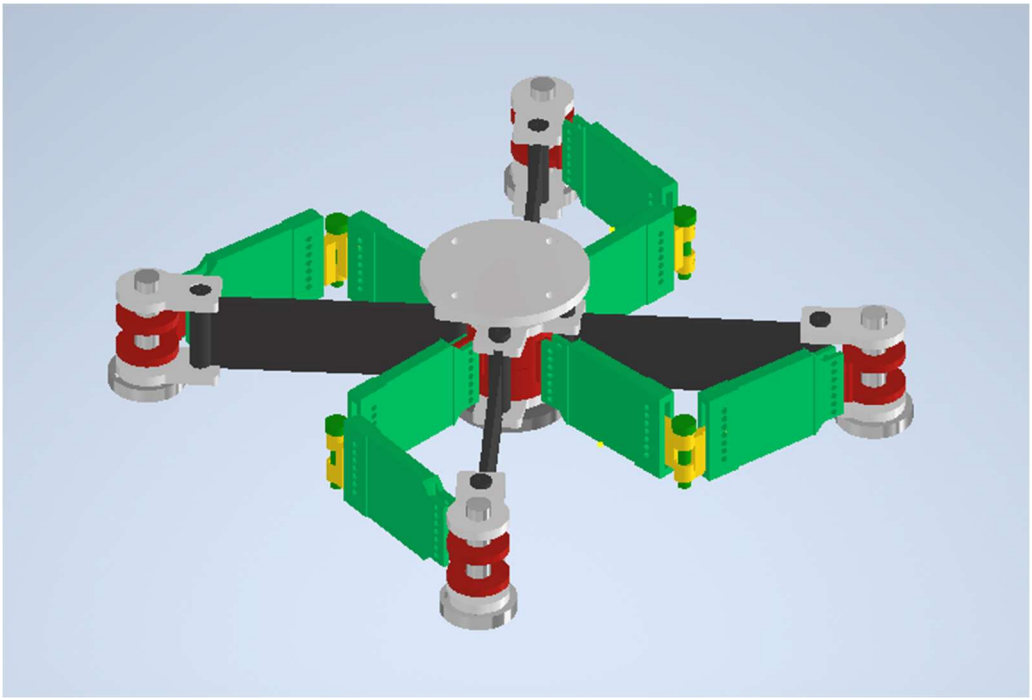

CAD design for Final model